12-1994

Effects of Blowing Ratio on Heat Transfer to the Throat Region of a Porous-Walled Nozzle

Joseph L. Lenertz

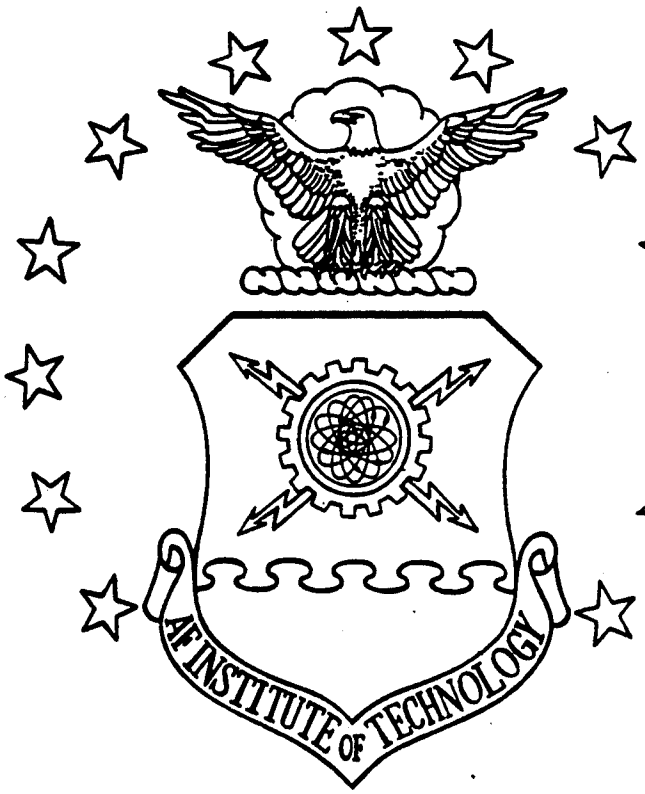

EFFECTS OF BLOWING RATIO ON HEAT TRANSFER TO THE THROAT REGION OF A POROUS-WALLED NOZZLE

THESIS

Joseph L. Lenertz, B.S.

AFIT/GA/ENY/94D-7

DEPARTMENT OF THE AIR FORCE
AIR UNIVERSITY
AIR FORCE INSTITUTE OF TECHNOLOGY

Wright-Patterson Air Force Base, Ohio

AFIT/GA/ENY/94D-7

Accesion For	
NTIS CRA&I	☒
DTIC TAB	☐
Unannounced	☐
Justification	
By	
Distribution /	
Availability Codes	
Dist	Avail and / or Special
A-1	

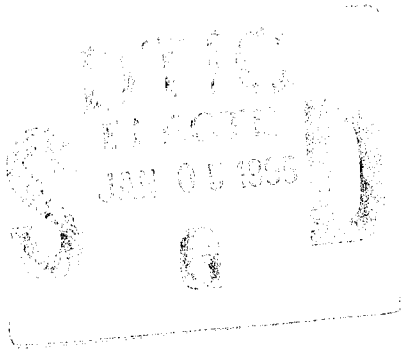

EFFECTS OF BLOWING RATIO ON HEAT TRANSFER TO THE THROAT REGION OF A POROUS-WALLED NOZZLE

THESIS

Joseph L. Lenertz, B.S.

AFIT/GA/ENY/94D-7

Approved for public release; distribution unlimited

AFIT/GA/ENY/94D-7

EFFECTS OF BLOWING RATIO ON HEAT TRANSFER TO THE THROAT REGION OF A POROUS-WALLED NOZZLE

THESIS

Presented to the Faculty of the Graduate School of Engineering

of the Air Force Institute of Technology

Air University

In Partial Fulfillment of the

Requirements for the Degree of

Master of Science in Astronautical Engineering

Joseph L. Lenertz, B.S.

Captain, USAF

December 1994

Preface

This report represents a part of the evolution of cooling research done in the AFIT Low Speed Shock Tube by a long line of previous researchers. It moves forward from past research in two important ways: By examining heat transfer in a nozzle in favor of continued flat plate studies, it introduces the added complexity of accelerating flow and pressure gradients. The second change, from film cooling to transpiration cooling, provides another dimension of variable cooling over the surface. These changes raise a number of new questions suitable for further research.

My greatest thanks in this effort go to Lt. Col. Jerry Bowman, who always made himself available, and answered many questions with superior knowledge and good humor. My gratitude also goes to Dr. Rodney Bowersox and Mr. Andrew Pitts for help with analytical and technical issues, and to Mr. Tim Hancock of the AFIT Machine Shop for his dedicated and precise construction of the nozzle and test section. My thanks also to Lt. David Keener, who worked the boundary layer growth problem using the same equipment, and without whom I might never have finished. Finally, special thanks and all my love to my wife [redacted] and children [redacted] for their patience and understanding.

Joseph Lenertz

Table of Contents

List of Figures

List of Tables

List of Symbols

Symbol	Description	Units
A	Area	m^2
A_i	Injection surface area	m^2
A_p	Nozzle cross sectional area	m^2
B	Blowing ratio $(\rho_i u_i / \rho_p u_p)$	
c	Specific heat of a solid	J/kg K
c_p	Specific heat at constant pressure	J/kg K
c_v	Specific heat at constant volume	J/kg K
D	Diameter of flat plate leading edge	m
DR	Density ratio (ρ_i / ρ_p)	
erfc	Complementary error function	
h	Convective heat transfer coefficient	W/m^2K
I	Electrical current	amperes
k	Thermal conductivity	W/m K
$\dot{m}$	Mass flow rate	kg/s
M	Mach number	
p	Pressure	Pa
Pr	Prandtl number $(c_p \mu / k)$	
q"	Heat flux	W/m^2
r	Recovery factor	
r_c	Throat radius of curvature in downstream direction	m
R	Electrical resistance	ohm
Re_x	Reynolds number $(\rho u x / \mu)$	
St	Stanton number $(h/\rho u c_p)$	
t	Time	s

T	Temperature	K
u	Velocity	m/s
V	Electrical potential	volts
x	Distance into substrate	m
α	Thermal Diffusivity	m^2/s
δ	Velocity boundary layer thickness	m
Δ	Thermal boundary layer thickness	m
γ	Ratio of specific heats (c_p / c_v)	
η	Nondimensional variable $(x/(4\alpha t)^{.5})$	
λ	Nondimensional variable $(ht^{.5}/(\rho ck)^{.5})$	
μ	Dynamic fluid viscosity	Ns/m^2
π	Geometric constant ($\cong$3.1416)	
θ	Angle from stagnation point on cylinder	deg
Θ	Nondimensional temperature $((T-T_i)/(T_o-T_i))$	
ρ	Density	kg/m^3
σ	Stefan Boltzmann constant	W/m^2K^4
$(\rho ck)^{.5}$	Thermal product	$J/m^2Ks^{.5}$

Subscripts

aw	Adiabatic wall
g	Primary gas
gly	Glycerin USP, 95%
i	Injection flow
inc	Incremental area
o	Stagnation condition
out	Ouput

p	Primary nozzle flow
w	Inner wall surface condition
x	Local, or based on distance

Abstract

This experiment analyzed the effects of blowing ratio on heat transfer to the throat region of a porous-walled nozzle, using the AFIT low speed shock tube. Heat flux data were taken from both sides of a two-dimensional Mach 2.0 ($Re/m=5.2x10^{7}$) nozzle using thin film resistance thermometers. One side was transpiration-cooled by secondary air injection through a sintered wall, while the other served as a control. Control results were validated using empirical relations, and cooled side results showed up to a 14% reduction in heat transfer coefficient at blowing ratios of 0.51%. The linear nature of cooling effectiveness at these low blowing ratios allowed a modification of nozzle heat transfer equations to include a blowing ratio parameter. Disturbance of primary flow was also minimal, causing no measurable reduction of nozzle performance.

EFFECTS OF BLOWING RATIO ON HEAT TRANSFER TO THE THROAT REGION OF A POROUS-WALLED NOZZLE

I. Introduction

1.1 Background

Aeronautical and astronautical engineers have for many years faced the challenge of increasing the performance of turbine and liquid rocket engines. One aspect of this challenge is the extreme heat flux imparted to the nozzle walls, especially near the throat. (Hill and Peterson, 1992:550) Film cooling techniques have achieved some success in raising allowable combustion temperatures and increasing nozzle lifetime, but they also have drawbacks (Sutton, 1976:281). Film cooling involves the injection of a relatively cool gas through one or several discrete holes in the nozzle wall to establish a protective film on the surface. It requires relatively large injection mass flow per unit area (10-300% of mainstream flow), which can cause thrust losses due to disturbance of the primary flow (Azevedo, 1993:44). A new cooling method that minimizes the disturbance of the primary flow while providing effective cooling in the throat area is desired. This is important not only to increased performance in turbine and liquid rocket engines, but also to provide a smooth primary flow for hypersonic wind tunnels.

Transpiration cooling involves the injection of a fluid (gaseous or liquid) through a porous material, over a relatively large surface area. This analysis proposes that transpiration cooling reduces heat transfer to the throat region of a supersonic nozzle, using lower injection flow rates than are typical for film cooling.

1.2 Problem

An acceptable heat flux can usually be fixed by maximum allowable throat temperature/nozzle lifetime criteria. Sufficient cooling for most applications is simply that which results in an acceptable heat flux. In order to minimize the disturbance to the primary flow, the minimum blowing ratio (see eq (1.1)) that affords sufficient cooling must be known. Therefore, this analysis provides an estimate of the heat transfer over a range of blowing ratios, defined by:

$$B(s) = \frac{\int_0^s \rho_i u_i ds \Big/ s}{\dot{m}_p \Big/ A_p(s)} \cong \frac{\sum_{j=1}^{n} \rho_{ij} u_{ij} \Delta s_j \Big/ s}{\dot{m}_p \Big/ A_p(s)} \tag{1.1}$$

where s is the distance along the nozzle wall, the symbols ρ and u represent density and velocity, and the subscripts i and p refer to injected flow and primary flow.

The heat exchange relations through the turbulent boundary layer near the wall of a supersonic nozzle are very complex, making analytical modeling very difficult. Some relations exist for the case of pure forced convection (no film cooling), but experimental research is necessary to correlate heat transfer with blowing ratio (Valencia, 1993:1.2). No generalized analytical relations exist for the prediction of heat flux in configurations with non uniform heat flux distribution, as is the case in supersonic nozzles (Beitel, 1993:49). This leaves the empirical approach as the best method to predict heat flux, in spite of its loss of accuracy as we depart from test conditions. Even numerical analysis techniques require "experimental data with well-known boundary conditions." (Wittig and Scherer, 1987:572)

1.3 Summary of Current Knowledge

Although transpiration cooling has defied solution by analytical methods until very recently, it is not a new idea. Experimental research in the area of transpiration cooling for aerospace applications has been conducted since 1946, and the first successful full scale demonstration of transpiration cooling occurred in 1967 with the firing of the Aerojet ARES, a 100,000 pound (445 kN) thrust chamber (May and Burkhardt, 1991:1). Transpiration cooling proved effective for the injector faces in the J-2 and space shuttle main rocket engines. It was selected because it was more effective than film cooling in this area, and usually required less propellant (Sutton, 1976:281).

Transpiration cooling has not been used in cooling the combustion chamber or nozzle regions of large liquid rocket engines. Due to the steep pressure gradients along the inner wall of the nozzle, especially near the throat, proper cooling requires variable porosity and/or thickness material. The manufacture of these large, complex shapes of porous materials is difficult and costly, and has been the greatest challenge of transpiration cooling. The structural strength of porous materials is typically lower than that of solid materials at a given temperature, but this drawback can be partially offset by lower porous wall temperatures. It is possible that advances in this area will create new interest in porous-walled cooling, but for the present, platelets are used for most transpiration cooling applications. Platelets are thin sheets of metal individually photo etched and either diffusion bonded or mechanically held together to form a wall with flow passages of any desired pattern (May and Burkhardt, 1991:1).

Because the aerothermal relationships remain the same whether using platelets or porous material, influencing factors and general results will be equally valid for either method, with the effect of surface roughness a possible exception. In addition, some of the factors found to influence the effectiveness of film cooling can be used as a starting point for transpiration cooling research.

May and Burkhardt (1991:1-53) studied the use of liquid RP-1 to transpiration cool the throat of a subscale rocket nozzle, and found some surprising benefits of transpiration cooling versus regenerative cooling. Analysis of the thermocouple temperature curves indicated a 97% reduction in heat flux at a mass flow ratio of 8.8%. Because cooling was so effective at that mass flow ratio, (causing a measured wall temperature of 366.5 K vs. predicted of 755.4 K) they recommended a reduction to a flow ratio of 2.9% for the full scale model. They also found that an increase in specific impulse, an increase in engine system life, or a combination of both can be achieved by using transpiration cooling versus regenerative cooling. The reasons for this are associated with the high pressure drop that results from regeneratively cooling the throat. The additional pumping required to force the coolant through the coolant lines reduces the turbopump's ability to pressurize the combustion chamber. Transpiration cooling, with little or no additional pressure drop, allows an increase in chamber pressure, which translates to a greater expansion ratio and higher specific impulse. An increase in specific impulse of 8.2-14.8 seconds was found to be possible due to higher chamber pressure alone. Another smaller performance benefit was found to be due to decreased kinetic and boundary layer losses (May and Burkhardt, 1991:D-2). To trade off some or all of this performance gain to achieve increased turbopump lifetime, the chamber pressure can be reduced towards regenerative cooling levels, and the savings in pressure drop will allow lower turbopump discharge pressures. In May's RP-1 engine, a complete shift to the engine life scheme using transpiration cooling would increase turbopump lifetime by a factor of nine.

One of the factors that made May's results so remarkable was the effectiveness of cooling due to the phase change of the injected fluid. This analysis used gaseous dry air as the injected fluid and met with substantially reduced cooling effectiveness.

Many other factors influence the effectiveness of cooling, but no empirical or analytical relations exist to quantify these effects for transpiration cooling near the throat. Many

empirical relations exist for film cooling, however, and may give insight into general relations in transpiration cooling. In film cooling, a blowing ratio of 0.55 was found to have maximum cooling effectiveness for density ratios near 1.0 (Goldstein et al., 1971:321-379). Cooling effectiveness could be increased by using higher density ratios, up to 4.17 with blowing ratios up to 1.68 (Pederson et al., 1977:620-627). Higher primary flow turbulence levels were found to increase heat flux, decrease cooling effectiveness, and increase the optimum blowing ratio (Rivir, 1987). Clearly these factors will also influence the effectiveness of transpiration cooling, but no quantifiable relations are available.

At about the same time, Poll (1991:27-31) developed an analytical method with good potential to predict heat flux with transpiration. He derived and solved the integral equations for mass, momentum, and energy within a boundary layer and with arbitrary transpiration. He used a reference temperature concept to correct for problems encountered with an earlier Pressure Gradient Closure technique. This allowed a more accurate relation between temperature and fluid viscosity at low wall-to-total enthalpy ratios. This technique solves the compressible boundary layer problem but cannot be easily used to predict heat flux to a transpiration cooled wall.

1.4 Scope and Objectives

This research addressed the determination of transpiration cooling effectiveness in the throat region of a supersonic nozzle, using the AFIT low speed shock tube. Because it involves a new method of cooling and complex geometries with pressure gradients, it was necessarily limited in scope. Stagnation conditions of primary flow were held as constant as possible (always within 2%) throughout the study. The composition and density of injected fluid, geometry and porosity of nozzle wall, and location of test instrumentation were all held fixed. Cooling results were obtained at two locations in the nozzle, where

the flow mach number was M=1.17 and M=1.54 respectively. A range of blowing ratios from B=-0.0035 to B=0.0051 were tested.

The main objectives of this research were:

1. To determine uncooled heat transfer rates and coefficients in the throat region of a supersonic nozzle.

2. To determine the effects of blowing ratio on heat transfer coefficient using transpiration cooling.

3. To create an empirical relationship between blowing ratio and heat transfer coefficient, and incorporate it into existing heat transfer relations.

4. To compare qualitatively transpiration cooling with film cooling, regarding heat transfer and primary flow disturbance.

1.5 Method

The AFIT low speed shock tube can create high pressure, high temperature conditions similar to those found in a turbine engine or wind tunnel nozzle. One advantage of shock tubes over other methods is its low operational cost, with a drawback of relatively short (a few milliseconds) testing times.

These short test times require highly responsive heat flux gauges and piezoresistive pressure transducers to measure the required data. The calibration of the pressure transducers was a straightforward and extremely reliable procedure. The calibration of the thin film heat flux gauges, however, is a nontrivial problem (see Chapter Three for a complete discussion of their calibration). These calibrations were accomplished while connected to the appropriate signal conditioners, amplifiers, filters, and data reduction computers that were to be used during the actual data taking. In this way, the entire data collection system was calibrated at once.

A Mach 2.0, two-dimensional nozzle was designed with the aid of several computer programs that used boundary layer corrections on the method of characteristics shape design. It was subject to a number of constraints to allow for good stagnation conditions following shock reflection and nearly perfect expansion to ambient room pressures. Both sides of the nozzle were designed to allow the installation of heat flux gauges and pressure transducers. The blowing side (bottom) included a pressurized plenum for secondary fluid injection through a porous wall, while the nonblowing side served as a control.

The porous material was selected to allow blowing ratios up to 0.1 based on isentropic flow predictions, expected allowable plenum pressures, and manufacturer's data. Manufacturer's data was later verified, but blowing ratios were limited to 0.0113 at the nozzle exit due to volumetric flow rate limits of the source.

After all test equipment was calibrated and installed in the test section of the shock tube, the shock tube was run several times (allowing at least five usable runs) at each blowing condition. Data was collected and stored by the Nicolet 500 Data Acquisition System, with 3000 points collected over each 3 millisecond run time. Run time of the nozzle was determined by pressure data and shadowgraph photos.

This data was processed by several computer programs. One used a numerical technique to find the heat transfer rate to the wall of the nozzle. Once the physical characteristics of a particular heat flux gauge are known (via calibration), a time history of the voltage output during a run will yield the heat transfer rate as a function of time (Cook and Felderman, 1965:561). This heat transfer rate is then averaged over the run time, and divided by a temperature difference to find the convective heat transfer coefficient:

$$q'' = h(T_{aw} - T_w) \tag{1.2}$$

where q" is the heat transfer rate per unit area, h is the convective heat transfer coefficient, T_{aw} is the adiabatic wall temperature and T_w is the current actual temperature of the inner wall surface.

Another program was written to numerically integrate the mass injection along the wall to get a cumulative blowing mass flow rate upstream of each heat flux gauge. This mass flow rate is divided by the injection area up to that point and primary flow ρu at that point. This defines a local blowing ratio.

Plotting heat flux versus blowing ratio, a linear relationship provided a satisfactory best fit curve over the range of blowing ratios considered. This allowed incorporation of the blowing ratio into the analytical heat flux relations.

II. Theory

2.1 Heat Transfer

In order to have some idea of the amount of cooling required in a nozzle, some basic knowledge of the mechanisms of heat transfer is required. There are three widely accepted modes of heat transfer: conduction, convection, and radiation. Each of these modes, as they apply to heat transfer through the boundary layer in a nozzle, will be discussed in turn.

Conduction exchanges energy by direct molecular interaction, and obeys Fourier's Law (White, 1984:12):

$$q_x^{"} = -k\frac{dT}{dx} \tag{2.1}$$

where $q_x^{"}$ is the heat transfer per unit area in the x direction, k is the material's thermal conductivity, and the ratio represents the slope of the temperature gradient. Assuming no internally generated heat and a large solid slab with a single plane surface exposed to the heat, and applying the first law of thermodynamics, the one-dimensional heat conduction equation becomes:

$$\frac{\partial}{\partial x}\left(k\frac{\partial T}{\partial x}\right) = \rho c_v\left(\frac{\partial T}{\partial t}\right) \tag{2.2}$$

where ρ is the material density and c_v is the specific heat (for a simple derivation, see White, 1984:97-98). Assuming thermal conductivity is not a function of location, and defining an important ratio called thermal diffusivity as:

$$\alpha = \frac{k}{\rho c_v} \qquad \text{we have} \qquad \frac{\partial T}{\partial t} = \alpha \frac{\partial^2 T}{\partial x^2} \tag{2.3}$$

the one dimensional unsteady conduction equation. Now, assume an initially isothermal slab is suddenly subjected to a heat flux due to surface convection by a gas with constant temperature T_0 and constant heat transfer coefficient h_0. Solving eq (2.3), the result is (White, 1984:171):

$$\Theta = \frac{T - T_i}{T_o - T_i} = erfc(\eta) - \exp(\lambda^2 + 2\eta\lambda) erfc(\eta + \lambda) \tag{2.4}$$

where T_i is the initial wall temperature, T_o is the gas temperature, erfc is a function called the complementary error function (see Figure 2.1), η and λ are dimensionless variables that allow a solution to eq (2.3).

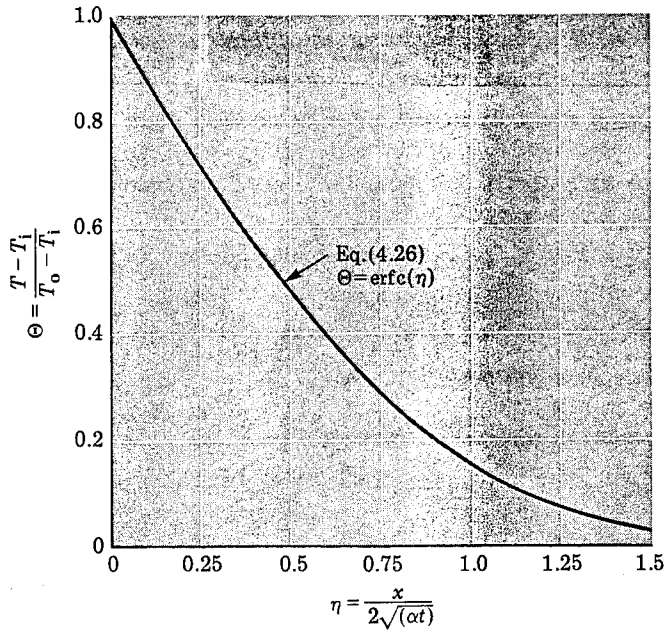

Fig. 2.1 Complementary Error Function (White, 1984:169)

The parameter λ is defined by:

$$\lambda = \frac{h}{(\rho c_v k)^{.5}} t^{.5} \tag{2.5}$$

where t is time. At the surface (x=0) η equals zero, so eq (2.4) simplifies to:

$$\Theta = 1 - \exp(\lambda^2) erfc(\lambda) \tag{2.6}$$

This is the exact solution for the time history of the temperature on the surface of the material (for an excellent derivation of this result, see White, 1984:166-172). This result was used in a computer program called TESTER (see Appendix C) to verify the method used to convert heat flux gauge voltages to convection heat transfer (film) coefficients.

Convection is the mode of heat transfer associated with macroscopic fluid motion. It is the heat transfer that takes place between a fluid and a solid surface as a consequence of the movement of the fluid relative to the solid surface (Ozisik, 1985:5). The convection heat transfer relation (eq (1.2)) is explained in Hill and Peterson, pages 545-546. Some useful equations used in high speed convection problems are:

$$r = \mathrm{Pr}^{1/3} = \frac{T_{aw} - T_g}{T_o - T_g} \tag{2.7}$$

where r is the recovery factor, Pr is the Prandtl number defined as $c_p \mu / k$, and T_g and T_o are the static and stagnation temperatures of the primary fluid. The parameters μ and c_p are the fluid viscosity and specific heat. Adiabatic wall temperature can be solved for with:

$$T_{aw} = T_g\left(1 + r\frac{\gamma - 1}{2}M^2\right) \tag{2.8}$$

where γ is the ratio of specific heats and M is the primary flow Mach number. This adiabatic wall temperature is used to find heat transfer coefficient from measured heat flux via eq(1.2).

Because the heat flux gauges were recalibrated near the leading edge of a flat plate, the solutions of the convection heat transfer coefficient for a flat plate and cylinder are given in addition to the nozzle solution. The heat transfer through the turbulent boundary layer of a flat plate with no film cooling and no primary flow turbulence is (Kays and Crawford, 1980:213):

$$St\,\mathrm{Pr}^{.4} = 0.0287\,\mathrm{Re}_x^{-.2} \tag{2.9}$$

where St is the Stanton number, Re_x is the Reynolds number, and they are defined as:

$$St = \frac{h}{\rho_p u_p c_p} \qquad \text{and} \qquad \mathrm{Re}_x = \frac{\rho_p u_p x}{\mu}$$

where ρ_p and u_p are the density and velocity of the primary flow fluid, respectively. This solution has slightly differing values among texts, with:

$$St\,\mathrm{Pr}^{1/3} = 0.0296\,\mathrm{Re}_x^{-.2} \tag{2.10}$$

the result given from other sources (White, 1984:261 and Ozisik, 1985:397). The empirical solution for flow past a circular cylinder is given in graphical form in Figure 2.2 (Giedt, 1949:377-380).

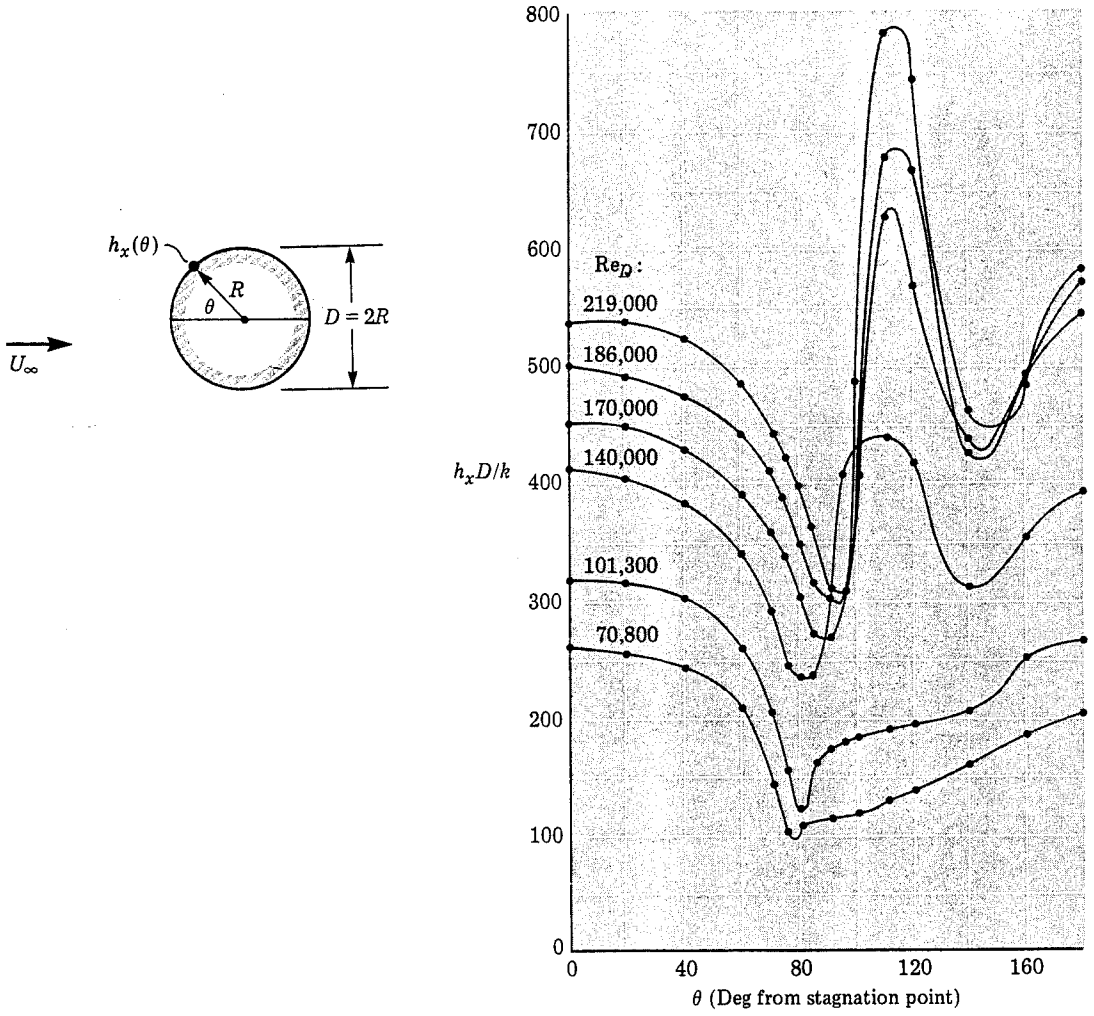

Fig. 2.2 Heat Transfer Distribution Over a Cylinder (Giedt, 1949:381)

Finally, after the heat flux gauges are calibrated, the heat flux data from the tests in the Mach 2.0 nozzle should be compared with some analytical model. This model will validate the calibrated values of thermal product of the gauges, and can serve as a baseline for a new heat transfer relation that includes a blowing ratio parameter. The relation yielding convective heat transfer coefficient in a supersonic nozzle is given by Bartz as:

$$h = \frac{.02443643(\rho^* u^*)^{.75}\mu_o^{.25}c_p}{(D^*)^{.1}(r_c)^{.1}\,\mathrm{Pr}^{.46}}\left(\frac{A^*}{A}\right)^{.75}\sigma\left(\frac{1}{\Delta}\right)^{1/7}\left(\frac{1}{\delta}\right)^{3/28} \tag{2.11}$$

where the asterisk superscript indicates conditions at the nozzle throat, the zero subscript indicates stagnation conditions, r_c is the throat radius of curvature along the direction of flow, and Δ, δ are the local thermal and velocity boundary layer thickness, respectively (Bartz, 1954:1238-1241). The parameter D is diameter, A is area, and σ is defined by:

$$\sigma = \left\{\left[.5\left(\frac{T_w}{T_o}\right)\left(1+\frac{\gamma-1}{2}M^2\right)+.5\right]^{.6}\left(1+\frac{\gamma-1}{2}M^2\right)^{.15}\right\}^{-1} \tag{2.12}$$

where for shock tubes, T_w is simply the ambient room temperature, since the wall temperature does not change appreciably during the test. The shape of this curve through the test nozzle is shown in Figure 2.3. The thermal and velocity boundary layer thickness were assumed equal for this turbulent flow, and the velocity boundary layer thickness was provided by Keener (1994:4-4).

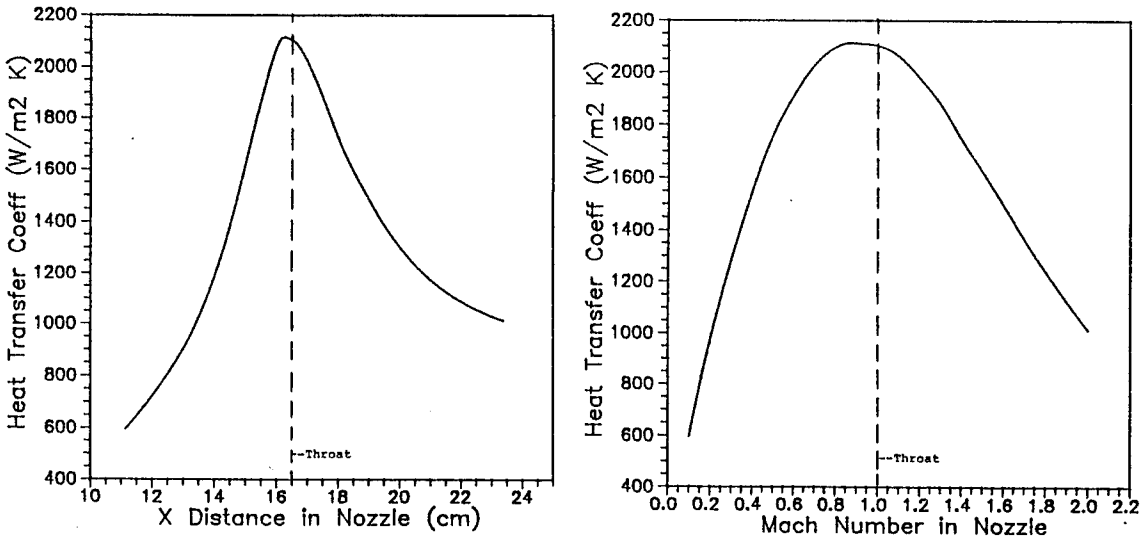

Fig. 2.3 Predicted Heat Transfer Coefficient along Wall of Mach 2 Nozzle

Hill and Peterson made additional assumptions about the boundary layer growth along the nozzle, allowing the removal of Δ and δ from Bartz's equation:

$$h = \left[\frac{.026(\rho^* u^*)^{.8} \mu_o^{.2} c_p}{(D^*)^{.1} (r_c)^{.1} \mathrm{Pr}^{.6}} \right] \left(\frac{A^*}{A} \right)^{.9} \sigma \tag{2.13}$$

where σ is defined as:

$$\sigma = \left\{ \left[.5 \left(\frac{T_w}{T_o} \right) \left(1 + \frac{\gamma - 1}{2} M^2 \right) + .5 \right]^{.68} \left(1 + \frac{\gamma - 1}{2} M^2 \right)^{.12} \right\}^{-1} \tag{2.14}$$

for a diatomic gas. These solutions are based on Prandtl numbers near unity, smooth primary flow, and certain nozzle geometries (see Bartz, 1954:1235-1242).

Although conduction and convection are certainly important factors in this study, radiation is not. Even if we assume the gas is a perfect emitter and the nozzle walls absorb as a black body (worst case assumptions), the radiation energy absorbed by the walls would be:

$$q'' = \sigma (T_g^4 - T_w^4) \tag{2.15}$$

where σ is the Stefan-Boltzmann constant, equal to 5.67 x 10^{-8} W/m^2K^4, T_g is the gas temperature, and T_w is the wall surface temperature. This translates to about 1.2% of measured convection heat flux under test conditions. In rocket nozzles, where temperatures can range from 2200 to 4100 K, radiation accounts for 5% to 35% of total heat transfer (Sutton, 1986:355).

2.2 Heat Flux Gauges

Because of the short test times (1-10 msec) associated with shock tube testing, high speed instrumentation is required. Heat flux gauges (more accurately referred to as thin film resistance thermometers) can be used to measure variations in surface temperature, through changes in the resistance of the film. By using the basic heat transfer relations set out in eqs (2.1) and (2.3), the surface temperature history can be used to determine heat transfer to the surface of the gauge.

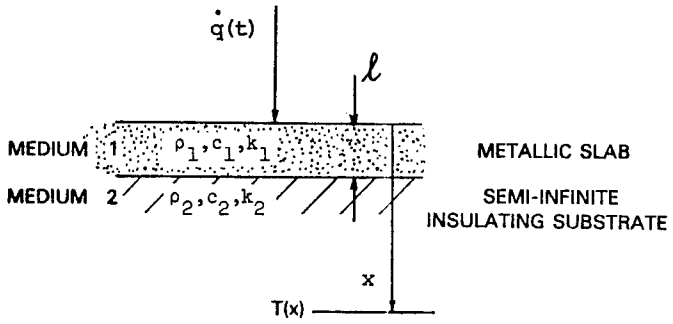

Fig. 2.4 Side View of Tip of Heat Flux Gauge (Schultz and Jones, 1973:89)

If the substrate of the gauge (see Figure 2.4) is assumed to be a semi-infinite slab and the film of platinum assumed to be so thin that it does not affect the temperature history of the surface of the substrate, the relation between the temperature history of the gauge and the heat flux imparted to the surface can be obtained (Schultz and Jones, 1973:4-7):

$$q''(t)=\left(\frac{\rho ck}{\pi}\right)^{.5}\left[\frac{T(t)}{t^{.5}}+.5\int_{o}^{t}\frac{T(t)-T(\tau)}{(t-\tau)^{1.5}}d\tau\right] \tag{2.16}$$

where the parameter $(\rho ck)^{.5}$ is called the thermal product. For a complete derivation of the above, see Appendix A. This form has a singularity at $t=\tau$ which will cause errors in the value of q'', so this relation is modified to allow an accurate numerical integration (Cook

and Felderman, 1965:561). The resulting summation can be further simplified by noticing that when t=0, the output of the gauge is zero:

$$q''(t_J) = 2\left(\frac{\rho ck}{\pi}\right)^{.5} \sum_{j=1}^{J} \frac{T(t_j) - T(t_{j-1})}{(t_J - t_j)^{.5} + (t_J - t_{j-1})^{.5}} \tag{2.17}$$

The above equation resulted after removing the T(0) portion of an earlier derivation (Bonafede, 1988:41). A good derivation of eq (2.17) is in Schultz and Jones (1973:35-37). If the heat flux were known to be constant, it can be shown that the surface temperature is (Schultz and Jones, 1973:7):

$$T(t) = \left[\frac{2q''}{(\pi\rho ck)^{.5}}\right] t^{.5} \tag{2.18}$$

A parabolic form vs. time. If we plotted the temperature against the square root of time, we would have a constant slope defined by the thermal product and the heat flux. This fact is used later in the calibration of the gauges to find their thermal products. Because we now expect a parabolic temperature output with a constant heat flux input, a constant, known heat flux would allow solution for the thermal product.

A computer program called TESTER was written to validate eq (2.17). If the exact solution of the temperature history of the gauge were known under conditions of sudden surface convection by a gas with constant temperature T_o and constant heat transfer coefficient h_o, then that temperature history could be plugged into eq (2.17) and we should be able to recover h_o with:

$$h_o = q''(t_J) / \left(T_{aw} - T(t_J)\right) \tag{2.19}$$

where T_{aw} is defined by eq (2.8). It just happens that the exact solution of the temperature history *is* known under the conditions described above. It is eq (2.6)! So, assuming some constant values for the thermal product and heat transfer coefficient, eq (2.5) defines λ and eq (2.6) provides the temperature history to place into eq (2.17). TESTER applied this method with good results: convergence to within 1% of h_o after only six time increments (see Appendix C). Now the heat flux history of the surface of a gauge can be found, if only the thermal product and temperature history of the gauge are known.

One method to obtain the thermal product is an electrical heating calibration. This technique consists of passing a constant current through the gauge for a short time so that ohmic heating produces a change in resistance of the thin film. A circuit able to provide this constant current is shown in Figure 2.5, in which R_o is the gauge to be calibrated, R_2 and R_3 are matched resistors, and R_1 is a potentiometer with a resistance range including the resistance of the gauge. The signal generator supplies the bridge with a constant voltage for 500 μs. Because the bridge is initially balanced, half of the R_s current will flow through the gauge. Over the heating time, the gauge resistance changes by less than 0.15%. As the resistance increases, the amount of current through the gauge decreases, so heat flux change over the heating time is negligible. If the amount of heat lost to the air is assumed small, then the heat transferred to the substrate is:

$$q'' = I_o^2 R_o / A \tag{2.20}$$

where I_o is the current through the gauge, R_o is the initial gauge resistance, and A is the thin film surface area.

A second calibration, where the heat flux gauge is immersed in glycerin, results in a lower heating rate of the substrate due to a portion of the heat being absorbed by the

glycerin. Schultz and Jones (1973:23-25) derived a relation yielding the thermal product of the substrate using this double calibration technique (see eq (2.21)).

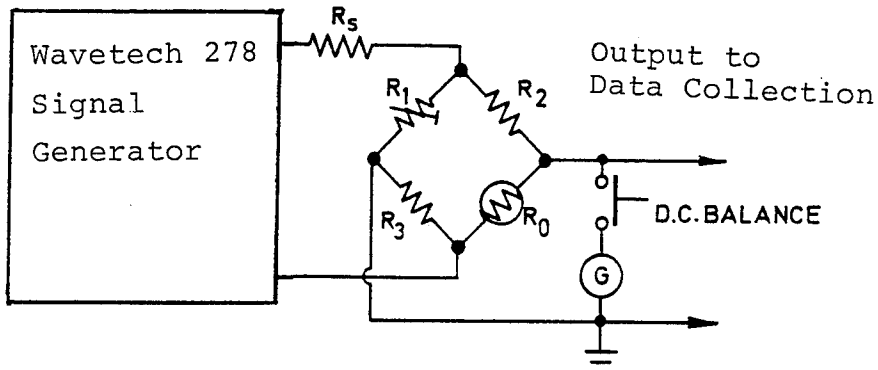

Fig. 2.5 Heating Calibration Circuit (Schultz and Jones, 1973:102)

$$(\rho ck)^{.5}_{sub} = \frac{(\rho ck)^{.5}_{gly}}{\frac{\Delta V_1/t^{.5}}{\Delta V_2/t^{.5}} - 1} \tag{2.21}$$

where the thermal product of glycerin is 925 $J/m^2K\ s^{.5}$ (±4%), ΔV_i is the voltage change of the bridge output in air, and ΔV_2 is the voltage change of the bridge output in glycerin. This method relies on a constant input heat flux producing a constant slope line when temperature (directly related to the bridge output voltage) is plotted against the square root of time. The errors introduced by this method come from the inexact thermal product of glycerin, the small variation of heat flux over time, and especially from the non-uniformity of the thin platinum film and the silicon monoxide coating . This last source of error alone can be 15% of the deduced value of the thermal product. Other calibration methods with higher claimed accuracy exist, and are mentioned again in chapter five (Seginer and others, 1964:25-30).

2.3 Fluid Flow Relations

The science of fluid dynamics is based on foundations of both theory and experiment. Theory, using four basic physical laws and assuming certain simplifying conditions exist, allows the prediction of fluid characteristics in a given situation. This project used many theoretical relations to predict the conditions in the shock tube and through the nozzle. The majority of these relations assume the compressible flow of a thermally and calorically perfect gas.

This report assumes the reader is familiar with these relations and offers other sources for a more complete review. In the preliminary analysis of flow through the nozzle, this research assumed isentropic flow. The governing equations of the isentropic flow of a perfect gas are (Shapiro, 1953:83):

$$\frac{p}{p_o}=\left(\frac{\rho}{\rho_o}\right)^{\gamma}; \qquad \frac{T}{T_o}=\left(\frac{p}{p_o}\right)^{\frac{\gamma-1}{\gamma}}; \qquad p=\rho RT; \quad \text{and} \quad \frac{T_o}{T}=1+\frac{\gamma-1}{2}M^2 \tag{2.22}$$

For choked flow in a converging-diverging nozzle, the additional relation:

$$\frac{A}{A^*}=\frac{1}{M}\left[\left(\frac{2}{\gamma+1}\right)\left(1+\frac{\gamma-1}{2}M^2\right)\right]^{\frac{\gamma+1}{2(\gamma-1)}} \tag{2.23}$$

is all that is required to define the conditions at any point in the nozzle. These relations are used to predict flow conditions throughout the nozzle, and were used in the initial design to size the nozzle, determine the final Mach number, and predict primary flow pressures during the selection of a porous material.

In a shock tube, it is the reflection of a shock wave from the converging portion of the nozzle that creates conditions which cause the nozzle to "start". During the short time

period when the nozzle is started, (or has a steady supersonic flow downstream of the throat), the above isentropic equations apply, albeit with less than perfect accuracy. All that is required to define fluid characteristics at any point in the nozzle is knowledge of the stagnation conditions, the ratio of specific heats, and the nozzle geometry.

To predict the stagnation conditions following the reflection of the shock wave, some understanding of shock wave relations and flow in ducts is required. The shock wave and fluid flow relations used in this study are widely known, so this paper makes no attempt to rederive or explain them. Shapiro provides an excellent discussion of "flow in constant area ducts with friction" (page 166), "analysis of moving shocks" (page 1000), shock tube analysis (page 1007), and many other related topics. Another good source for shock tube theory and performance is "Shock Tubes" by Glass. These relations were incorporated into a computer program called SHOCKTUN (Bowersox, 1990). It calculated the conditions in each region of the shock tube for given test conditions, including the conditions following the reflection of the shock from a flat wall.

The converging portion of the nozzle does not reflect a shock wave in the same manner as a flat wall, however. The curved wall of the converging portion of the nozzle causes numerous oblique shock waves with larger total pressure losses than a single normal shock. In addition, the throat allows a portion of the shock to pass through unreflected. For these reasons, the SHOCKTUN program was used as a first estimate of conditions following shock reflection. It was vital to know, however, whether the pressure following reflection would be high enough to "start" the nozzle, creating supersonic flow. Some experimental method was required. Zuppan (1965:Abstract) found that an area ratio of shock tube cross section over throat area was a good parameter in determining the efficiency of shock reflection. By applying Zuppan's results to this research's expected test conditions, it was found that sufficient pressure would exist following shock reflection to start the nozzle. He found that contraction ratios of 10.65 to 13.3 provided maximum

flow duration and stability. For this work, a contraction ratio of 10.65 was selected to maximize the available area in the nozzle for instrumentation. This fixed the nozzle throat height.

Based on the range of possible driver pressures and the desire to have a perfectly expanded nozzle without a vacuum in the driven section, a Mach 2.0 nozzle was selected. The shape of the nozzle was determined using the computer codes NOZZ and BLCORR (Bowersox, 1990). The codes used the method of characteristics (see Shapiro, page 462) with a correction for boundary layer growth. The computer programs were designed to allow some flexibility in the number of reflections in the supersonic region and the shape of the subsonic region. This made it possible to increase the length of the nozzle to make room for instrumentation.

Once the nozzle geometry had been determined, the analysis of porous materials to be used for mass injection could begin. Selecting a porous material for the transpiration cooled side of the nozzle involved a structural analysis and a mass flow rate analysis. Mott Metallurgical Corporation provided strength, porosity, and geometric specifications for a wide variety of porous products. Using 316L stainless steel (the cheapest choice), even the highest porosity (weakest) grade material offered 354 kN of strength from 66 cm^2 of bonded material. The design plenum pressure was set at 552 kPa (80 psi) because this allowed some adjustment upward to the maximum plenum pressure of 690 kPa (100 psi) defined by pressure transducer limits. Since the blowing area was set at 58 cm^2, the maximum pressure force on the porous material would be 4 kN. The tensile strength offered by the material was clearly enough for these conditions.

Since any grade of porous material would be strong enough to withstand the expected pressure forces, the grade providing the desired mass flow rate was selected. Mott Metallurgical manufactured their material in 1.57 mm (0.0625 in) thick sheets. This meant that four layers of material would be necessary in order to properly mount pressure

transducers and heat flux gauges. Mass flow through porous material is related to the pressure drop across the material, so it was assumed that each layer would experience one fourth of the total pressure drop.

In order to fully determine the grade of porous material, not only the pressure drop, but also the injection velocity, must be specified (see Figure 2.6). Because the effective blowing ratios for transpiration cooling are much less than 0.1 (Azavedo, 1993:44), the desired blowing ratios at the throat were arbitrarily selected at 0.01 and 0.05.

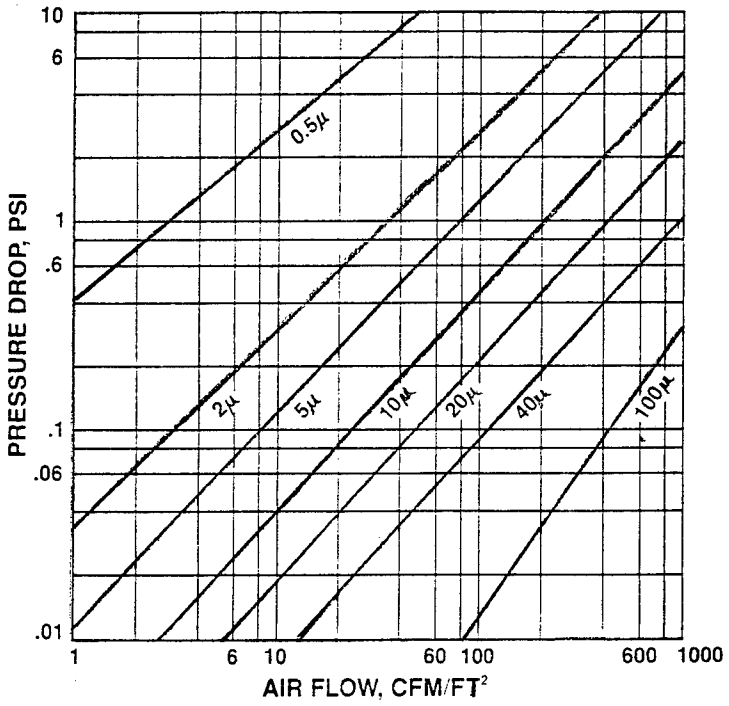

Fig. 2.6 Porous Material Flow Curves (Mott Metallurgical, 1986)

Now that the blowing ratio was selected, it could be used to find an injection velocity. Predicted stagnation conditions at the nozzle entrance of 538 kPa (78 psi) and 491 K and

isentropic relations allowed the calculation of ρu of the nozzle flow at the throat. The injection parameter $\rho_i u_i$ was then found by eq (1.1).

Bottled air was the source of injection fluid. Knowing the pressure and temperature in the bottle and assuming adiabatic flow to the plenum, the plenum air density, ρ_p, could be estimated using a Mollier diagram for nitrogen. Then, assuming incompressible flow through the porous material, $\rho_i = \rho_p$, so injection velocity could be calculated.

From Figure 2.6, it was possible to create equations of the form:

$$\Delta p = A u_i^B \tag{2.24}$$

for each of the porosity grades. Here Δp is pressure drop, A and B are constants determined from the chart, and u_i is the injection velocity. Inserting the design pressure drop and injection velocity into eq (2.24), it was found that the 2 micron grade was closest for B=0.01, and the 10 micron grade was best for B=0.05. The data supplied by Mott, and this analysis, was later validated to within 2% using a pressure transducer and flow meter.

III. Experimental Apparatus and Procedure

3.1 Calibration

In order to have confidence in experimental data, the instrumentation and data collection systems must first be calibrated with known standards. Three types of instruments were used to take measurements in the test section: An Omega T-type thermocouple, ten 100 psi (689 kPa) Endevco piezoresistive absolute pressure transducers, and (initially) eight Medtherm platinum thin film resistance thermometers.

Thermocouples rely upon known voltages produced from the contact of two different types of metal (in this case copper and constantan wires) at a given temperature, and require no calibration. The wires were attached to an Omega model 415B digital readout which supplied temperature to the nearest tenth of a degree Fahrenheit.

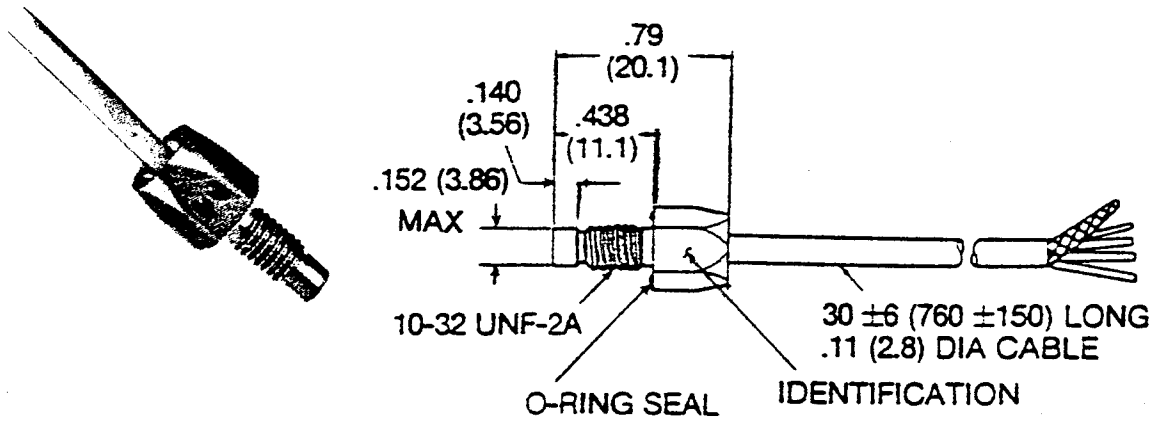

Fig. 3.1 Model 8530A Pressure Transducer (Endevco Corp., 1985)

The pressure transducers (see Figure 3.1) were calibrated using a dead weight calibration technique using an Ametek model HK-500 pneumatic pressure tester. Each

transducer was calibrated with its associated cable and Endevco model 4423 signal conditioner attached and set to the same gain as in test conditions. These transducers had less than 0.5% standard deviation from a linear best fit over their stated range of 100 psi (689 kPa). Appendix B contains the calibration plots and linear least squares fits for the pressure vs. voltage data.

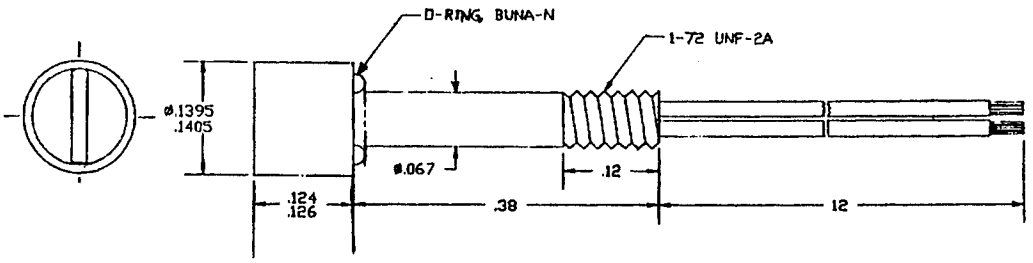

Fig. 3.2 Model PTF 100-20404 Heat Flux Gauge (Medtherm Corp., 1994)

The thin film heat flux gauges (see Figure 3.2) were a great deal more challenging to calibrate. The initial calibration involved finding the steady-state conversion factor from voltage output to temperature (the slope of the voltage-temperature curve) for each gauge. This was accomplished by placing all heat flux gauges and two thermocouples in a controlled temperature circulating water bath. An aluminum holder (see Figure 3.3) containing the heat flux gauges was covered with a protective sheet of thin latex and lowered into a beaker of distilled water. One of the two thermocouples was immersed in the water while the other was placed in the holder with the heat flux gauges.

The heat flux gauge wires were attached to a shielded cable which fed into Transamerica PSC 8115 bridge supply modules. These modules, in conjunction with PSC 8015 amplifiers, provide the input power to the gauges by supplying a constant 2.5 Volts DC to a Wheatstone bridge. The heat flux gauge acts as one leg of the initially balanced bridge, so as the temperature (and hence the resistance) of the gauge changes, the bridge

becomes unbalanced and creates an output voltage. This output voltage is then amplified (and filtered if desired) by the PSC 8015 amplifier before being fed into the Nicolet 500 Data Acquisition System (see Figure 3.4). This set-up was necessary even in the calibration. In this way, the entire chain of systems is calibrated at once, and small variations between bridges or amplifiers are accounted for in the calibration.

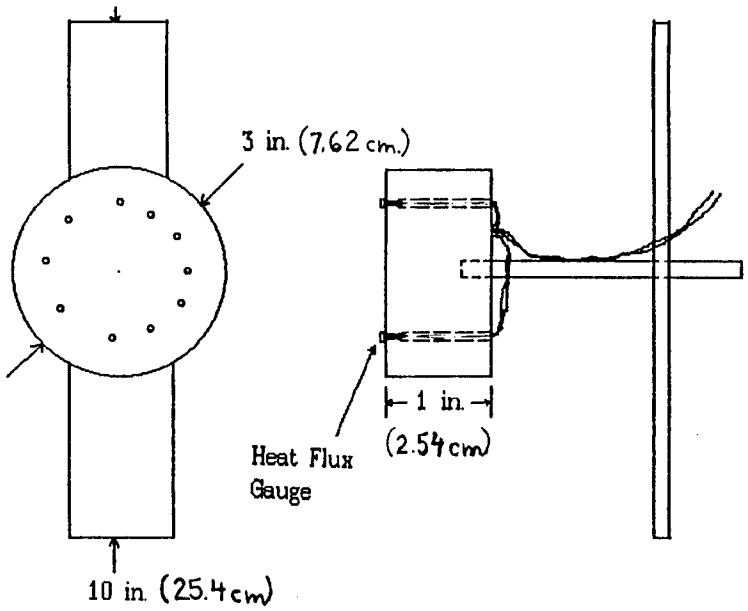

Fig. 3.3 Heat Flux Gauge and Thermocouple Holder (Eads, 1992:Fig. 15)

During the static calibration, a magnetic stirrer was used to maintain an even water temperature distribution, and a hot plate was used to increase water temperature to the next calibration point. Thermocouple temperature measurements were recorded against the voltage change from each heat flux gauge bridge. Nine temperature points were taken for each gauge, ranging from 296 K (72.8 °F) to 313 K (103 °F). Lines were fit to the points using a linear least squares technique, (see Appendix B) and their slopes were used as a voltage coefficient for temperature. The worst case results were a standard deviation of 1.2% from a linear best fit over a range of approximately 800 mV. The gauges had a

sensitivity range of 42 to 59 mV/K. The thermocouple located in the holder, under the same conditions as the heat flux gauges, had a lower sum of the squares of residuals in the linear fit than the thermocouple in the water, so the data from the thermocouple in the holder was used for calibration.

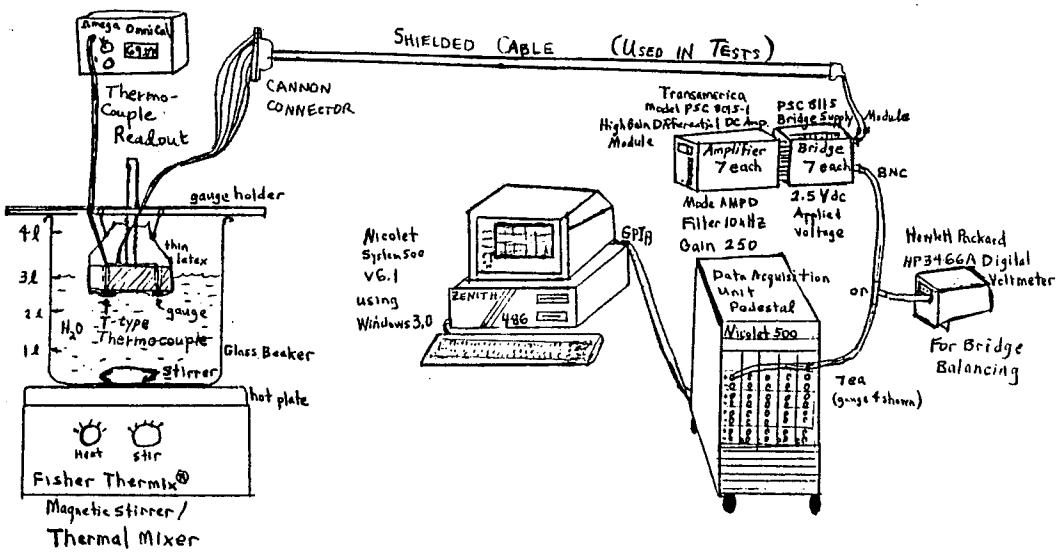

Fig. 3.4 Heat Flux Gauge Static Calibration Apparatus (Eads, 1992:A.3)

The electrical heating calibration described in chapter two was required in order to find a dynamic characteristic of the gauge, called the thermal product. The thermal product is required in order to use eq (2.17) to find heat flux into the gauge from a gauge temperature history. The goal here was to achieve constant heat flux into the gauge substrate via ohmic heating.

This was accomplished by supplying a Wheatstone bridge with a constant 5.0 Volts over a short period of time. This caused approximately 0.02 Amperes of current to pass through the heat flux gauge. Because the gauge resistance does not change by more than 0.15% during this time, the power through the gauge can be considered constant. A wave generator was used to supply the short burst of voltage, and the Nicolet 500 was used to

record the bridge output voltage. The equipment set-up and discharge calibration procedure was:

1. Create a separate Wheatstone bridge to avoid the additional circuitry in the bridge supply modules. Use two matched 120 Ohm resistors for two legs and a third 120 Ohm resistor in parallel with a 5,000 Ohm ten turn potentiometer for the third leg, and the gauge to be calibrated for the fourth leg.

2. Hang the gauge in air (or glycerin) with a thermocouple alongside to record the ambient temperature.

3. Supply the bridge with 2.5 Volts ungrounded (floating ground) dc power, and balance the bridge to zero output using the potentiometer. Read output voltage with a Hewlett Packard 3468A multimeter set to floating ground dc Volts.

4. Disconnect power supply and connect a Wavetech model 278 signal generator to the bridge input. Set for 200 Hz, 5 Volt amplitude, and a single square pulse.

5. Connect output voltage to a channel on the Nicolet 500, making certain the Nicolet input is set up and used in the ungrounded mode. Select one shot on Nicolet and trigger the wave generator.

This procedure was used to record six voltage histories of each gauge in air, and another six in glycerin. The data was plotted against time and appeared to be parabolic, as expected from eq (2.18). When plotted vs. square root time, however, it was clear that some of the curves were not linear (not parabolic with time-see Appendix B). The fact that a few gauges *were* reacting normally led to the belief that the bridge and wave generator were causing constant ohmic heating, as desired, and that it was the gauges themselves that were the problem. One gauge (Serial Number 42) was not only nonlinear vs. square root time, but it appeared to react somewhat differently to each voltage pulse,

even though all the pulses were equal. In spite of these difficulties, several methods were employed to find a thermal product using eq (2.19).

Since eq (2.19) requires the ratio of the slope of the air calibration curve (vs. square root time) to the slope of the glycerin calibration curve, one method simply fit a best fit line to the data regardless of the shape of the data curve. Another method used a quadratic fit, and then computed the slope at the time corresponding to 225 μsec. The resulting thermal products with associated standard deviation values (normal distribution) are shown in Table 3.1. Knowing that the Pyrex 7740 substrate has a thermal product of 1520 $J/m^2K\ sec^{.5} \pm 5\%$ (Schultz and Jones, 1973:99), the results of this calibration technique generally did not fall within an expected range of values.

Table 3.1 Thermal Product of Gauge Substrate Using Linear and Quadratic Fits

Gauge Serial Number	3	6	36	42	55	65
Linear Fit Thermal Product	1705	1408	2216	3441	1443	2265
Linear Standard Deviation	11.3	68.8	337.2	544.6	9.6	54.8
Quadratic Fit Thermal Prod.	1706	1433	2226	3432	1444	2267
Quadratic Standard Deviation	10.9	41.7	341.2	508.0	9.6	29.4

Possible explanations of this difference between theoretical and measured values of thermal product include nonuniformity of the platinum film or silicon monoxide coating, unseen transients in the signal generator or data collection device, contamination of the interior of the gauge with glycerin, and insufficient ohmic heating to get a clear parabola. The sensitivity of eq (2.19) to very small changes in slopes as the ratio approaches unity also increases the apparent error in thermal product.

3.2 The Shock Tube

The facility used for this experiment was the AFIT low speed shock tube located in room 146 of building 641. The shock tube is 8 in (20.32 cm) tall, 4 in (10.16 cm) wide, and has a 4 ft (1.22 m) long driver section, a 16 ft (4.88 m) driven section, and a 4 ft (1.22 m) test section. A .007 in (.18 mm) thick mylar diaphragm separates the high pressure driver section from the low pressure driven section.

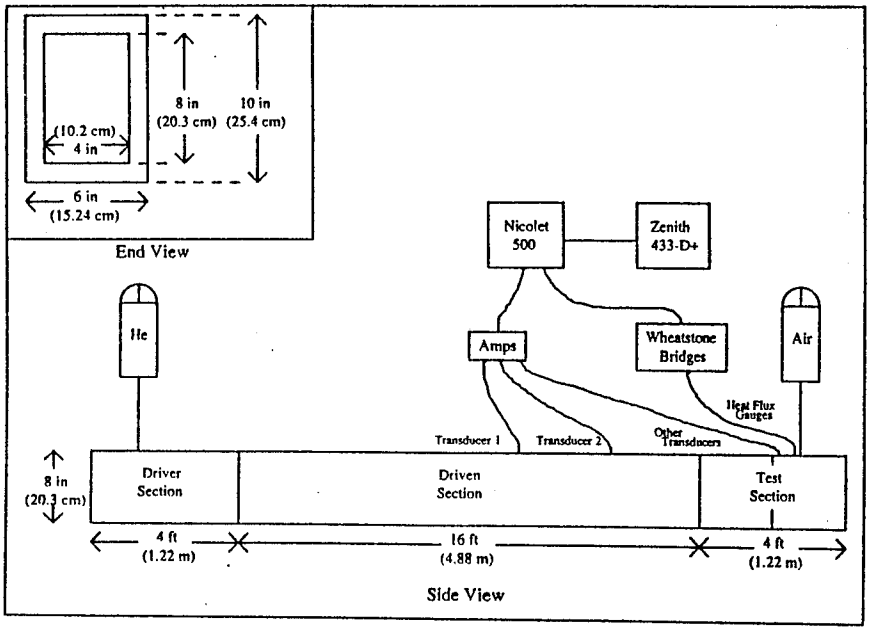

Fig. 3.5 Shock Tube Apparatus

An air and helium mixture was used in the driver to increase the speed of sound over a 100 percent air mixture, which increases the strength of the shock in the shock tube. The partial pressures of air and helium in the driver section were approximately 98.6 kPa (14.3 psi) and 482.6 kPa (70 psi) respectively, for all testing. This allowed the computation of the ratio of specific heats and gas constant of the mixture by using the Gibbs-Dalton Law (Hill and Peterson, 1992:38). At test conditions, the ratio of specific heats was 1.5992 and the gas constant was 1009.5 J/kg K. This mixture created stronger shocks than air alone, creating stagnation conditions just upstream of the nozzle entrance of 513 kPa

(74.4 psi) and 498 K. This was a high enough pressure to allow near-perfect expansion through the nozzle to ambient room pressures. The end of the shock tube was left open to the room to avoid undesirable shock reflections.

3.3 Flat Plate Recalibration

The unexpected results of the electrical discharge calibration method mandated another attempt at calibration of the heat flux gauges. The new method involved exposing the gauges to equal heat fluxes on a flat plate in the shock tube, and then forcing the temperature plots to yield the same value of heat transfer coefficient from eq (2.17) by using the thermal product as a variable.

A flat plate was modified to hold eight heat flux gauges aligned perpendicular to the flow. The plate, 1.85 cm thick with a rounded leading edge (radius of 0.925 cm), was positioned horizontally, and vertically centered within the tube. The heat flux gauges were positioned 5 mm back from the point of tangency between the round nose and flat portion (see Figure 3.6).

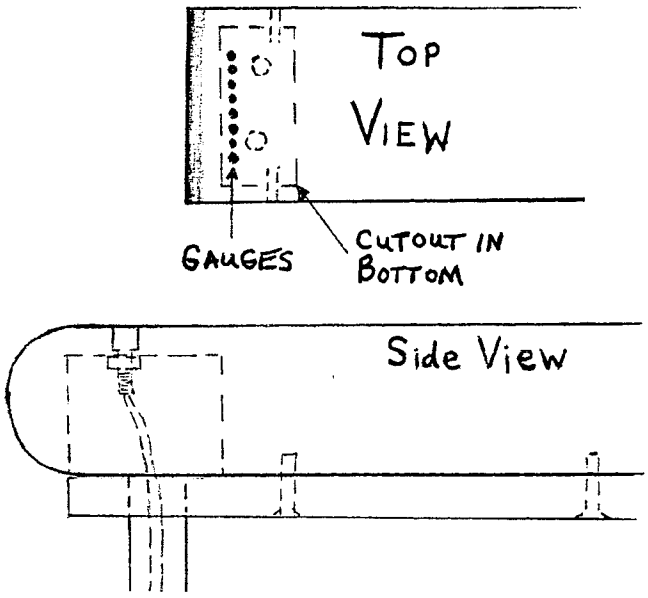

Fig. 3.6 Flat Plate with Heat Flux Gauges

Shocks were run using 369 kPa (53.5 psi) air only in the driver section, to save helium. Six sets of data for each gauge were recorded. The data were input into a program called FLTPLT (see Appendix C) which computed the heat flux and heat transfer coefficient at the gauge for one particular flow condition. The thermal product values from the initial discharge calibration (fourth row of Table 3.1) were used, with the following results:

Table 3.2 Flat Plate Heat Transfer Coefficients Using Original Thermal Products

Gauge Serial Number	3	42	55	65
Gauge Thermal Product	1706	3432	1444	2267
Voltage Coefficient (K/Volt)	17.016	17.411	19.057	18.624
Heat Flux (W/m^2)	83275.4	170884	74980.5	99720.8
Heat Transfer Coefficient (W/m^2 K)	1390.54	2834.53	1256.32	1625.29

Comparing these values to flat plate solutions for turbulent boundary layer heat transfer coefficients showed that these values were of the correct order of magnitude. Using a Reynolds number of 200,000 to 400,000 (depending on the definition of the front edge of the plate) and Prandtl number of 0.7, eqs (2.9) and (2.10) yield heat transfer coefficients from 1482 to 1715 W/m^2K. Now, considering the gauges to be so close to the round nose of the flat plate that they are heated as if at the θ=120° point of a cylinder, and extrapolating Figure 2.2, the predicted heat transfer coefficient is approximately 1840 W/m^2K, again of the same order of magnitude as measured values.

Now having some confidence in the gross magnitude of values produced by the gauge data, the gauge's thermal products were recalibrated to yield the same heat transfer coefficient using a weighted averaging technique. The results are shown in Table 3.3.

Table 3.3 Flat Plate Heat Transfer Coefficient Using Averaged Thermal Products

Gauge Serial Number	3	42	55	65
Gauge Thermal Product	1622.4	1627.5	1520.0	1786.4
Voltage Coefficient (K/Volt)	17.016	17.411	19.057	18.62
Heat Flux (W/m^2)	79195	78050	78927	78303
Heat Transfer Coefficient (W/m^2 K)	1297.3	1296.9	1297.0	1297.9

These recalibrated values of thermal product are closer to the accepted value of Pyrex 7740 and have much less variance between gauges. At the least, all of the gauges should provide a good measure of relative heat flux, since they will produce the same results for a given equal heat flux.

Although the flat plate calibration was successful in using an equal heat flux to recalibrate the gauge thermal products, the positioning of the gauges was not optimum. Rounded leading edges cause some turbulence and instability of the flow up to a distance downstream of 1.4 plate diameters (Mehendale and others, 1991:847). The gauges in this study were placed within one plate diameter of the beginning of the flat portion. Therefore, no empirical relations could accurately predict the heat transfer coefficient at that location, so no accurate check of experimental results was available.

3.4 Mach 2.0 Nozzle

The test article in this experiment was a two dimensional flow, converging diverging nozzle. This section will deal primarily with the physical features, dimensions, and instrumentation of the nozzle.

The nonblowing side (top) of the nozzle had a 3 in (7.62 cm) circular cavity and twin instrumentation channels hollowed out to allow installation of four pressure transducers and four heat flux gauges. The heat flux gauges were placed .5 in (1.27 cm) from centerline at positions 2 in (5.08 cm) prior to, and 0.219 in (5.56 mm), 0.828 in (2.1 cm), and 2.172 in (5.517 cm) downstream of the throat (see Figure 3.7). Because the subsonic gauge position was never filled with a working gauge, the locations downstream of the throat were termed positions 1, 2, and 3. The Mach number at these positions was M_1=1.1713, M_2=1.54405, and M_3=1.9368 respectively. The sides of the nozzle had O-rings to create a seal with the inner wall of the shock tube.

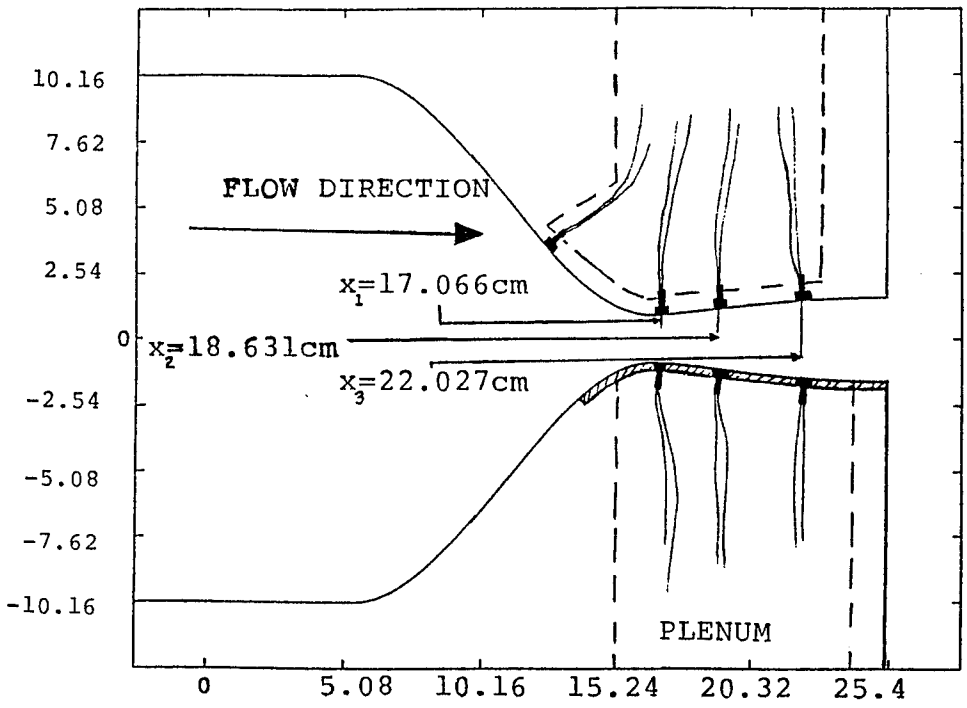

Fig. 3.7 Side View of Mach 2.0 Nozzle, Heat Flux Gauge Locations

The blowing side (bottom) of the nozzle had a 3 by 3 in (7.62 cm) square cavity drilled completely through the wall from the bottom. From the top, a 4 by 4.8 in (10.16 by 12.19 cm) shelf was cut 1/4 in (6.35 mm) deep, centered over the cavity. This allowed four

layers of the 0.0625 in (1.59 mm) thick porous plates to fit onto the shelf and be level with the inner wall of the nozzle (see Figure 3.8). Once the porous plates were bent to the contour of the nozzle and attached to the shelf, the plenum was complete. Once sealed onto the bottom of the shock tube with O-rings, this cavity can be pressurized and will allow transmission of a gas at a rate dependent on the pressure difference across the four layers of porous material. The instrumentation on the blowing side of the nozzle mirrored that of the nonblowing side except it had no provision for instrumentation prior to the throat.

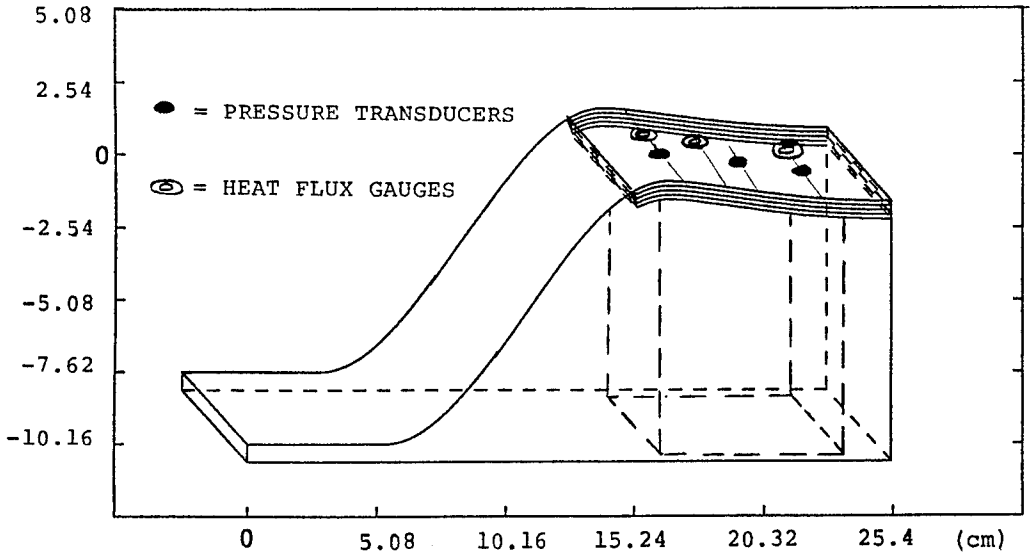

Fig. 3.8 Nozzle Blowing Side

Some difficulties were experienced with installation of gauges into relatively small but deep cavities. Special tools are required to avoid destroying the extremely fragile wires of the heat flux gauges. Also, because the surface of the gauge is flat, it can never truly conform with the curved contour of the nozzle, so some tripping of the flow was expected.

3.5 Data Collection

This section will focus on the data collection procedures followed during the testing, since the majority of the data collection apparatus was discussed in section 3.1. At each blowing ratio, it was desired to have at least five good sets of data. The collection and reduction of data fell into three natural phases: preparation, testing, and recording/reducing.

Before each test, much of the equipment required prepping. The bridges of all heat flux gauges were balanced, pressure transducer output was zeroed, and the Nicolet 500 system was configured. Next, the shock tube was flushed with dry air for 5 minutes to avoid the variable humidity associated with room air. Finally, ambient pressure and temperature, and air and helium bottle pressures were recorded.

The testing procedure was fairly quick and simple. A mylar diaphragm was installed in the shock tube, the helium was connected to the driver section and a valve opened to begin pressurization. A timing circuit was enabled and the room darkened for film exposure (if necessary). Just before the desired driver pressure was reached, the air bottle used to supply gas for transpiration cooling was opened to a pre-set level. This pressurized the plenum and started the injection airflow. The Nicolet 500 was enabled, and the shock tube was fired.

Following each firing of the tube, the raw experimental data was transferred to files in the Zenith 433D+ computer. When all the tests were complete, the data was converted into useful form and sent to the Sun network for processing. The Sun Sparc 20 computers were then used to manipulate the raw data to obtain heat flux, heat transfer coefficient, and blowing ratio values.

IV. Results and Discussion

4.1 Nozzle Shock Interaction

During a firing of the shock tube, the interaction between the shock and the nozzle has a strong influence on the measured values of heat transfer coefficient. When the shock moves down the tube, most of it is reflected by the converging portion of the nozzle, creating the stagnation conditions. A fraction of the shock is not reflected, however, and is "swallowed" by the nozzle.

The nonreflected portion of the original shock expands due to and reflects off of the diverging section of the nozzle. The passage of the ensuing oblique shocks and turbulent flow over the heat flux gauges causes a rapid rise in heat flux (see Figure 4.1). Following the initial jump, there is a fairly quick drop to the steady flow run time heat flux, followed by a slow, steady drop off to near zero heat flux at the time the nozzle unstarts.

The reason behind this heat flux behavior lies in the nature of the boundary layer . In nozzle flow, the boundary layer acts as a thermal insulator. A thicker boundary layer will tend to be a better insulator than a thin boundary layer. Until the first shock wave passes over the heat flux gauge, there has been no flow and therefore no boundary layer, so the heat flux quickly reaches a maximum. Following the passage of the shock, the boundary layer grows and begins to insulate the nozzle walls. Once steady flow has been achieved and the boundary layer is fully developed, there is nearly constant heat flux. The steady drop off in heat flux at the end of the run is due to lower primary flow temperatures as the nozzle begins to unstart. The beginning and end of the steady flow run time (0.65 and 2.4 ms) were established from pressure transducer data and shadowgraphs of the nozzle (Keener, 1994).

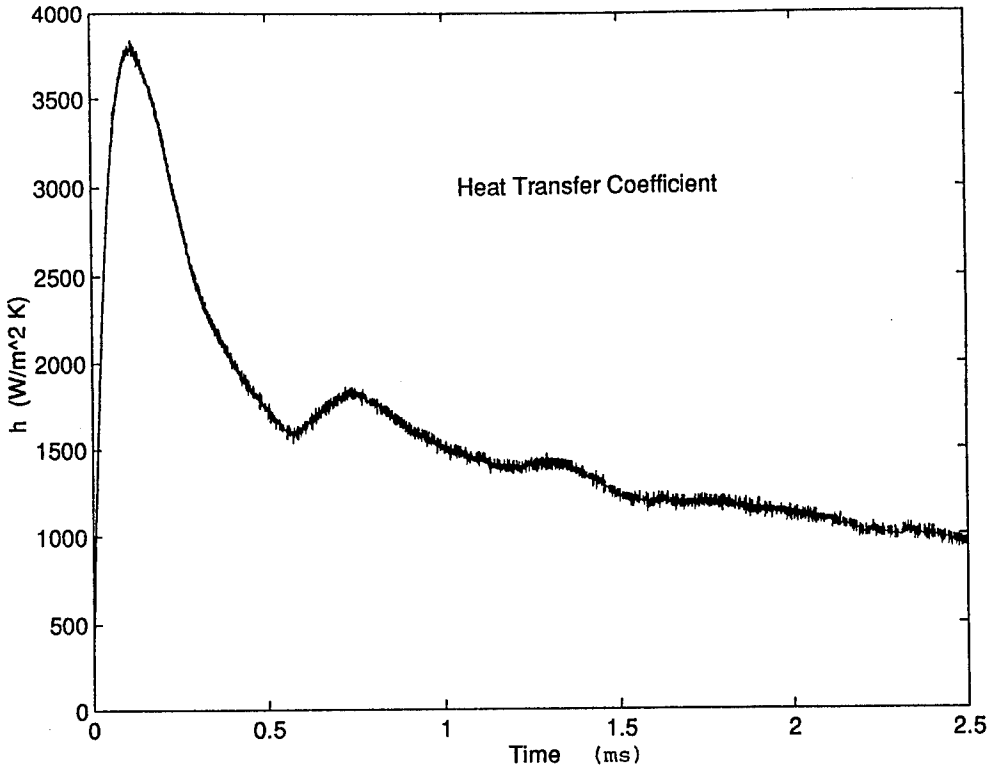

Fig. 4.1 Nozzle Heat Transfer Coefficient History

4.2 Uncooled Heat Flux

The nonblowing side of the nozzle provided reference heat flux data (no transpiration cooling) throughout the testing. Unfortunately, due to severe attrition of the heat flux gauges, only four of the six positions in the supersonic portion of the nozzle could be filled with working gauges. Positions one and three (see Figure 3.7) of the nonblowing side were filled, along with positions one and two on the blowing side.

The blowing side of the nozzle can never truly measure "uncooled" heat flux. Because the pressure of the primary flow decreases in the downstream direction, there can be at most one point where the pressure equals the plenum pressure. At all other locations, the plenum will either be suctioning or blowing, depending on whether the plenum pressure is lower or higher than the primary flow pressure at that point. In the baseline case, the low

plenum pressure was suctioning the primary flow up to both gauge locations, causing a reduction in thickness of the boundary layer on the blowing side of the nozzle. This resulted in higher than nonblowing heat transfer rates along the blowing side of the nozzle. Five runs of data were taken and processed, with the results shown in Table 4.1.

Table 4.1 Nonblowing Heat Transfer Coefficients (W/m^2K)

Gauge Position	1/Nonblowing	3/Nonblowing	1/Blowing	2/Blowing
Run 1	1518.3	1139.8	1996.6	1746.5
Run 2	1459.3	1093.5	1925.6	1634.5
Run 3	1626.8	1047.0	1997.2	1669.8
Run 4	1610.0	1065.0	2179.7	1680.4
Average of 4 Runs	1553.6	1086.3	1974.8	1682.8

Plotting this data versus the predicted heat transfer coefficient from eq (2.11), there is good agreement except for the position one nonblowing gauge data, which is about 22% low (see Figure 4.2). Upon inspection, the gauge appeared to be recessed into the nozzle wall by approximately 1.5 mm, while the rest of the gauges were essentially flush with the surface. This depression may be the cause of lower heat transfer coefficients at that location.

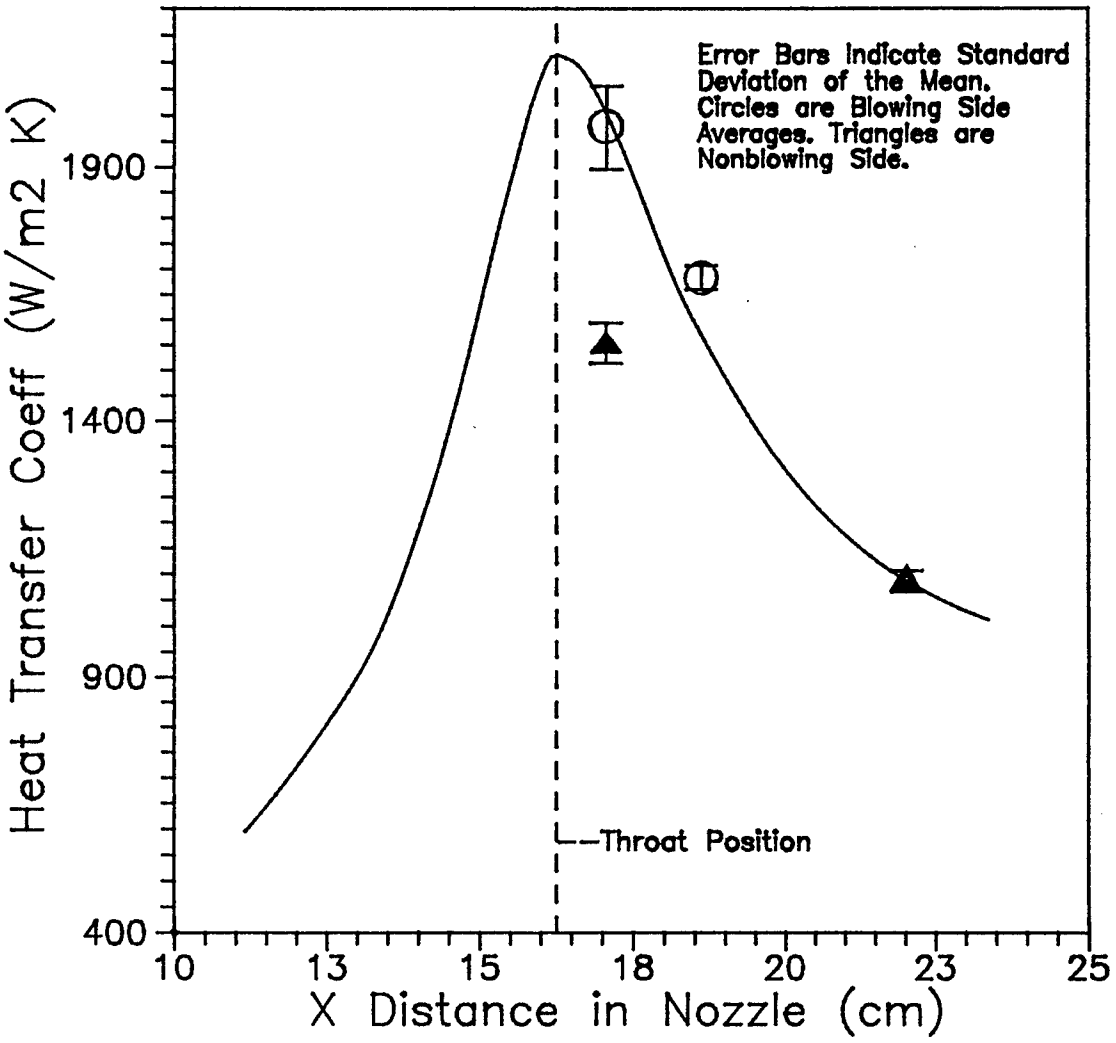

Fig. 4.2 Measured and Predicted Uncooled Heat Transfer Coefficient

4.3 Effects of Transpiration Cooling

The heat flux data on the blowing side of the nozzle was measured for various blowing ratios to determine the effectiveness of transpiration cooling. Five sets of heat flux gauge voltage data at each of five blowing ratios were evaluated. The heat flux gauges occupied

positions one and two on both sides of the nozzle. The resulting heat transfer coefficients are shown in Table 4.2.

Table 4.2 Heat Transfer Coefficients at Various Plenum Pressures (W/m^2K)

Plenum Pressure	Gauge 1 Nonblowing	Gauge 2 Nonblowing	Gauge 1 Blowing	Gauge 2 Blowing
98.6 kPa	1547.9	1774.3	2159.2	1738.9
262 kPa	1591.6	1791.7	2033.9	1564.9
296 kPa	1684.3	1868.3	2033.9	1566.9
338 kPa	1559.3	1758.7	1866.3	1387.7
379 kPa	1575.4	1788.1	1866.2	1393.0

This data appears to have a general trend towards cooling as the plenum pressure (blowing ratio) increases, but it is quite scattered. Notice that when the nonblowing heat flux is high, there appears to be less of a drop in blowing heat flux. This scatter could be a result of nonconstant shock strength from one data set to the next. To better see the actual effect of cooling, the data was normalized using the position two, nonblowing heat transfer coefficient. This effectively removed the scatter and made the nonblowing values nearly constant (less than 1.1% standard deviation) with different plenum pressures, as expected. Table 4.3 summarizes the results, showing a steady trend of decreasing heat flux with increasing plenum pressure (blowing ratio) on the blowing side of the nozzle.

Table 4.3 Normalized Heat Transfer Coefficients at Various Plenum Pressures (W/m^2K)

Plenum Pressure	Gauge 1 Nonblowing	Gauge 2 Nonblowing	Gauge 1 Blowing	Gauge 2 Blowing
98.6 kPa	1567.0	1796.2	2185.9	1760.4
262 kPa	1595.6	1796.2	2039.0	1568.8
296 kPa	1619.3	1796.2	1955.4	1506.4
338 kPa	1592.5	1796.2	1906.1	1417.3
379 kPa	1582.5	1796.2	1874.7	1399.3

In order to compare these heat transfer coefficients with a meaningful cooling parameter instead of just the plenum pressure, a blowing ratio must be defined. In film cooling, the blowing ratio is simple to define. Since the blowing generally occurs at only one point along the direction of flow, the blowing ratio is constant at all points downstream of the blowing. In transpiration cooling, since the blowing occurs continuously over an area, the blowing ratio is a function of downstream position in the nozzle. In addition, the pressure difference between the plenum and mainstream flow (across the porous wall) is continuously increasing in the downstream direction, so the local blowing is much higher near the nozzle exit than at the throat. This means that the blowing ratio for transpiration cooling requires an integration of blowing along the nozzle wall, up to the point of interest.

A computer code called BLOWDOT (see Appendix C) was written to perform this integration. It solves for mainstream pressure in the nozzle using isentropic relations with a correction factor based on experimental pressure data. For a given plenum pressure, this provides the pressure difference across the porous wall at each point in the nozzle.

Assuming the pressure difference is constant over a small increment of area, the incremental injection mass flow rate can be computed using eq (2.24) and:

$$\dot{m}_{inc} = \rho_i u_{inc} A_{inc} \tag{4.1}$$

When all increments up to a given point have been summed and divided by injection area up to that point, $\rho_i u_i$ is known. Then, evaluating the primary flow $\rho_p u_p$ at that point allows computation of the local blowing ratio. Figure 4.3 depicts blowing ratio as a function of downstream distance for the five plenum pressures tested.

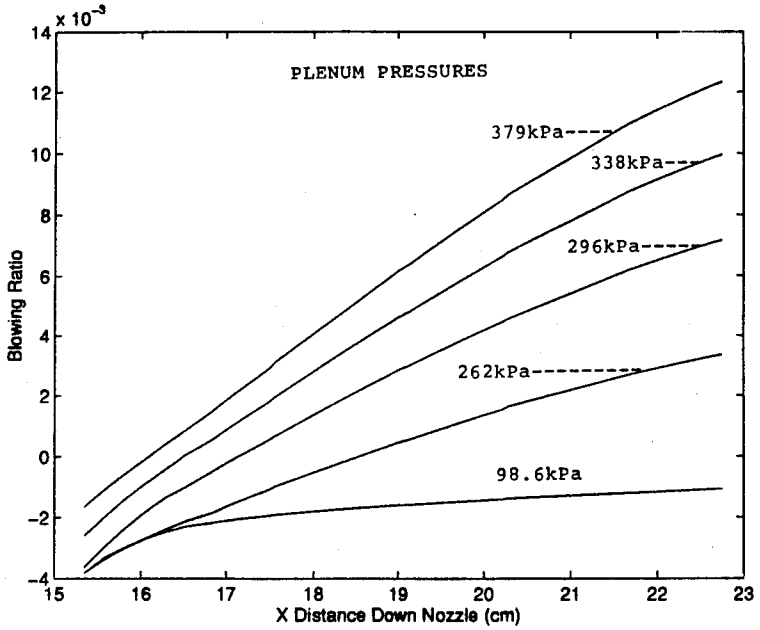

Fig. 4.3 Blowing Ratio vs. Downstream Location for Several Plenum Pressures

This technique resulted in negative blowing ratios for those cases where the plenum pressure was below the primary flow pressure up to the point of interest. Based on shadowgraphs of the flow, it appears this suction pulls the boundary layer partially into the plenum. This results in heat transfer coefficients up to 9% higher than zero blowing heat transfer. Positive blowing resulted in reduced heat transfer coefficients, down to

approximately 86% of nonblowing heat transfer coefficient at the maximum tested blowing ratio of 0.0051.

Defining relative heat flux as a ratio of measured blowing to nonblowing heat transfer coefficient, and plotting this against blowing ratio, Figure 4.4 shows the linear nature of cooling effectiveness. The open data points are position 1 (M=1.17) results; filled data points are results from position 2 (M=1.54). The slope is a linear best fit with a standard deviation of 0.63%. The upper horizontal line represents a limiting heat flux after the boundary layer thickness has been reduced due to suction.

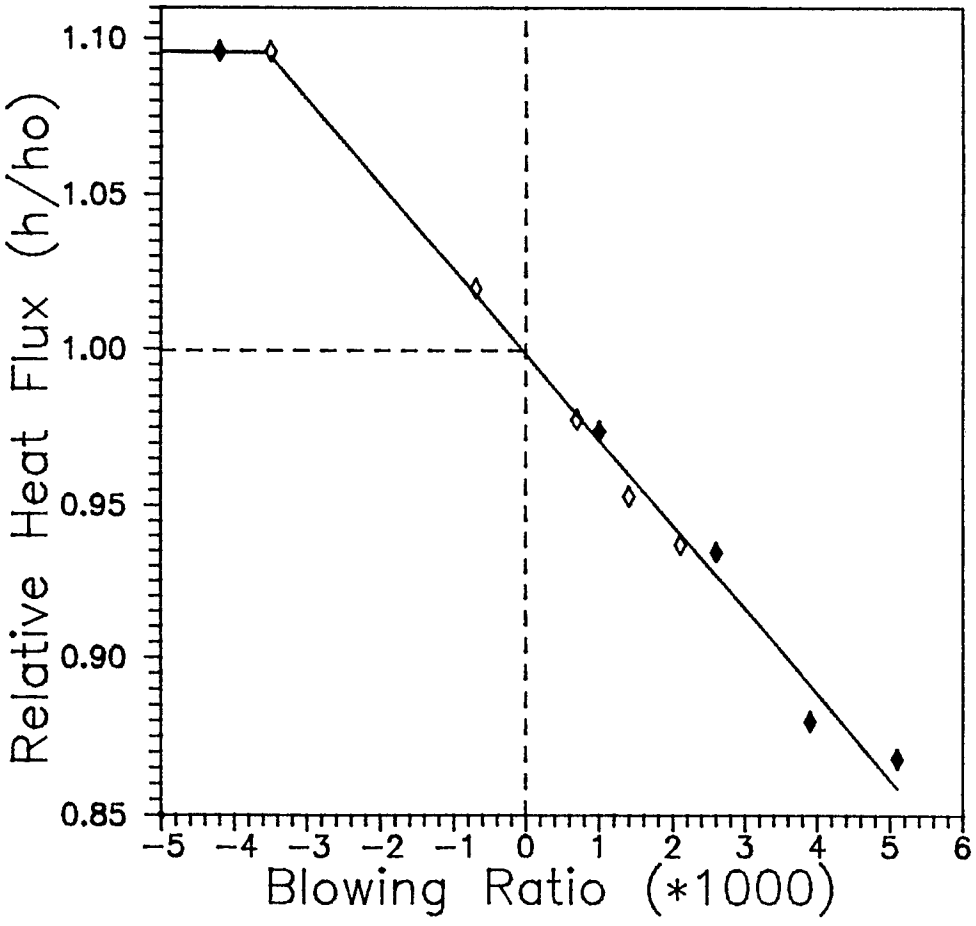

Fig. 4.4 Cooling Effectiveness of Transpiration Cooling in Mach 2.0 Nozzle

Based on the linear least squares fits of each position individually, there does not appear to be a significant difference in the cooling effectiveness at the two different locations in the nozzle. A given blowing ratio at either location would provide about the same amount of cooling. Because the pressure drop across the porous material was higher at the location further downstream, the blowing ratio and cooling effectiveness were also higher at the downstream location. This would be an unfortunate result in an actual rocket or wind tunnel nozzle, as it would provide the least cooling where it was needed the most: just prior to the nozzle throat. However, for the present study, this was not a limitation.

This slope would indicate a modification of eq (2.11) is required if the wall is porous and is being transpiration cooled. Defining local blowing ratio B as above, eq (2.11) should read:

$$h = \frac{.02443643\left(\rho^* u^*\right)^{.75} \mu_o^{.25} c_p}{\left(D^*\right)^{.1} \left(r_c\right)^{.1} \mathrm{Pr}^{.46}} \left(\frac{A^*}{A}\right)^{.75} \sigma \left(\frac{1}{\Delta}\right)^{1/7} \left(\frac{1}{\delta}\right)^{3/28} (1 - 27.381B) \qquad (4.2)$$

Using this relation, a plot of heat flux with transpiration cooling as a function of nozzle location was created. Figure 4.5 depicts the heat transfer coefficient vs. downstream location in the nozzle for the baseline and highest blowing cases.

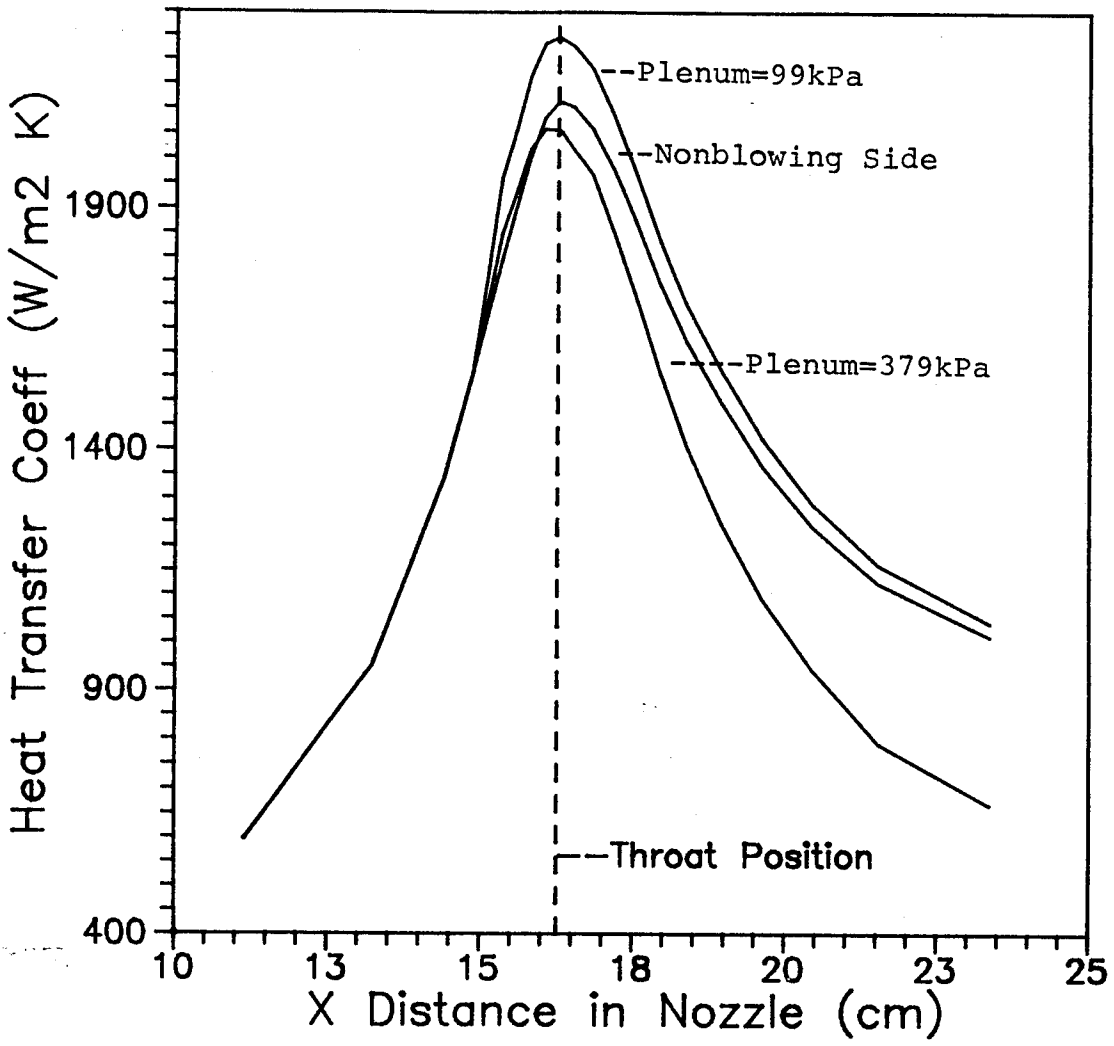

Fig. 4.5 Heat Transfer Coefficient along Nozzle at Different Blowing Rates

V. Conclusions and Recommendations

5.1 Conclusions

A study of transpiration cooling with applications to rocket nozzle cooling was performed. Overall heat flux values for "nonblowing" (ambient pressure plenum conditions on the blowing side) were within 7.7% of predicted values except for a gauge not flush with the nozzle wall. Transpiration cooling was effective at reducing heat flux at blowing ratios much lower than typical for film cooling. Heat flux varied linearly with blowing ratio over the range B=-0.0035 to B=0.0051, causing heat flux values from 109% to 86% of the nonblowing case, respectively.

Transpiration cooling compares well against film cooling, which has required blowing ratios on the order of 0.2 to 0.4 to achieve a 14% reduction in heat flux (Pederson et al., 1977:620 and Valencia, 1993:A33). The difference between film cooling and transpiration cooling injection velocity can be quite large under conditions of equivalent cooling effectiveness. According to Valencia, injection velocities of approximately 60 m/s would be required to achieve a 14% heat reduction near the nozzle throat, while transpiration cooling required an injection velocity of only 1.6 m/s. The substantially higher injection velocities associated with film cooling can disturb the primary flow and can reduce nozzle performance (Azavedo, 1993:44).

Although not a direct result of this research, a collaboration with another researcher found that the nozzle performance was unaffected by the transpiration cooling. A blowing ratio of 0.012 caused a 47% growth in the velocity boundary layer thickness and a reduction of local Mach near the porous wall, but the overall change in performance was calculated as a 0.5% *improvement* (Keener, 1994). Taking this improvement as statistically negligible, the overall potential of transpiration cooling is still impressive: A

14% reduction in heat transfer using a blowing ratio of .0051 with virtually no loss in performance.

The accurate calibration of a heat flux gauge to determine thermal product is a difficult but necessary step towards meaningful heat flux measurements. The electric discharge calibration method failed to provide consistent, predictable results. The results were unsatisfactory, and used only as a starting point in the known heat flux to a flat plate calibration. Although measured heat transfer coefficient values following the flat plate calibration are near the theoretical values of eq (2.11), there is still no statistical representation of the accuracy of the thermal products.

5.2 Recommendations

The recommendations of this project are twofold: to provide guidance gained by experience to other researchers contemplating similar research, and to provide ideas and methods of expanding this research to include wider ranges and more variables.

Thin film resistance thermometers are so fragile and difficult to calibrate, that whatever methods exist to avoid exposing them to currents or physical manipulation will be well worth using. Due to the numerous physical and electrical set-ups required to calibrate the gauges as outlined in this report, severe attrition of the gauges resulted. From a total of twelve gauges acquired during the study, only two remained operational at the end. Although two of these failures occurred while the gauges were subjected to conditions within their specifications, the majority of failures were avoidable.

Another method uses the same principle of electrical heating through a circuit to provide a constant heat flux, but it avoids the double air-and-glycerin calibration (Seginer and others, 1964:25-30). It also removes the requirement to analyze ratios of the response slopes to find the thermal product, and claims a 1% accuracy vs. the 10-15%

accuracy of the air and glycerin electrical heating method. This may avoid some handling of the gauges and provide more accurate heat transfer coefficient results.

This research focused on a narrow range of blowing ratios using only one type of injection fluid (a single density ratio) and only one grade of porous material. Some avenues of additional research naturally follow given the limited nature of this initial study. A bottled gas regulator with higher volumetric flow rate would allow greater blowing ratios, and the simple change to a helium bottle would allow the study of a different density injection fluid. A change to the 10 micron grade porous material from the present 2 micron grade would allow testing on the effects of surface roughness, and additional heat flux gauges would give better coverage of the entire nozzle.

In order to achieve more cooling near the nozzle throat, where it is most needed, several methods are possible: Covering the downstream portion of the porous material from inside the plenum would enable the fluid supply system to achieve higher plenum pressures and therefore greater blowing ratios near the throat. Another more challenging possibility is to create a variable porosity sandwich to cover the plenum. This method would use the two outer layers of porous material to hold the smaller sectioned inner layers in place. By choosing relatively coarse grades near the throat with progressively finer grades downstream, the desired blowing ratio at each section could be adjusted to meet cooling requirements.

Appendix A

This section consists of a simple derivation of eq (2.16), the relation that creates a heat flux history on the surface of a heat flux gauge from the gauge's thermal product and temperature history. A simpler approach than other available derivations was deemed necessary so that novices entering heat flux research could follow and understand the results.

Referring to Figure 2.4, notice a semi-infinite slab made up of two mediums is subjected to a certain heat flux (W/m^2). Medium 1 has a finite thickness L. Denoting the thermal diffusivities (m^2/sec) of the two mediums as $\alpha_1 = k_1/\rho_1 c_1$ and $\alpha_2 = k_2/\rho_2 c_2$, we have:

A1
$$\frac{\partial^2 T_1}{\partial x^2} = \frac{1}{\alpha_1}\frac{\partial T_1}{\partial t}$$

A2
$$\frac{\partial^2 T_2}{\partial x^2} = \frac{1}{\alpha_2}\frac{\partial T_2}{\partial t}$$

from eq (2.3), the one dimensional unsteady conduction equation. This is the equation defining what the temperature T is at some distance x into the medium and some time t.

Then, assuming a certain heat flux $\dot{q}_s$ at the surface, there will be a temperature gradient in medium 1, with the slope of that gradient being the thermal conductivity, k (W/m K).

A3
$$\dot{q}_s = -k_1 \frac{\partial T_1}{\partial x} \quad \text{(at x=0)}$$

Similarly, at the junction of the two mediums we can say:

A4 $$k_1 \frac{\partial T_1}{\partial x} = k_2 \frac{\partial T_2}{\partial x} \quad \text{and} \quad T_1 = T_2 \quad (\text{at x=L})$$

Finally, assuming medium 2 has infinite thickness,

A5 $$T_2 = 0 \quad (\text{at x}=\infty)$$

This set of equations (A1-A5) defines the problem and supplies boundary conditions. Performing the LaPlace transform on A1 and A2, we have:

$$\mathbf{L}\left(\frac{\partial^2 T_1}{\partial x^2}\right) = \mathbf{L}\left(\frac{1}{\alpha_1}\frac{\partial T_1}{\partial t}\right)$$

$$\frac{\partial^2}{\partial x^2}\left(\mathbf{L}(T_1)\right) = \frac{1}{\alpha_1}\mathbf{L}\left(\frac{\partial T_1}{\partial t}\right)$$

$$\frac{\partial^2}{\partial x^2}\left(\mathbf{L}(T_1)\right) = \frac{s}{\alpha_1}\mathbf{L}(T_1)$$

Now, denoting $\mathbf{L}(T_1)$ as simply $\overline{T_1}$, we have:

$$\frac{\partial^2 \overline{T_1}}{\partial x^2} = \frac{s}{\alpha_1}\overline{T_1} \qquad \text{and similarly} \qquad \frac{\partial^2 \overline{T_2}}{\partial x^2} = \frac{s}{\alpha_2}\overline{T_2}$$

These are simply second order differential equations of the form:

$$\ddot{y} + 0\,\dot{y} - \frac{s}{\alpha} y = 0$$

and have the general solution:

$$y = A\exp\left(\left(\frac{s}{\alpha}\right)^{1/2} t\right) + B\exp\left(-\left(\frac{s}{\alpha}\right)^{1/2} t\right)$$

So, we know:

A6
$$\overline{T_1} = A\exp\left(\left(\frac{s}{\alpha_1}\right)^{1/2} x\right) + B\exp\left(-\left(\frac{s}{\alpha_1}\right)^{1/2} x\right)$$

A7
$$\overline{T_2} = C\exp\left(\left(\frac{s}{\alpha_2}\right)^{1/2} x\right) + D\exp\left(-\left(\frac{s}{\alpha_2}\right)^{1/2} x\right)$$

Now, performing the LaPlace transform on A3-A5, we have:

$$\overline{\dot{q}_s} = -k_1 \frac{\partial \overline{T_1}}{\partial x} \quad \text{(at x=0)}, \qquad k_1 \frac{\partial \overline{T_1}}{\partial x} = k_2 \frac{\partial \overline{T_2}}{\partial x}, \quad \overline{T_1} = \overline{T_2} \quad \text{(at x=L)}, \quad \text{and} \quad \overline{T_2} = 0 \quad \text{(at x=}\infty\text{)}$$

Substituting the solutions from A6 and A7 into the four equations above, we have four equations in the four unknowns A, B, C, and D:

A8
$$\overline{\dot{q}_s} = -k_1\left[A\sqrt{\frac{s}{\alpha_1}}\exp\left(\left(\frac{s}{\alpha_1}\right)^{1/2} x\right) - B\sqrt{\frac{s}{\alpha_1}}\exp\left(-\left(\frac{s}{\alpha_1}\right)^{1/2} x\right)\right]$$

A9
$$k_1\left[A\sqrt{\frac{s}{\alpha_1}}\exp\left(\left(\frac{s}{\alpha_1}\right)^{1/2} x\right) - B\sqrt{\frac{s}{\alpha_1}}\exp\left(-\left(\frac{s}{\alpha_1}\right)^{1/2} x\right)\right]$$

$$= k_2\left[C\sqrt{\frac{s}{\alpha_2}}\exp\left(\left(\frac{s}{\alpha_2}\right)^{1/2} x\right) - D\sqrt{\frac{s}{\alpha_2}}\exp\left(-\left(\frac{s}{\alpha_2}\right)^{1/2} x\right)\right] \quad \text{(at x=L)}$$

A10 $$A\exp\left(\left(\frac{s}{\alpha_1}\right)^{1/2}x\right)+B\exp\left(-\left(\frac{s}{\alpha_1}\right)^{1/2}x\right)=C\exp\left(\left(\frac{s}{\alpha_2}\right)^{1/2}x\right)+D\exp\left(-\left(\frac{s}{\alpha_2}\right)^{1/2}x\right)$$

(at x=L), and

A11 $$C\exp\left(\left(\frac{s}{\alpha_2}\right)^{1/2}x\right)+D\exp\left(-\left(\frac{s}{\alpha_2}\right)^{1/2}x\right)=0 \quad (\text{at } x=\infty)$$

Algebraic manipulation of A8-A11 will allow the removal of A, B, C, and D. Then, solving for $\overline{T_1}$ and $\overline{T_2}$ yields:

$$\overline{T_1}=\frac{\overline{\dot{q}_s}\sqrt{\alpha_1}\left[(1+a)\exp\left(-(x-L)\sqrt{\frac{s}{\alpha_1}}\right)+(1-a)\exp\left((x-L)\sqrt{\frac{s}{\alpha_1}}\right)\right]}{k_1\sqrt{s}\left[(1+a)\exp\left(L\sqrt{\frac{s}{\alpha_1}}\right)-(1-a)\exp\left(-L\sqrt{\frac{s}{\alpha_1}}\right)\right]}$$

$$\overline{T_2}=\frac{2\overline{\dot{q}_s}\sqrt{\alpha_1}\exp\left((L-x)\sqrt{\frac{s}{\alpha_2}}\right)}{k_1\sqrt{s}\left[(1+a)\exp\left(L\sqrt{\frac{s}{\alpha_1}}\right)-(1-a)\exp\left(-L\sqrt{\frac{s}{\alpha_1}}\right)\right]}$$

where $a=\left(\frac{\rho_2 c_2 k_2}{\rho_1 c_1 k_1}\right)^{1/2}$. These are the most general forms of the solution.

For heat flux gauges with very thin films, L will approach zero. In this case, the temperature at x distances inside the gauge is determined only by the thermal properties of medium 2, the substrate. The relation for $\overline{T_2}$ simplifies under this assumption, to:

$$\overline{T_2}=\frac{\overline{\dot{q}_s}\sqrt{\alpha_1}\exp\left(-x\sqrt{\frac{s}{\alpha_2}}\right)}{ak_1\sqrt{s}}=\frac{\overline{\dot{q}_s}}{\sqrt{\rho_2 c_2 k_2}}\frac{1}{\sqrt{s}}\exp\left(-x\sqrt{\frac{s}{\alpha_2}}\right)$$

At the surface of the gauge, this simplifies further, to:

A12
$$\overline{T_2} = \frac{\overline{\dot{q}_s}}{\sqrt{\rho_2 c_2 k_2}} \frac{1}{\sqrt{s}} \quad \text{(at x=0)}$$

Now taking the inverse LaPlace of this last relation, we have:

$$T = \frac{1}{\sqrt{\pi \rho c k}} \int_0^t \frac{\dot{q}_s(\tau)}{(t-\tau)} d\tau$$

where T is the temperature of the surface of the gauge and all thermal properties are those of the substrate. Alternatively, we could solve A12 for $\overline{\dot{q}_s}$ and then inverted the Laplace transform, finding:

A13
$$\dot{q}_s = \left(\frac{\rho c k}{\pi}\right)^{1/2} \int_0^t \frac{\frac{dT}{d\tau}(\tau)}{(t-\tau)^{1/2}} d\tau$$

This last equation is acceptable in a purely analytical sense, but for experimental use it must be modified. In all experimental data there is some noise inherently recorded along with the signal. Because of the high frequency nature of noise, we expect that the time derivative of temperature will fluctuate more wildly than the temperature itself. This would make A13 difficult to use and too noisy for good data reduction. A different form of equation A13 overcomes this problem.

Integrating A13 by parts using z=T(t)-T(τ) and T(0)=0, we have eq (2.16):

$$\dot{q}_s = \left(\frac{\rho c k}{\pi}\right)^{1/2} \left[\frac{T(t)}{\sqrt{t}} + \frac{1}{2} \int_0^t \frac{T(t)-T(\tau)}{(t-\tau)^{3/2}} d\tau\right]$$

Appendix B

This section contains the calibration plots of the thin film heat flux gauges. The plots are intended to display pictorially the linearity and repeatabilityof each gauge during calibration.

The heat flux gauges were rated from the manufacturer in English units and calibrated in Fahrenheit. Convert with K=5/9(°F+459.67) to use metric units. Calibration plots are shown only for the four gauges that were operational through the entire project. The order of plots 1 through 4 represent the nonblowing side of the nozzle at M=1.17 and M=1.54 locations, then the blowing side M=1.17 and M=1.54 locations. These positions were filled with gauge serial numbers 3, 42, 55, and 65 respectively. The remaining plots are labeled by serial number and include the air calibrations, the glycerin calibrations, and finally a comparison of the response slopes in air vs. glycerin.

Notice gauges 3 and 55 were much closer to linear (when plotted vs. square root time) than gauges 42 and 65. Gauges 3 and 55 were also much more repeatable, with lower deviations from the norm. This meant higher confidence in their thermal products of 1706 and 1444 $J/m^2Ks^{.5}$ respectively. These values compare well against the 1520± 5% value given for the Pyrex 7740 substrate. Gauges 42 and 65, however, had thermal products of 3432 and 2267 respectively, demonstrating the difficulty of accurate calibration of gauges of this type.

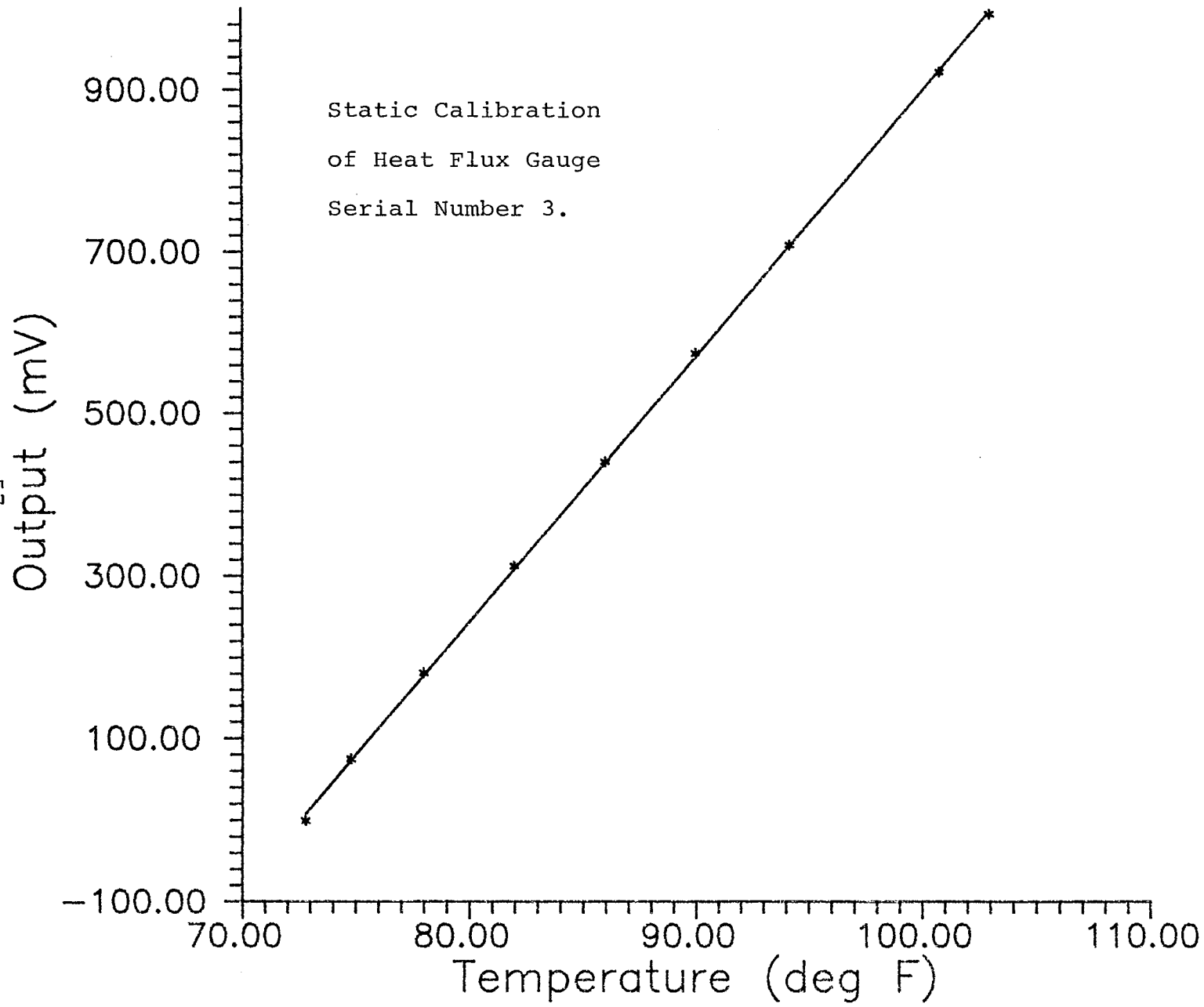
Static Calibration
of Heat Flux Gauge
Serial Number 3.
900.00
700.00
500.00
300.00
100.00
-100.00
Output (mV)
70.00
80.00
90.00
100.00
110.00
Temperature (deg F)

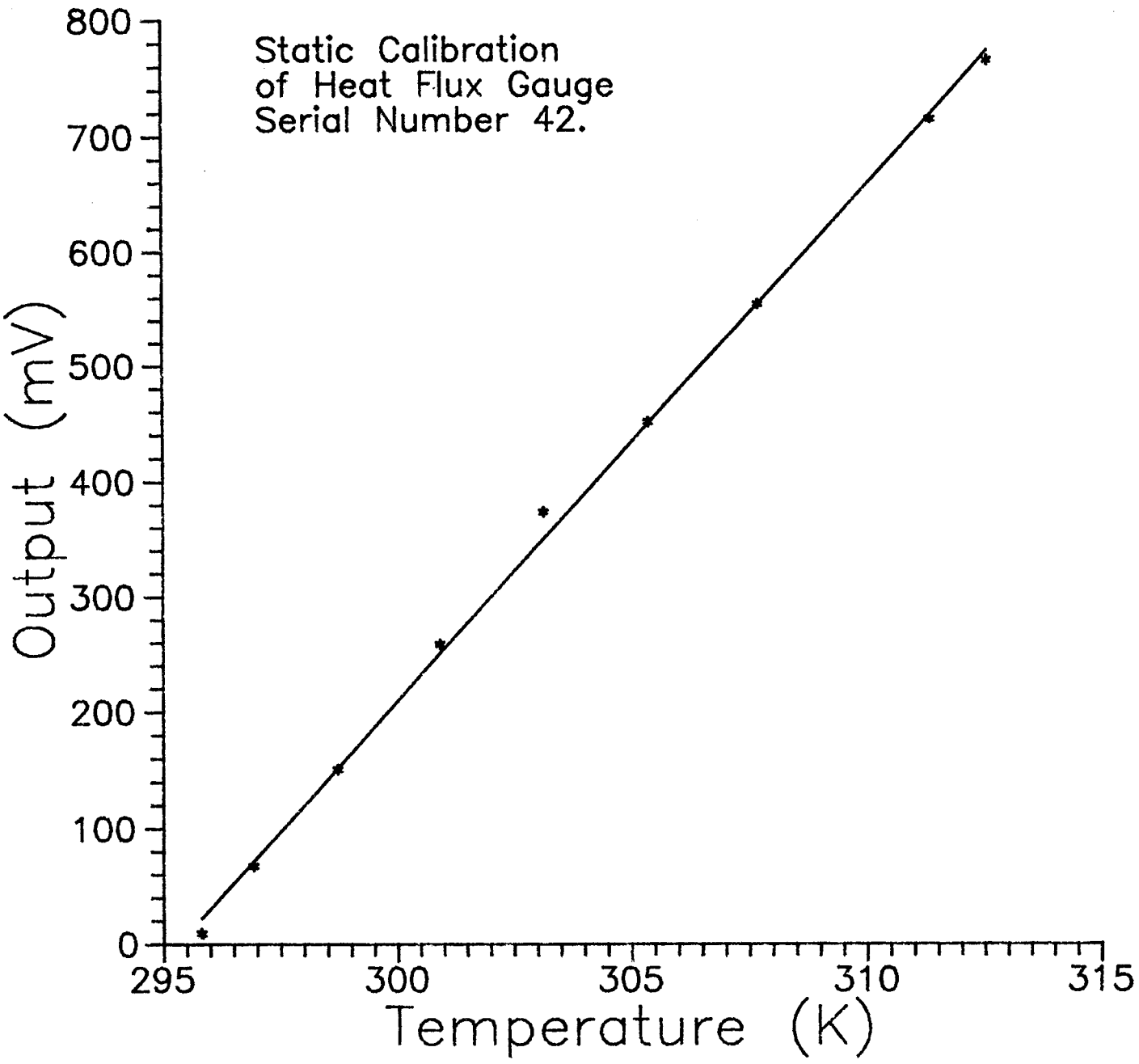
Static Calibration
of Heat Flux Gauge
Serial Number 42.
Output (mV)
800
700
600
500
400
300
200
100
0
295
300
305
310
315
Temperature (K)

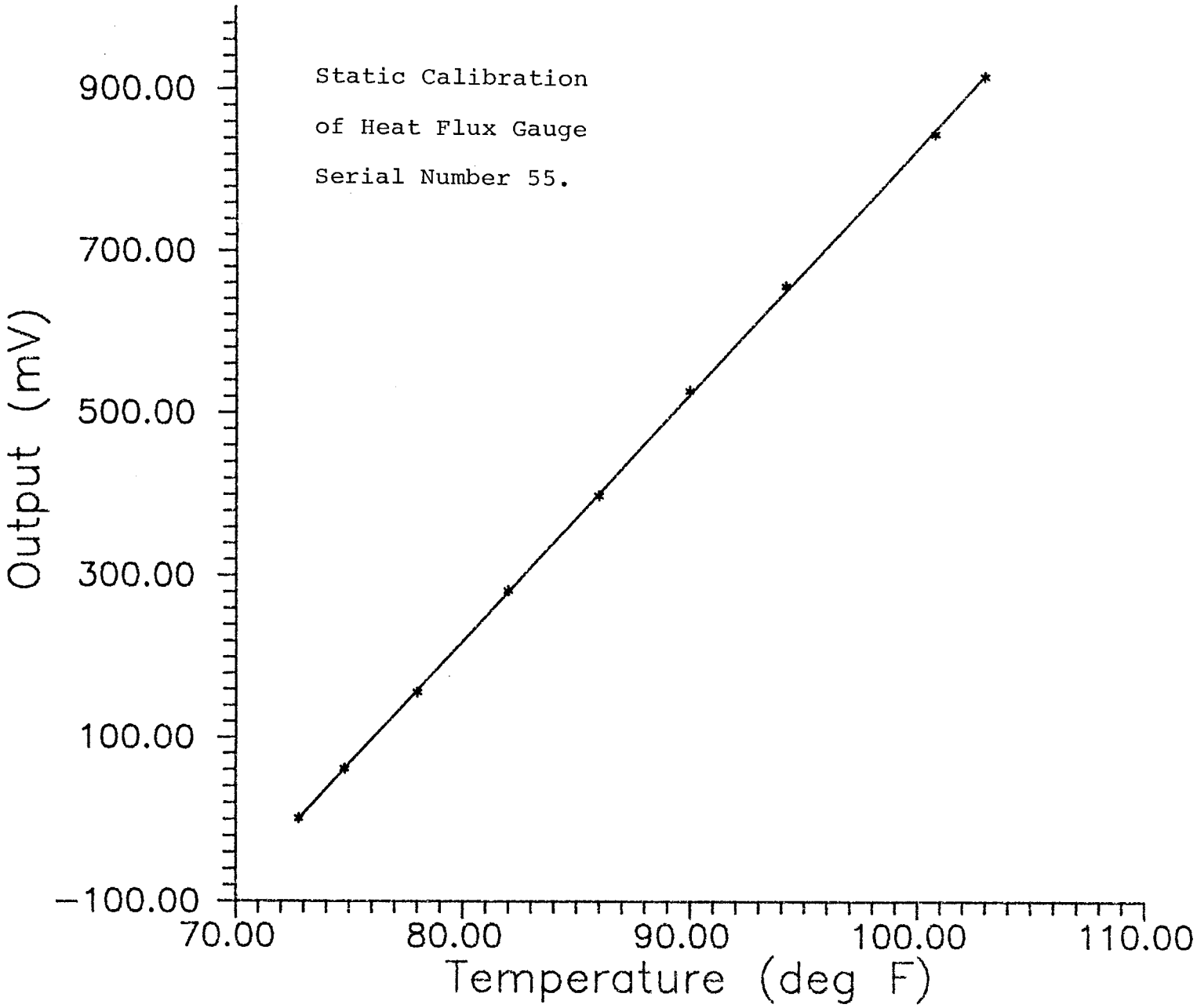
Static Calibration
of Heat Flux Gauge
Serial Number 55.
900.00
700.00
500.00
300.00
100.00
-100.00
Output (mV)
70.00
80.00
90.00
100.00
110.00
Temperature (deg F)

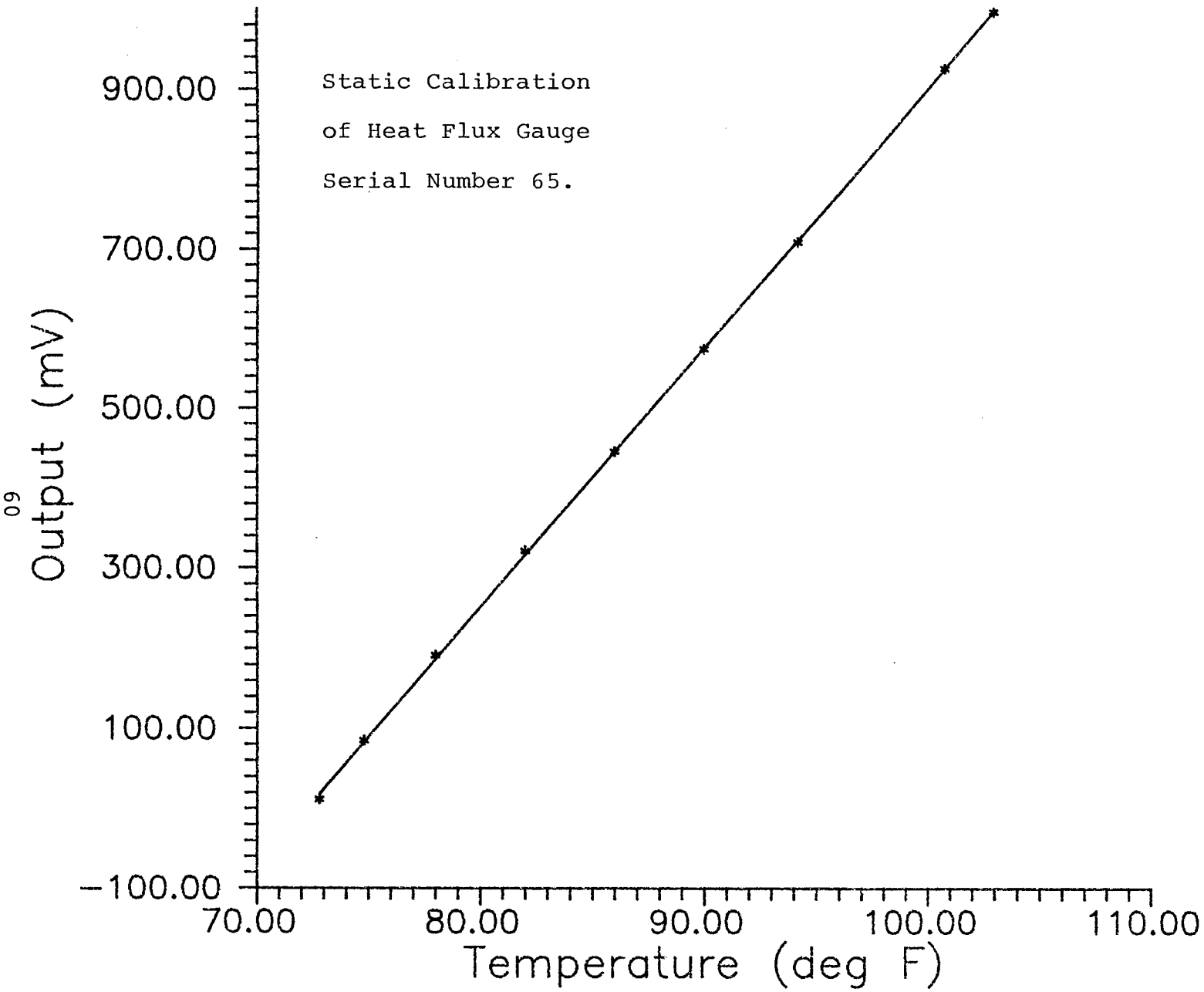
Static Calibration
of Heat Flux Gauge
Serial Number 65.
900.00
700.00
500.00
300.00
100.00
-100.00
Output (mV)
60
09
70.00
80.00
90.00
100.00
110.00
Temperature (deg F)

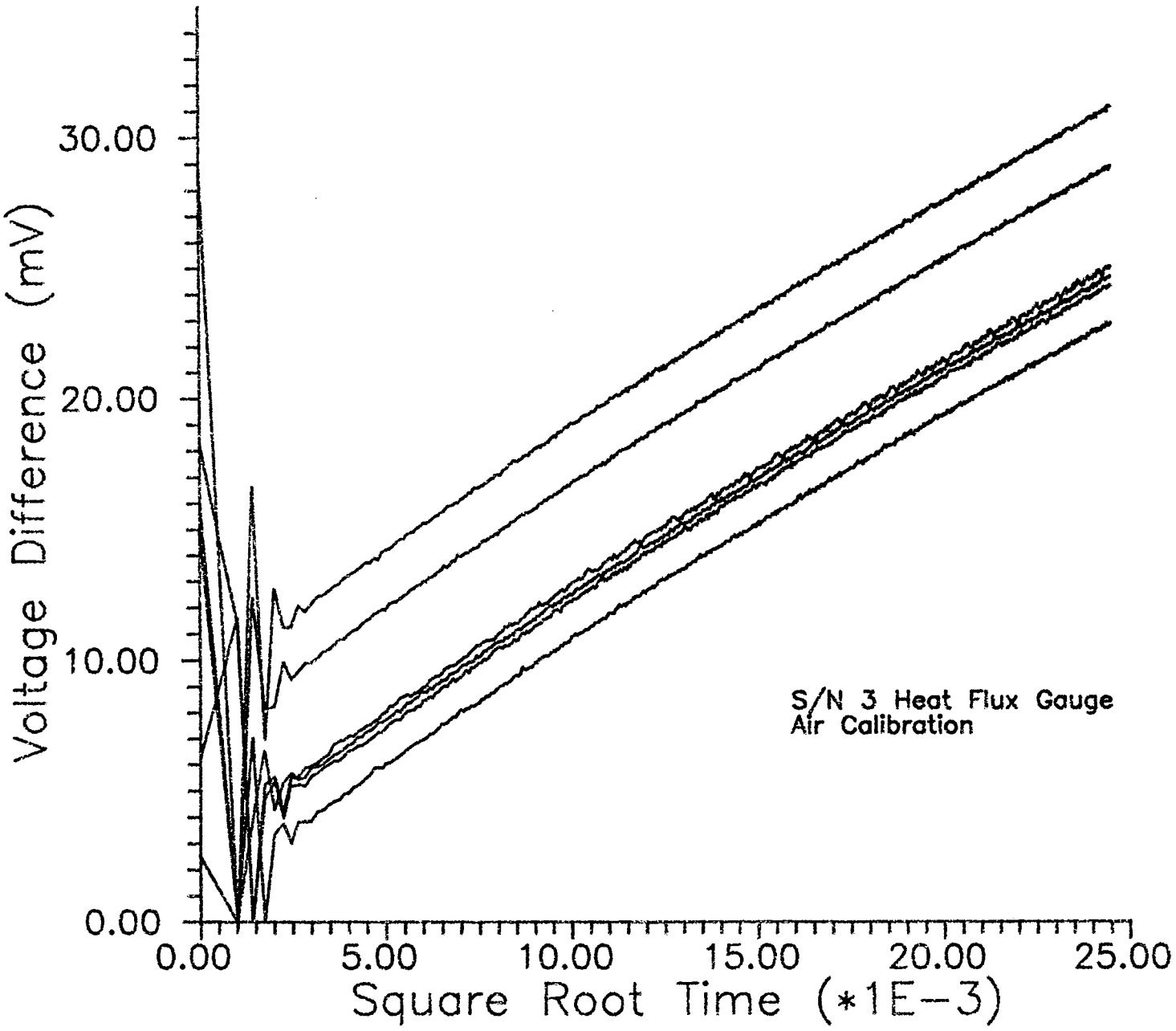
Voltage Difference (mV)
30.00
20.00
10.00
0.00
0.00
5.00
10.00
15.00
20.00
25.00
Square Root Time (*1E-3)
S/N 3 Heat Flux Gauge
Air Calibration

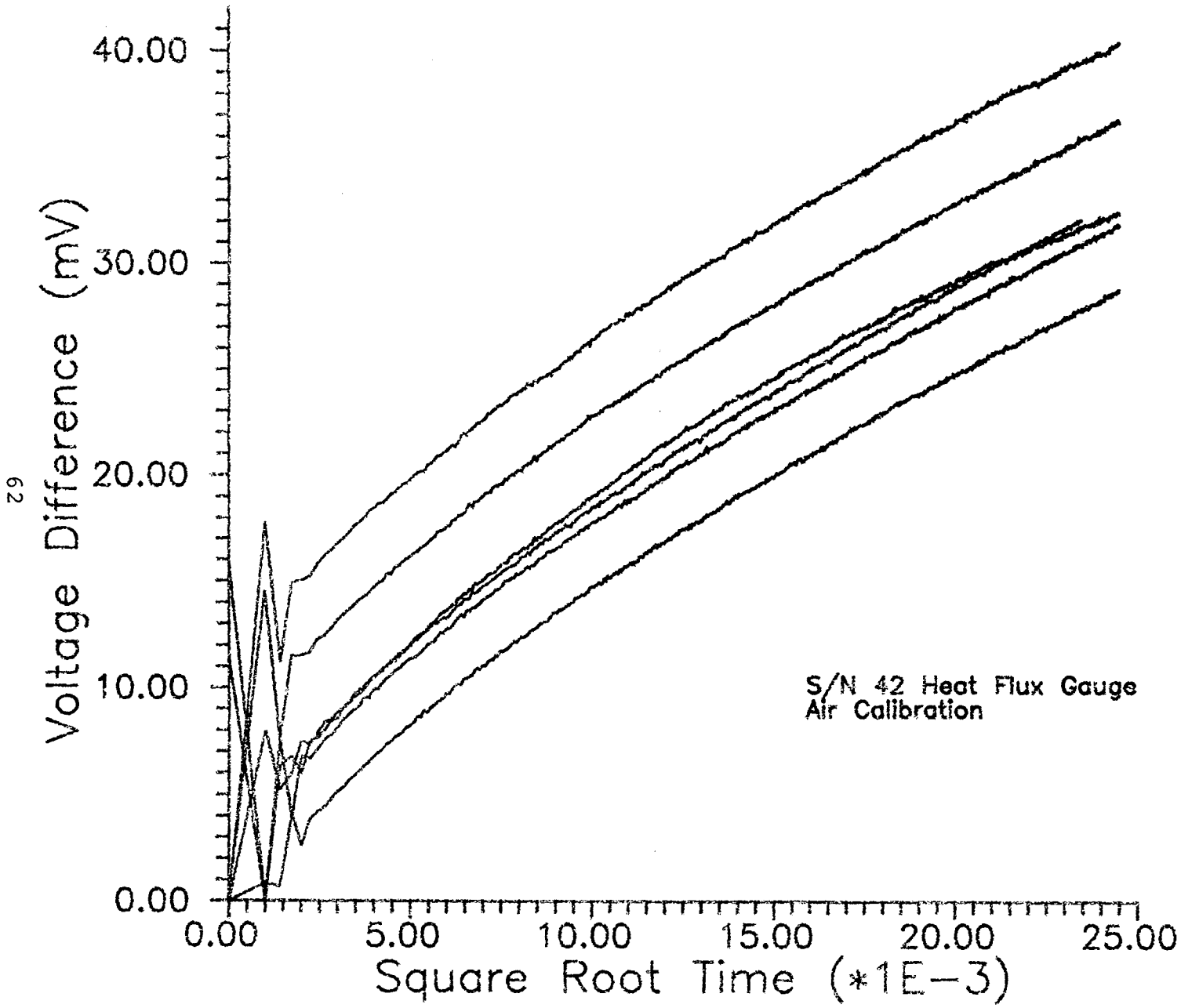
40.00
30.00
20.00
10.00
0.00
Voltage Difference (mV)
0.00
5.00
10.00
15.00
20.00
25.00
Square Root Time (*1E-3)
S/N 42 Heat Flux Gauge
Air Calibration

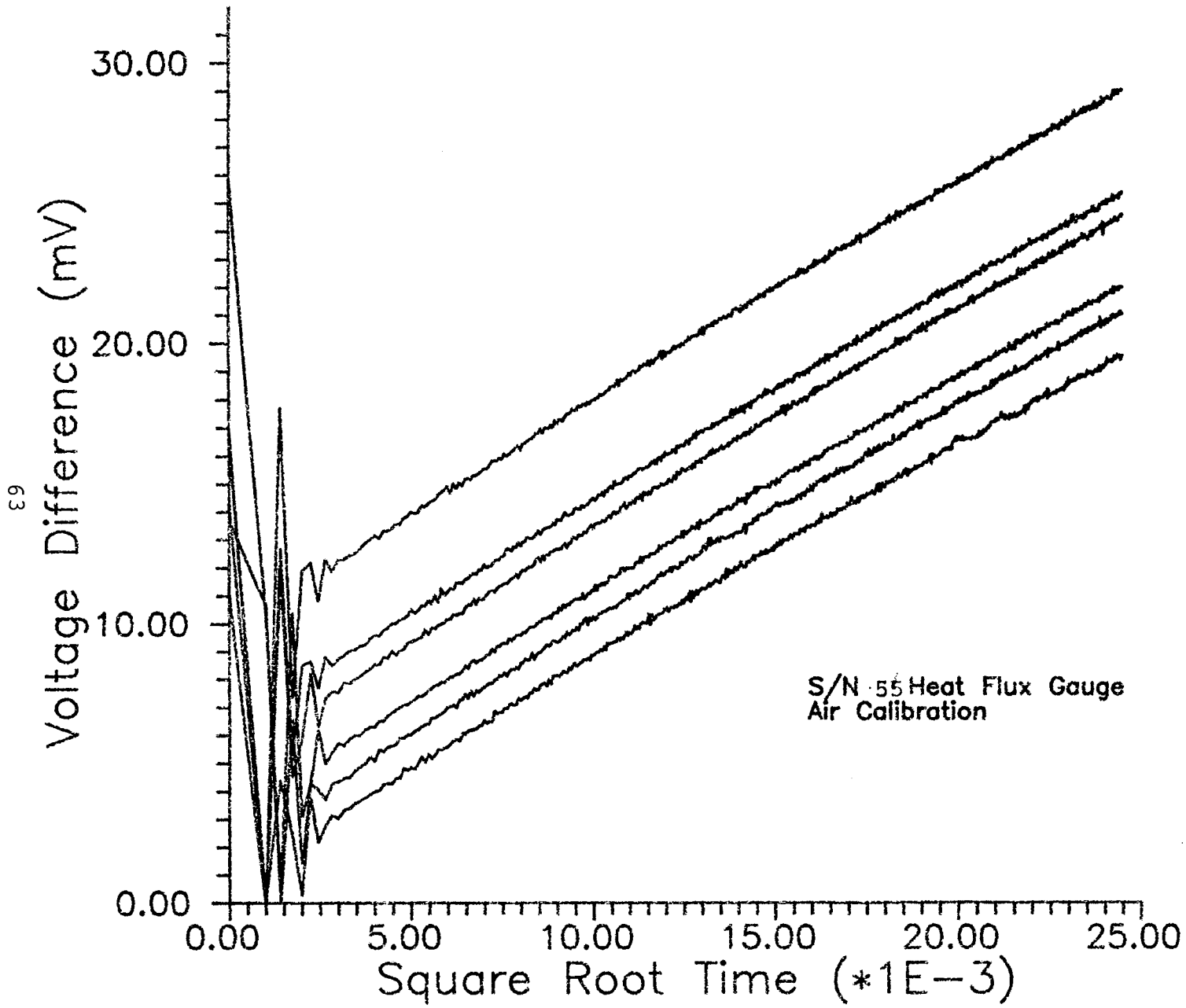
30.00
20.00
10.00
0.00
Voltage Difference (mV)
0.00
5.00
10.00
15.00
20.00
25.00
Square Root Time (*1E-3)
S/N 55 Heat Flux Gauge
Air Calibration

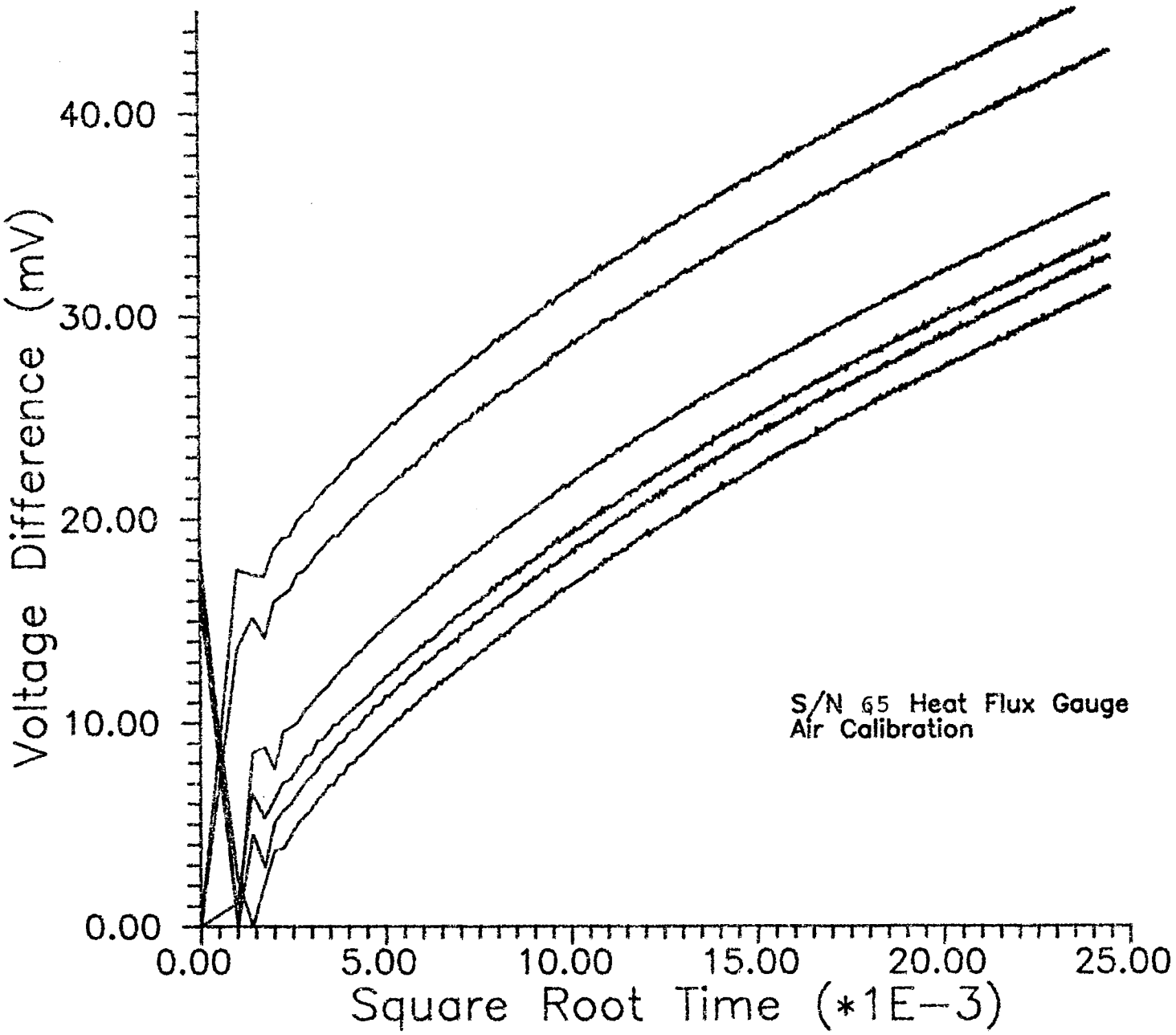
40.00
30.00
20.00
10.00
0.00
Voltage Difference (mV)
0.00
5.00
10.00
15.00
20.00
25.00
Square Root Time (*1E-3)
S/N 65 Heat Flux Gauge
Air Calibration

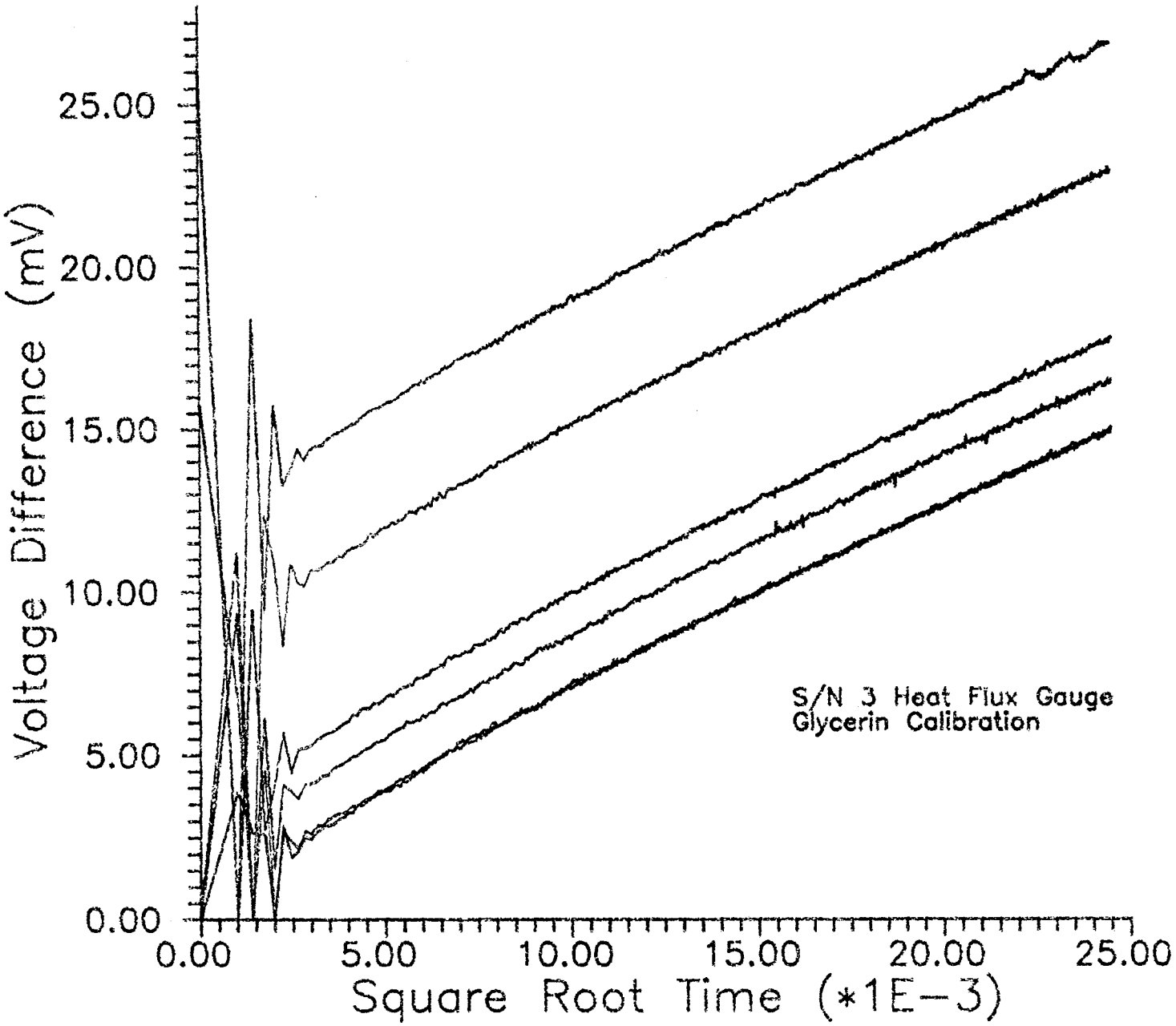
Voltage Difference (mV)
25.00
20.00
15.00
10.00
5.00
0.00
0.00
5.00
10.00
15.00
20.00
25.00
Square Root Time (*1E-3)
S/N 3 Heat Flux Gauge
Glycerin Calibration

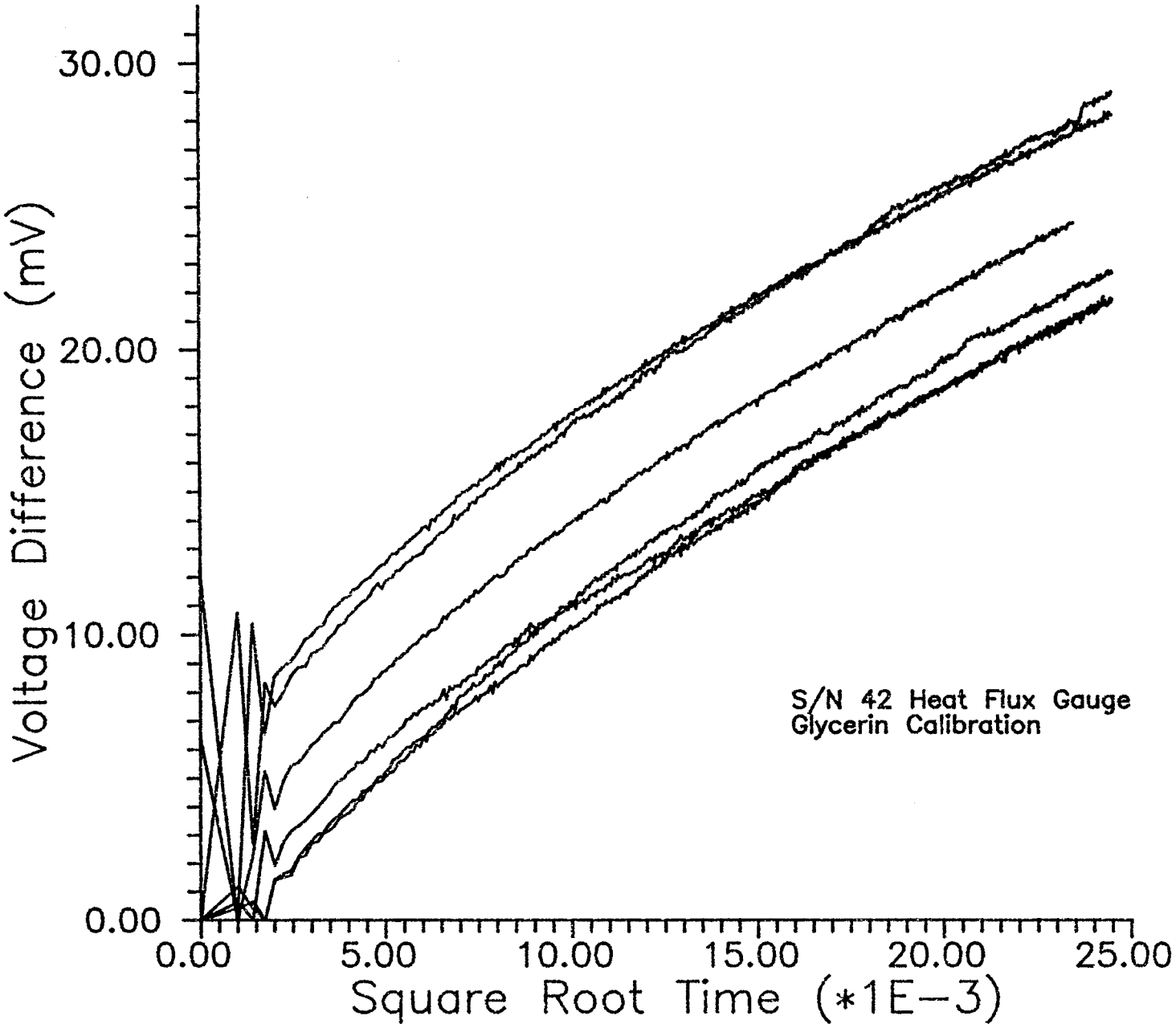
30.00
20.00
10.00
0.00
Voltage Difference (mV)
0.00
5.00
10.00
15.00
20.00
25.00
Square Root Time (*1E-3)
S/N 42 Heat Flux Gauge
Glycerin Calibration

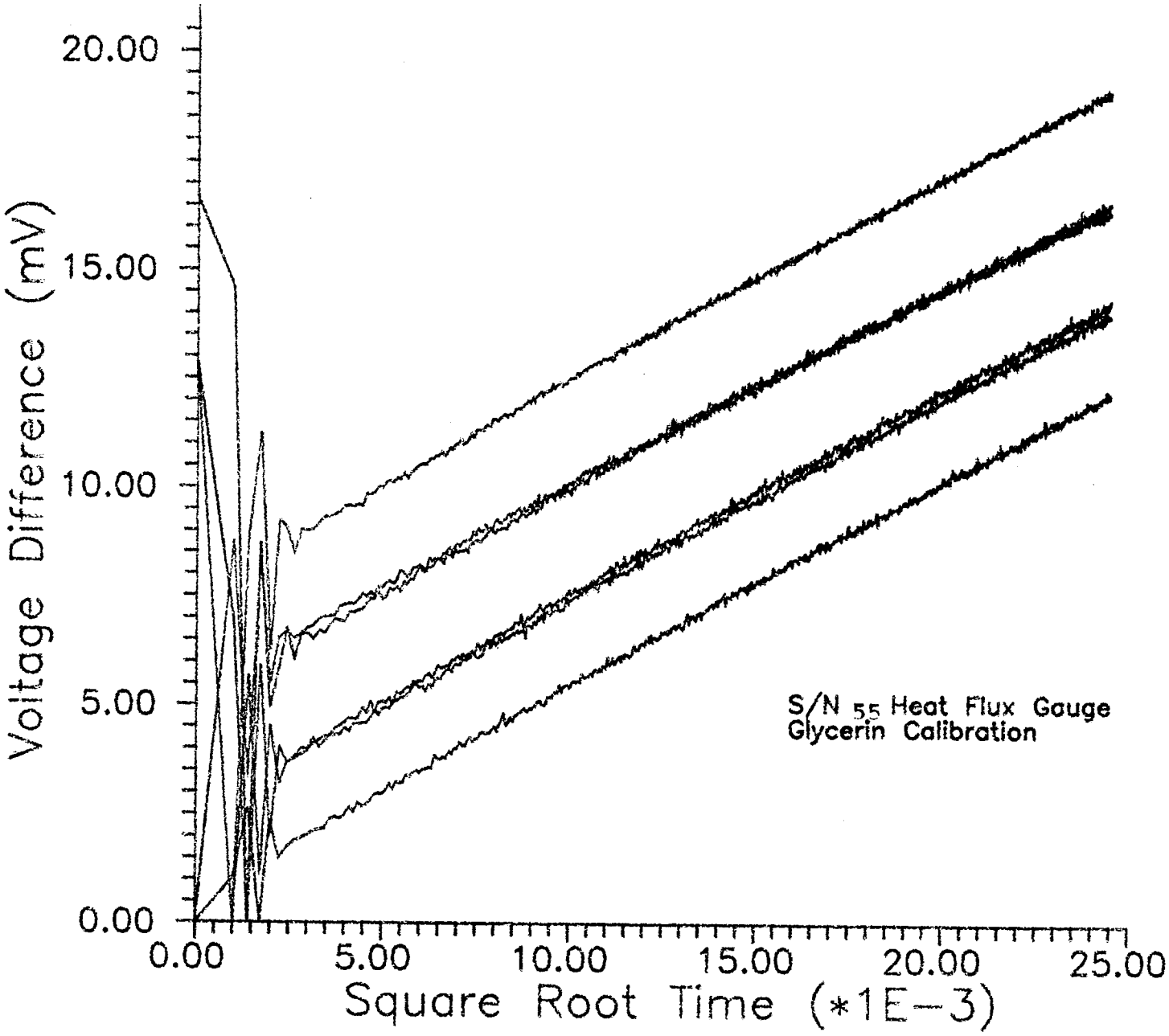
20.00
15.00
10.00
5.00
0.00
Voltage Difference (mV)
0.00
5.00
10.00
15.00
20.00
25.00
Square Root Time (*1E-3)
S/N 55 Heat Flux Gauge
Glycerin Calibration

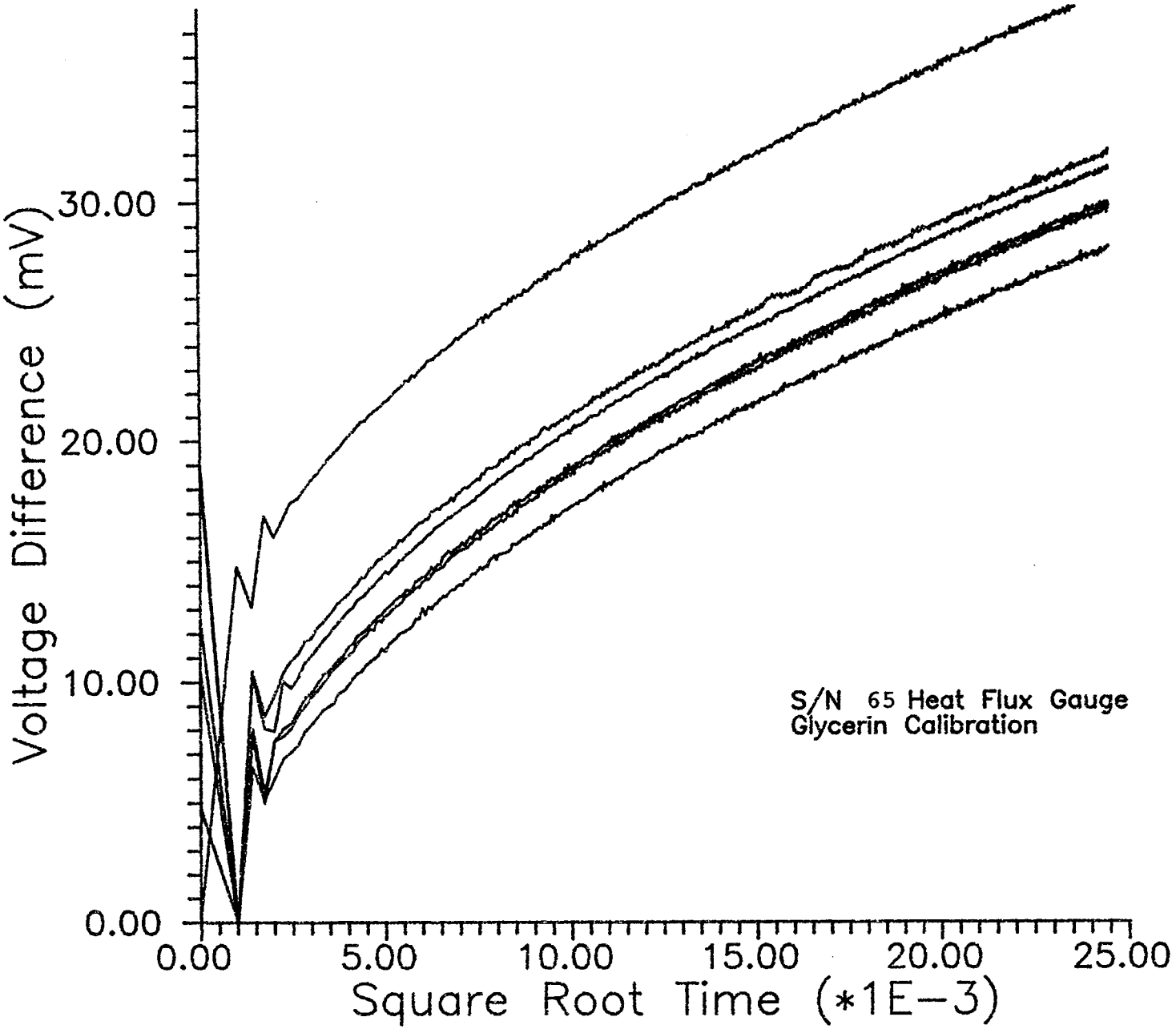
Voltage Difference (mV)
30.00
20.00
10.00
0.00
0.00
5.00
10.00
15.00
20.00
25.00
Square Root Time (*1E-3)
S/N 65 Heat Flux Gauge
Glycerin Calibration

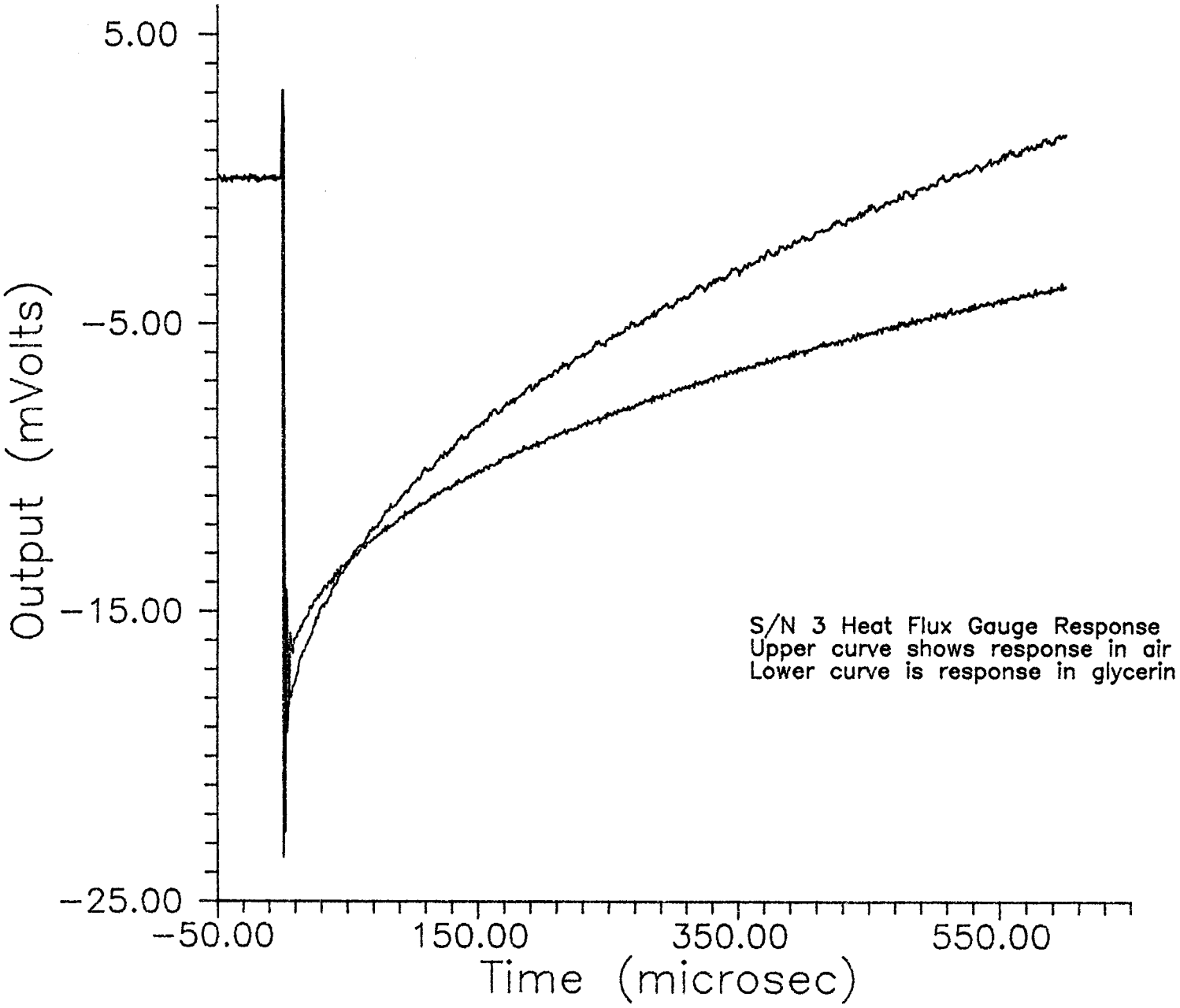
5.00
-5.00
-15.00
-25.00
Output (mVolts)
-50.00
150.00
350.00
550.00
Time (microsec)
S/N 3 Heat Flux Gauge Response
Upper curve shows response in air
Lower curve is response in glycerin

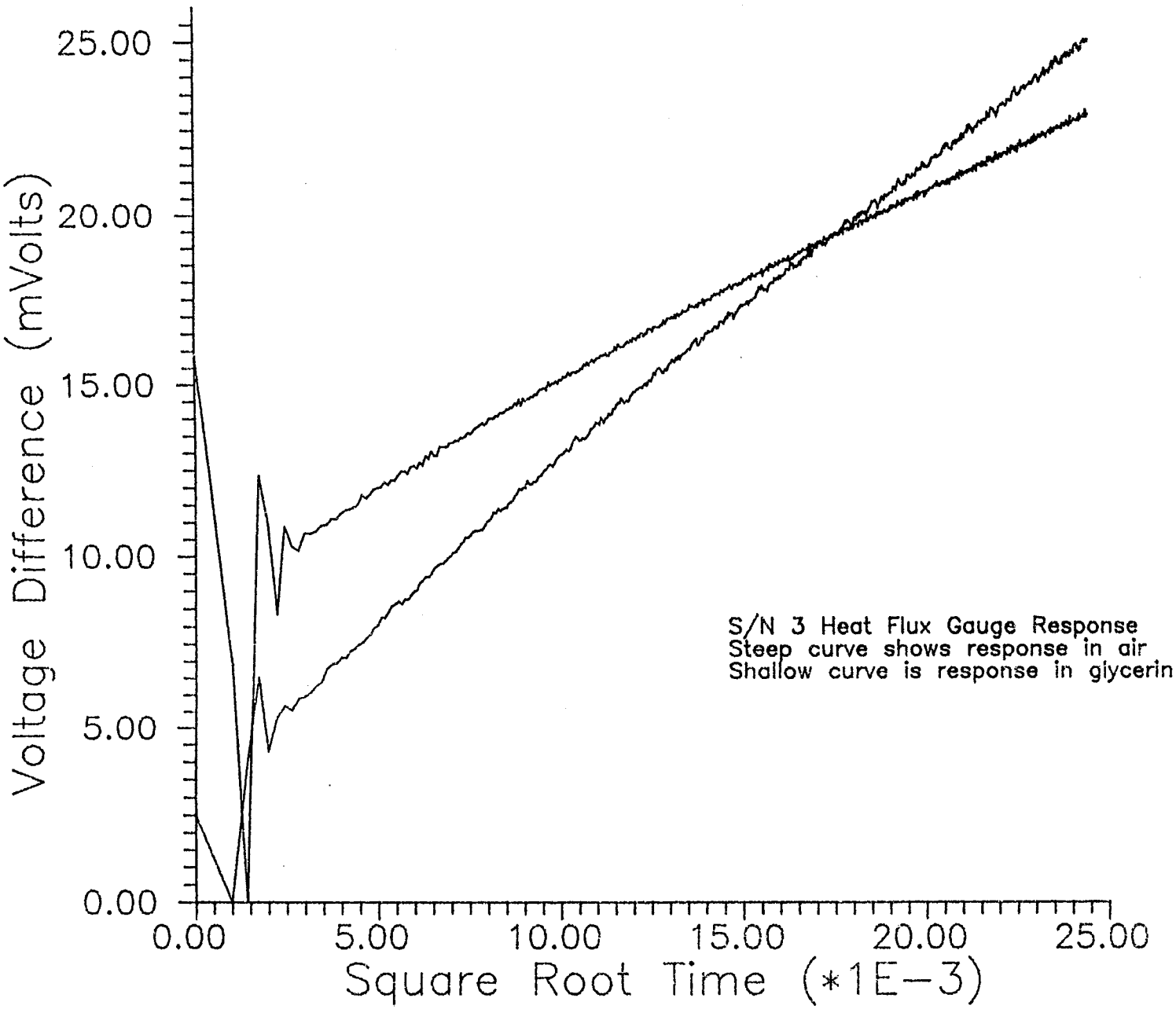
25.00
20.00
15.00
10.00
5.00
0.00
Voltage Difference (mVolts)
0.00
5.00
10.00
15.00
20.00
25.00
Square Root Time (*1E-3)
S/N 3 Heat Flux Gauge Response
Steep curve shows response in air
Shallow curve is response in glycerin

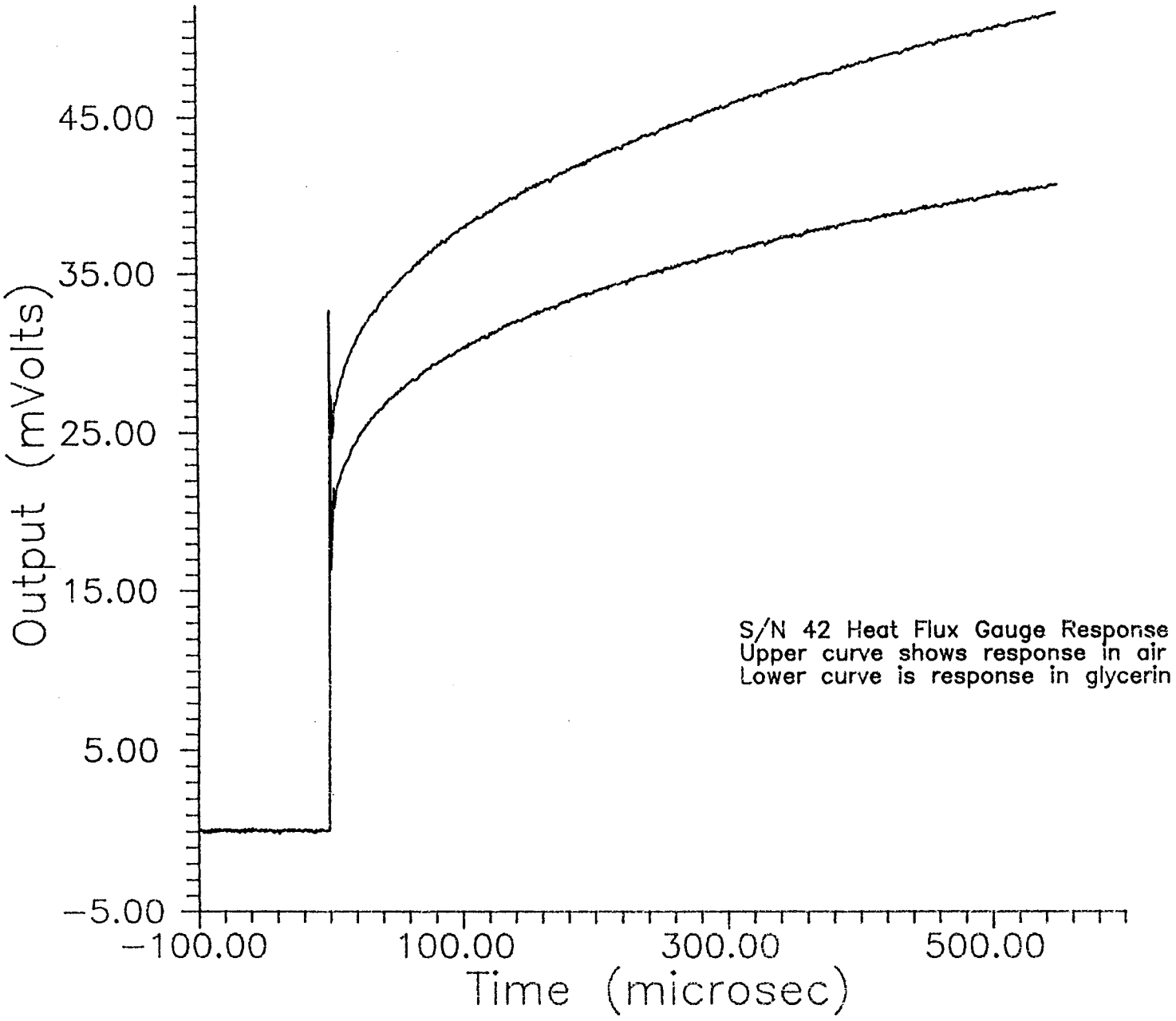
45.00
35.00
25.00
15.00
5.00
−5.00
Output (mVolts)
−100.00
100.00
300.00
500.00
Time (microsec)
S/N 42 Heat Flux Gauge Response
Upper curve shows response in air
Lower curve is response in glycerin

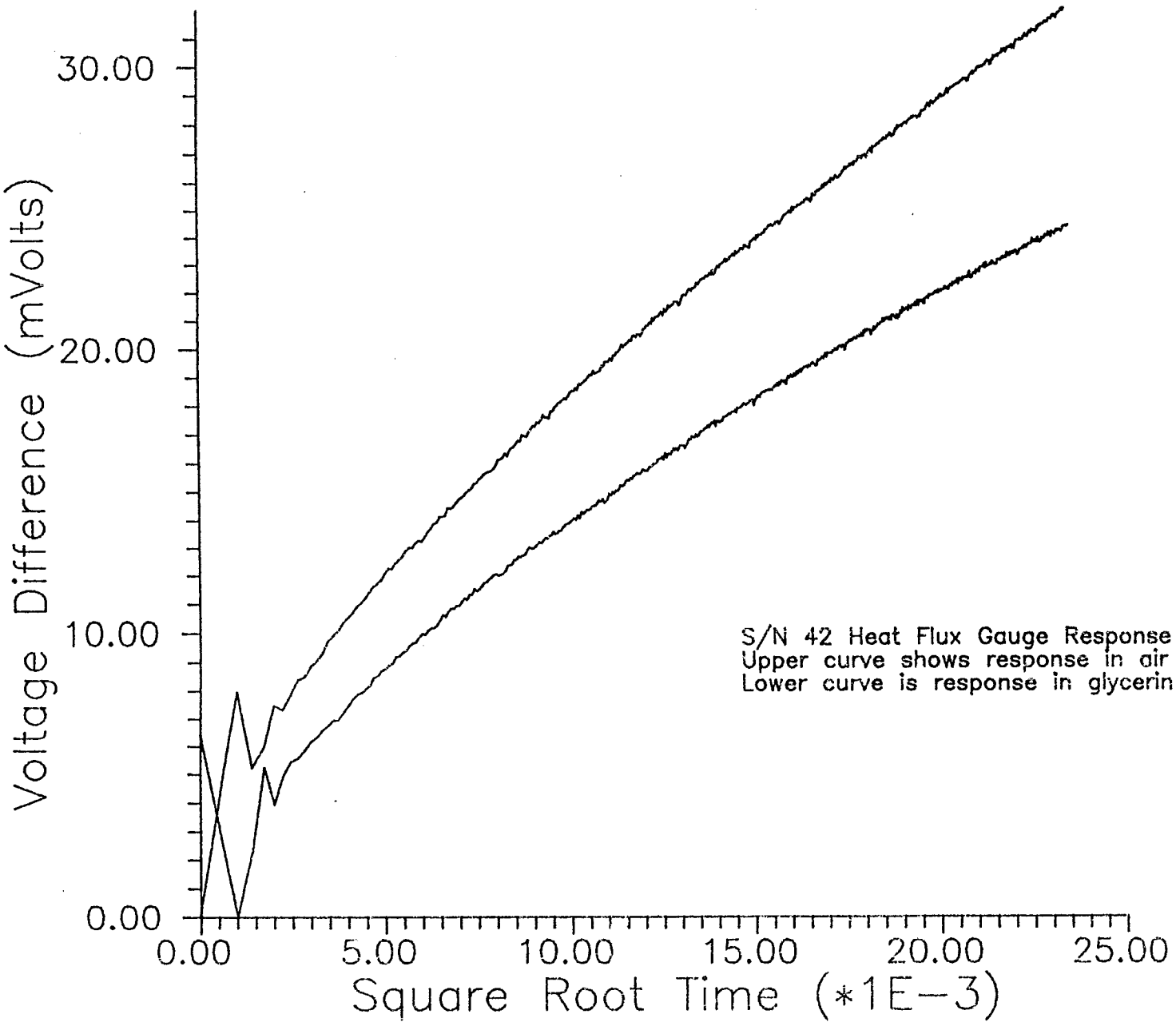
30.00
20.00
10.00
0.00
Voltage Difference (mVolts)
0.00
5.00
10.00
15.00
20.00
25.00
Square Root Time (*1E-3)
S/N 42 Heat Flux Gauge Response
Upper curve shows response in air
Lower curve is response in glycerin

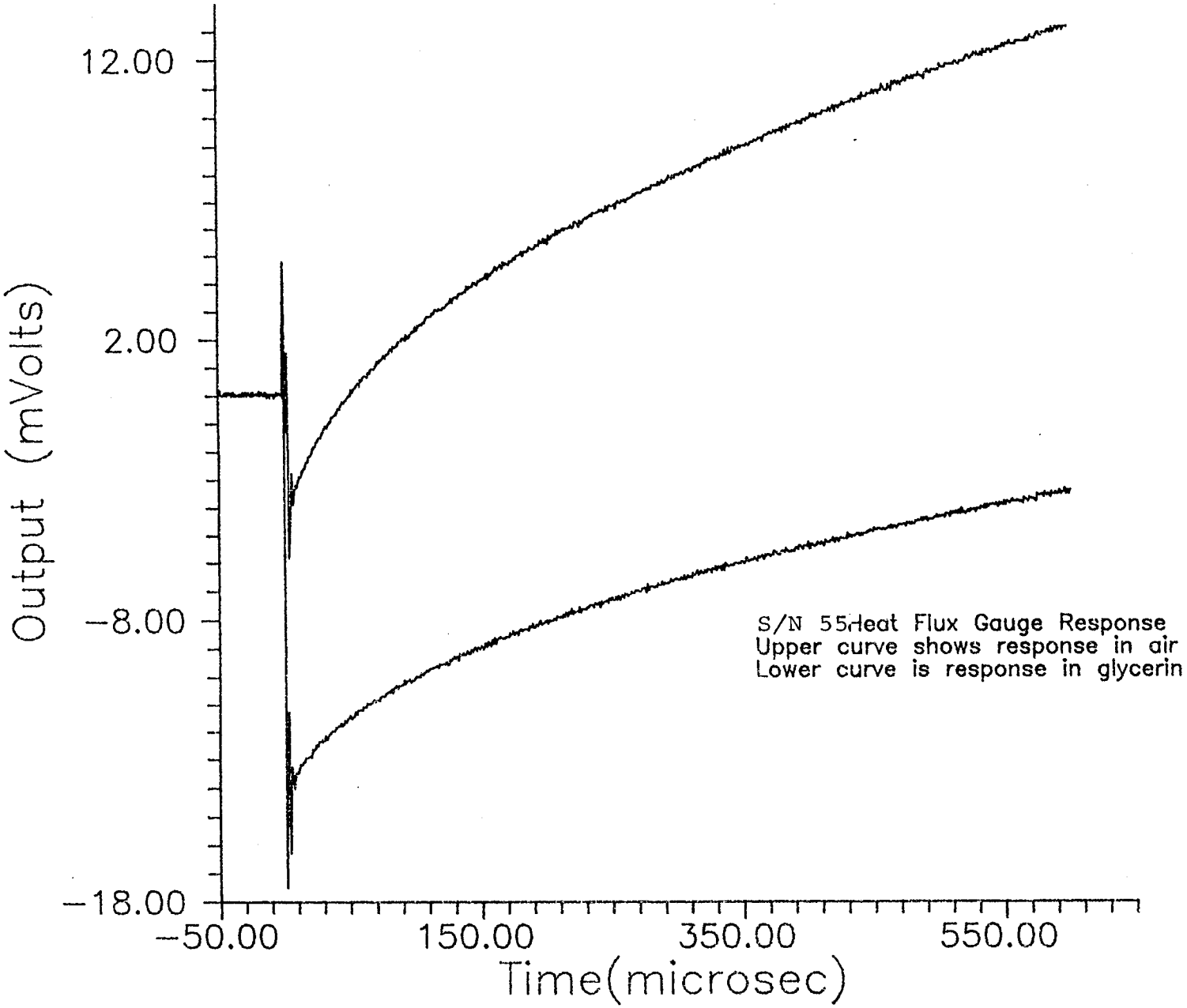
12.00
2.00
-8.00
-18.00
Output (mVolts)
-50.00
150.00
350.00
550.00
Time(microsec)
S/N 55Heat Flux Gauge Response
Upper curve shows response in air
Lower curve is response in glycerin

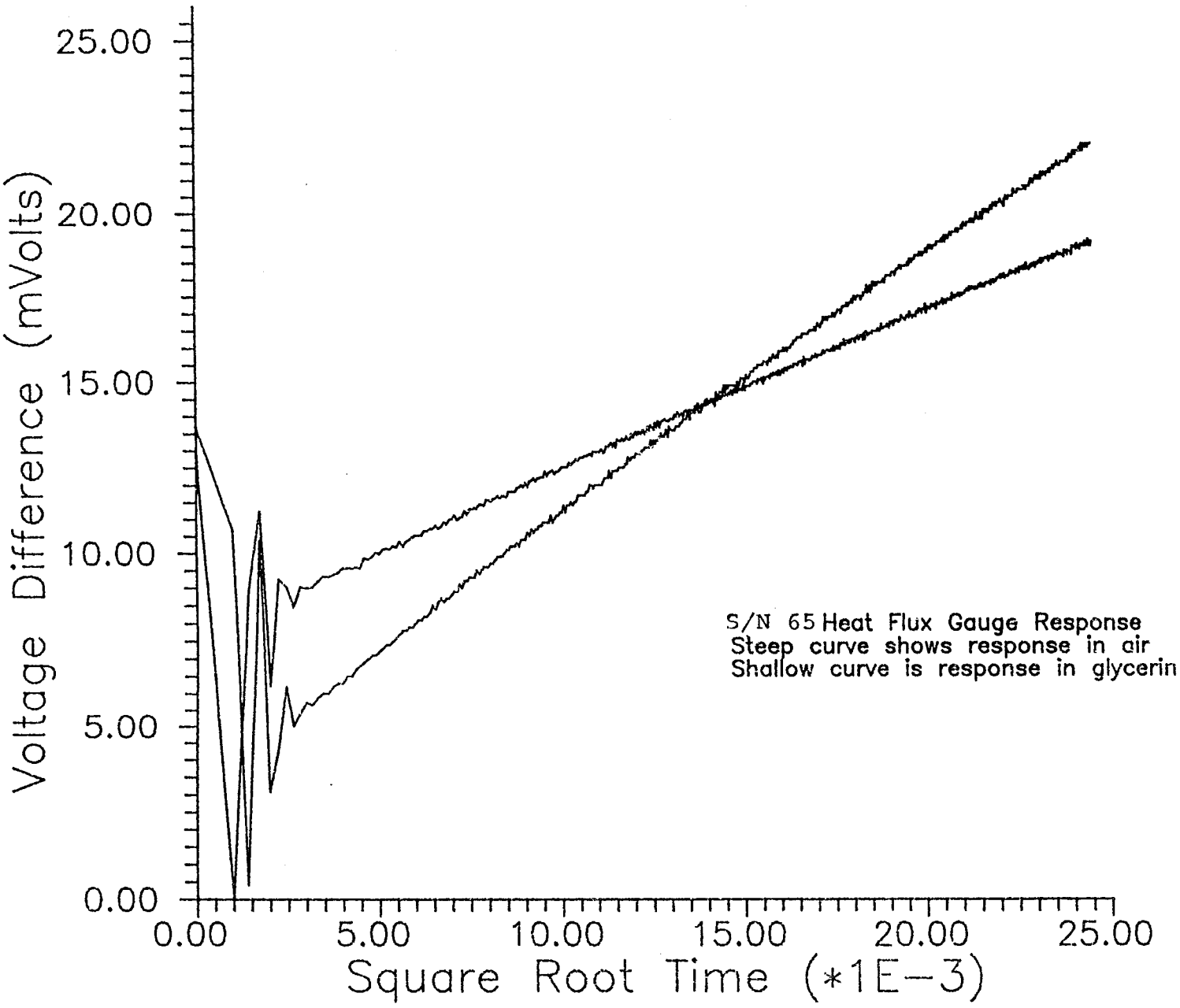
25.00
20.00
15.00
10.00
5.00
0.00
Voltage Difference (mVolts)
0.00
5.00
10.00
15.00
20.00
25.00
Square Root Time (*1E-3)
S/N 65 Heat Flux Gauge Response
Steep curve shows response in air
Shallow curve is response in glycerin

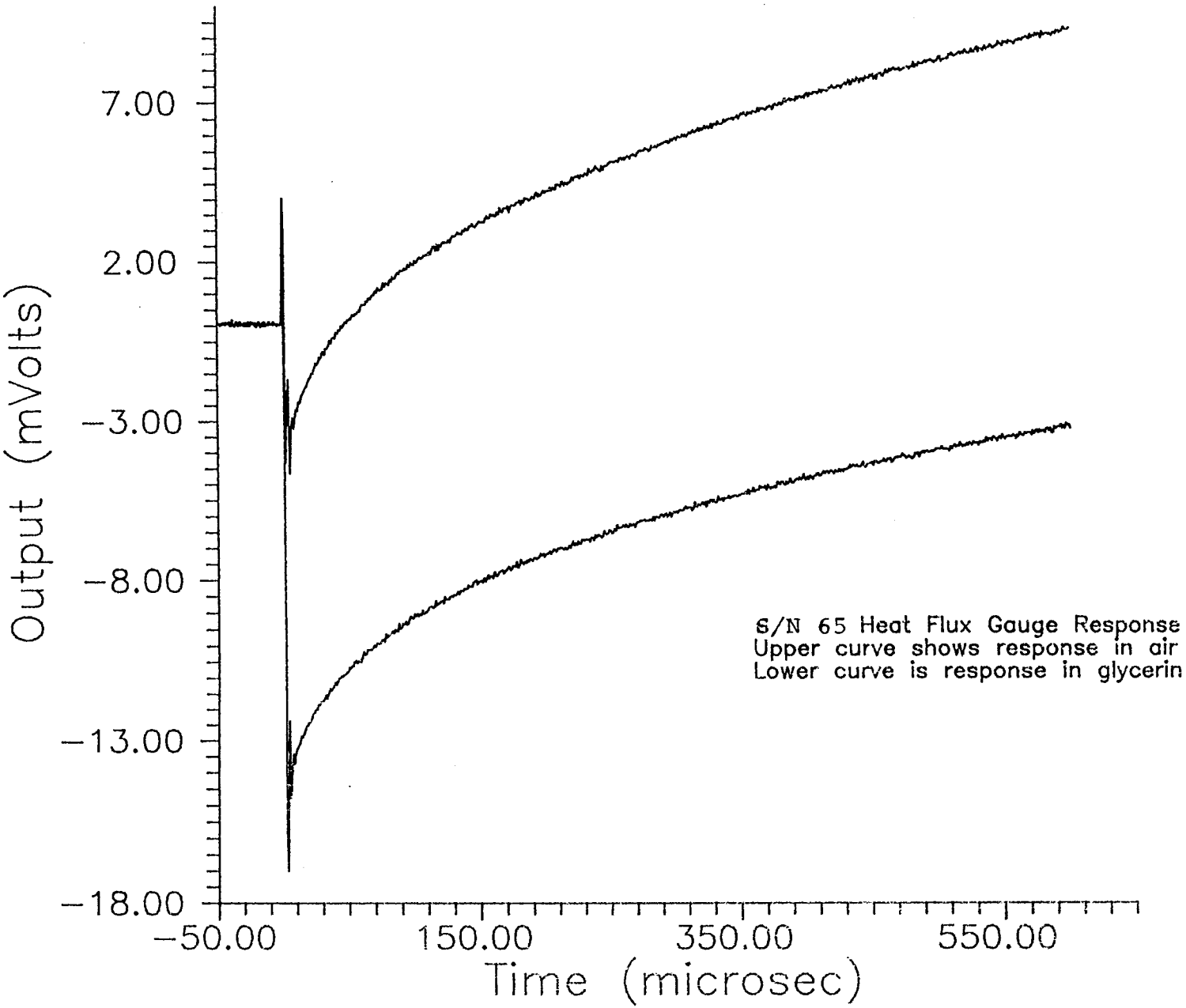
7.00
2.00
-3.00
-8.00
-13.00
-18.00
Output (mVolts)
-50.00
150.00
350.00
550.00
Time (microsec)
S/N 65 Heat Flux Gauge Response
Upper curve shows response in air
Lower curve is response in glycerin

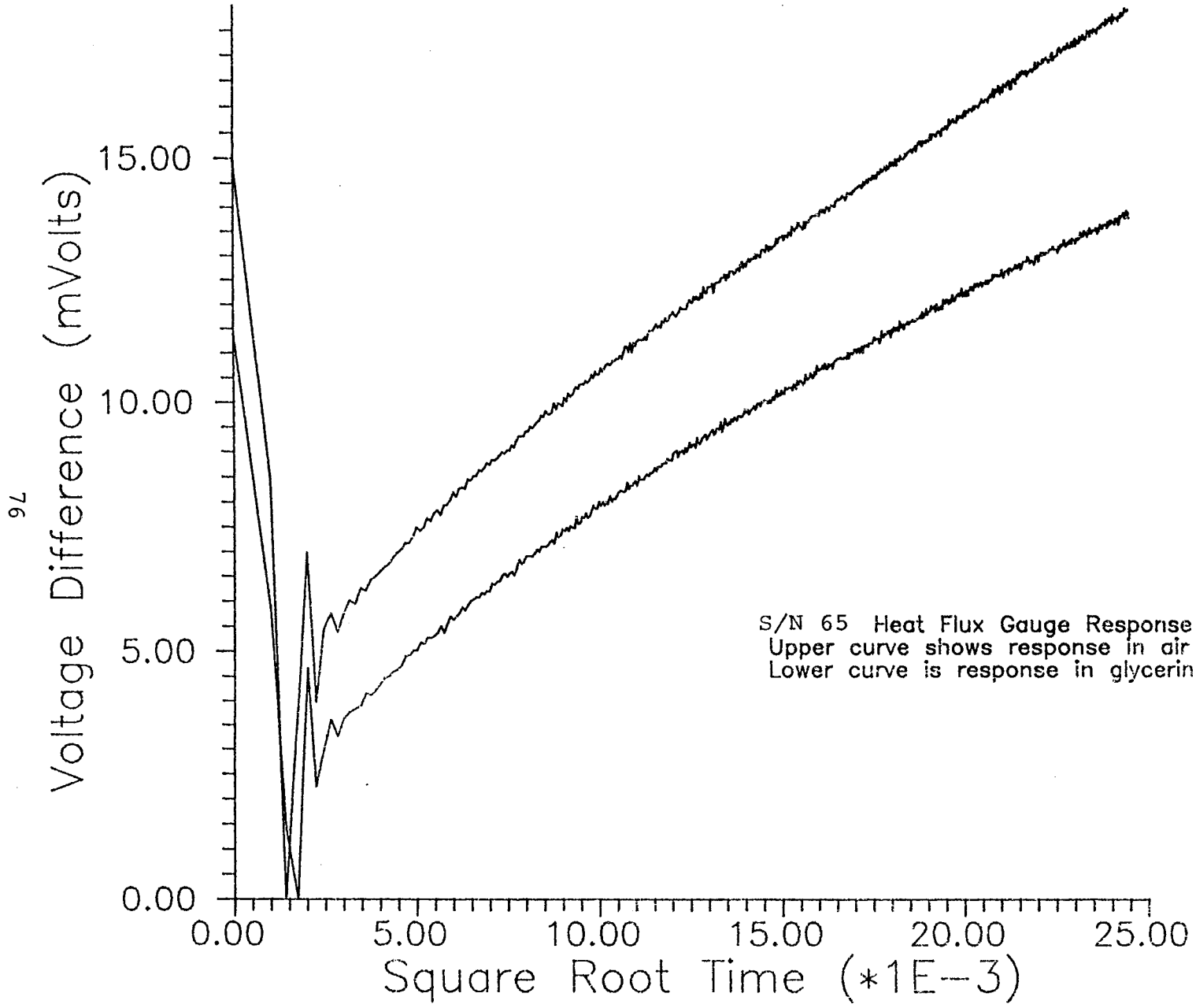
Voltage Difference (mVolts)
15.00
10.00
5.00
0.00
0.00
5.00
10.00
15.00
20.00
25.00
Square Root Time (*1E-3)
S/N 65 Heat Flux Gauge Response
Upper curve shows response in air
Lower curve is response in glycerin

Appendix C

This section contains the computer codes used to analyze data, listed in the order used: TESTER, FLTPLT, CRUNCHER, and BLOWDOT. The codes include their own introduction and explanations where necessary, and are followed by representative input and output files, shortened in some cases to save space.

```
      program tester
*
*  This program creates a temperature profile from the exact solution of a
*  semi-infinite flat plate convection problem, for the surface of the plate.
*  This solution assumes a constant h, and known properties
*  of the slab, such as rho, cp, and k.  It then uses this temperature profile
*  as a check for a heat transfer algorithm.  First derived by Cook and
*  Felderman and later simplified by Bonafede, this algorithm seeks to give
*  the surface heat flux into a thin film heat-flux gauge as a function of time,
*  given a temperature profile and the aforementioned slab characteristics.
*
*  Enter in the properties of the slab, heat transfer coefficient, and time
*  increment between data points, temperature of air, temp of wall.
*
       real lam,inc
       dimension t(1001),temp(1001)
*
      write(*,*) 'enter sqrt(rho*cp*k)'
      read(*,*) rck
*
      write(*,*) 'enter h, time increment between data points'
      read(*,*) h,inc
*
      write(*,*) 'enter air temp, initial wall temp'
      read(*,*) ta,tw
*
       lam=0.00d0
       pi=3.1415926535898d0
       n=1000
       temp(1)=tw
       t(1)=0.00d0
       write(*,*) '  __# ___time____lambda____erf(lam)___Temp'
*
        do 10 i=2,n
        t(i)=t(i-1)+inc
        lam=(h*sqrt(t(i))/rck)
        sq=lam**2.d0
        theta=1.d0-exp(sq)*(1.d0-erf(lam))
        temp(i)=theta*(ta-tw)+tw
        write(*,*) i,t(i),lam,erf(lam),temp(i)
*
 10      continue
*
*  Part Two
*
       write(*,*) 'time         calc q         calc h'
       t(1)=0.00d0
        do 20 j=2,n
        t(j)=t(j-1)+inc
        term1=0.0d0
        term2=0.00d0
        do 30 k=2,j
         sum=(temp(k)-temp(k-1))/(sqrt(t(j)-t(k))+sqrt(t(j)-t(k-1)))
         term2=term2+sum
 30      continue
*
         q=2.d0*rck/sqrt(pi)*(term1+term2)
         h2=q/(ta-temp(j))
         write(*,*) t(j),q,h2
 20      continue
*
         stop
         end
```

```
copperhead:@~> tester

enter sqrt(rho*cp*k)
1520.d0

enter h
200.d0

enter time increment between data points
5.e-6d0

enter air temp
600.d0

enter wall temp
295.d0
```

#	time	lambda	erf(lam)	Temp
2	5.00000E-06	2.94219E-04	3.31991E-04	295.101
3	1.00000E-05	4.16089E-04	4.69506E-04	295.143
4	1.50000E-05	5.09603E-04	5.75025E-04	295.175
5	2.00000E-05	5.88439E-04	6.63982E-04	295.202
6	2.50000E-05	6.57895E-04	7.42355E-04	295.226
7	3.00000E-05	7.20688E-04	8.13209E-04	295.248
8	3.50000E-05	7.78431E-04	8.78366E-04	295.268
9	4.00000E-05	8.32178E-04	9.39013E-04	295.286
10	4.50000E-05	8.82658E-04	9.95973E-04	295.304
11	5.00000E-05	9.30404E-04	1.04985E-03	295.320
12	5.50000E-05	9.75816E-04	1.10109E-03	295.336
13	6.00000E-05	1.01921E-03	1.15005E-03	295.350
14	6.50000E-05	1.06082E-03	1.19701E-03	295.365
15	7.00000E-05	1.10087E-03	1.24220E-03	295.379
16	7.50000E-05	1.13951E-03	1.28580E-03	295.392
17	8.00000E-05	1.17688E-03	1.32796E-03	295.405
18	8.50000E-05	1.21310E-03	1.36883E-03	295.417
19	9.00000E-05	1.24827E-03	1.40852E-03	295.429
20	9.50000E-05	1.28247E-03	1.44712E-03	295.441
21	1.00000E-04	1.31579E-03	1.48471E-03	295.452
22	1.05000E-04	1.34828E-03	1.52137E-03	295.463
23	1.10000E-04	1.38001E-03	1.55718E-03	295.474
24	1.15000E-04	1.41103E-03	1.59217E-03	295.485
25	1.20000E-04	1.44138E-03	1.62642E-03	295.495
26	1.25000E-04	1.47110E-03	1.65995E-03	295.506
27	1.30000E-04	1.50023E-03	1.69283E-03	295.516
28	1.35000E-04	1.52881E-03	1.72508E-03	295.525
29	1.40000E-04	1.55686E-03	1.75673E-03	295.535
30	1.45000E-04	1.58442E-03	1.78783E-03	295.545
979	4.88998E-03	9.20111E-03	1.03820E-02	298.141
980	4.89498E-03	9.20581E-03	1.03873E-02	298.143
981	4.89998E-03	9.21051E-03	1.03927E-02	298.144
982	4.90498E-03	9.21521E-03	1.03980E-02	298.146
983	4.90998E-03	9.21990E-03	1.04033E-02	298.147
984	4.91498E-03	9.22460E-03	1.04085E-02	298.149
985	4.91998E-03	9.22929E-03	1.04138E-02	298.150
986	4.92498E-03	9.23398E-03	1.04191E-02	298.152
987	4.92998E-03	9.23866E-03	1.04244E-02	298.154
988	4.93498E-03	9.24334E-03	1.04297E-02	298.155
989	4.93998E-03	9.24802E-03	1.04350E-02	298.157
990	4.94498E-03	9.25270E-03	1.04403E-02	298.158
991	4.94998E-03	9.25738E-03	1.04455E-02	298.160
992	4.95498E-03	9.26206E-03	1.04508E-02	298.162
993	4.95998E-03	9.26673E-03	1.04561E-02	298.163
994	4.96498E-03	9.27140E-03	1.04613E-02	298.165
995	4.96998E-03	9.27606E-03	1.04666E-02	298.166

996	4.97498E-03	9.28073E-03	1.04719E-02	298.168
997	4.97998E-03	9.28539E-03	1.04771E-02	298.170
998	4.98498E-03	9.29005E-03	1.04824E-02	298.171
999	4.98998E-03	9.29471E-03	1.04877E-02	298.173
1000	4.99498E-03	9.29936E-03	1.04929E-02	298.174

time	calc q	calc h
5.00000E-06	77644.2	254.656
1.00000E-05	64323.8	210.997
1.50000E-05	62672.4	205.601
2.00000E-05	62009.5	203.445
2.50000E-05	61717.6	202.503
3.00000E-05	61538.3	201.929
3.50000E-05	61395.8	201.474
4.00000E-05	61305.7	201.191
4.50000E-05	61235.5	200.972
5.00000E-05	61202.9	200.876
5.50000E-05	61153.7	200.725
6.00000E-05	61115.1	200.608
6.50000E-05	61132.4	200.674
7.00000E-05	61074.0	200.491
7.50000E-05	61042.6	200.397
8.00000E-05	61049.2	200.427
8.50000E-05	61041.1	200.409
9.00000E-05	61029.3	200.378
9.50000E-05	60993.8	200.269
1.00000E-04	60998.7	200.293
1.05000E-04	60999.5	200.303
1.10000E-04	60987.3	200.270
1.15000E-04	60957.5	200.179
1.20000E-04	61000.7	200.328
1.25000E-04	60966.6	200.222
1.30000E-04	60946.6	200.163
1.35000E-04	60940.1	200.148
1.40000E-04	60953.5	200.199
1.45000E-04	60945.6	200.179
1.50000E-04	60925.7	200.120
1.55000E-04	60916.6	200.096
4.90498E-03	60385.1	200.047
4.90998E-03	60372.0	200.005
4.91498E-03	60370.1	200.000
4.91998E-03	60346.1	199.921
4.92498E-03	60383.2	200.045
4.92998E-03	60371.9	200.009
4.93498E-03	60371.3	200.008
4.93998E-03	60371.6	200.010
4.94498E-03	60372.2	200.013
4.94998E-03	60373.1	200.017
4.95498E-03	60350.8	199.944
4.95998E-03	60389.1	200.072
4.96498E-03	60355.6	199.962
4.96998E-03	60369.7	200.010
4.97498E-03	60349.7	199.945
4.97998E-03	60389.4	200.077
4.98498E-03	60356.9	199.971
4.98998E-03	60348.5	199.944
4.99498E-03	60389.7	200.081

```
      program fltplt
*
*   This program reads in a data file of volts and time (the output of a
*   thin film heat flux gauge), along with a measured p5 and ambient (initial
*   wall) temperature.  It then solves for a "measured" T5 by using predicted p5
*   and T5 from SHOCKTUN and measured p5 through an isentropic relation.
*   Using this T5 as stagnation temp. and adiabatic, calorically perfect
*   assumptions, solve for adiabatic wall temp. by using a recovery factor.
*
      real m
      character name*10
      dimension volt(1001), t(1001), temp(1001), vneg(101), tneg(101)
      dimension q(1001),h2(1001)
*
      write(*,*) 'enter sqrt(rho*cp*k), temp coefficient (K/Volt)'
      read(*,*) rck,conv
      write(*,*) 'enter file name'
      read(*,*) name
      write(*,*) 'enter ambient temp (F), press. ("Hg) at start of test time'
      read(*,*) tamb,pamb
      write(*,*) 'enter deltaVolts from p gauge'
      read(*,*) v2
*
      pi=3.1415926535898d0
      tamb=(tamb+459.67d0)*5.d0/9.d0
      pamb=pamb*3386.38816
*
*   In next lines also replace .4,1.4,and .2's with a better gamma.
*
      temp2p=355.5287
      m=.430147
      p2pred=1.84368453e5
      p2=v2*47950.8533+pamb
      temp2=temp2p*(p2/p2pred)**(.398/1.398)
      taw=temp2*(1.d0+.199d0*m**2.d0)
      write(*,*) 'p2    Temp2    Taw'
      write(*,*) p2,temp2,taw
*
      write(*,*) 'time    Volts    temp'
       open(1,file=name,status='old')
       do 3 i=1,99
         read(1,*) vneg(i),tneg(i)
 3      continue
        read(1,*) volt(1),t(1)
        volt1=volt(1)
        volt(1)=0.0d0
        temp(1)=tamb
        write(*,*) t(1),volt(1)
        do 10 i=2,900
         read(1,*) volt(i), t(i)
         volt(i)=volt(i)-volt1
         temp(i)=conv*volt(i)+tamb
         write(*,*) t(i),volt(i),temp(i)
 10      continue
*
      write(*,*) name
      write(*,*) 'time          calc q          calc h'
       do 20 j=2,900
*
       term1=0.0d0
*
       term2=0.00d0
       do 30 k=2,j
        sum=(temp(k)-temp(k-1))/(sqrt(t(j)-t(k))+sqrt(t(j)-t(k-1)))
        term2=term2+sum
 30     continue
```

```
*
        q(j)=2.d0*rck/sqrt(pi)*(term1+term2)
        h2(j)=q(j)/(taw-temp(j))
        write(*,*) t(j),q(j),h2(j)
 20     continue
*
        qsum=0.d0
        hsum=0.d0
        do 40 l=521,720
         qsum=qsum+q(l)
         hsum=hsum+h2(l)
 40      continue
*
        qave=qsum/200.d0
        have=hsum/200.d0
        write(*,*) '   avg q    avg h'
        write(*,*) qave,have
        stop
        end
```

INPUT

enter sqrt(rho*cp*k), temp coefficient (K/Volt)

1520, 19.05735

enter file name

run75.dat

enter ambient temp (F), press. ("Hg) at start of test time

69.8, 29.025

enter deltaVolts from p gauge

1.224

OUTPUT

p2	Temp2	Taw
156982.	339.619	352.124

time	Volts	temp
5.00000E-06	9.60002E-04	294.168
1.00000E-05	1.76000E-03	294.184
1.50000E-05	2.72000E-03	294.202
4.48500E-03	0.175200	297.489
4.49000E-03	0.175200	297.489
4.49500E-03	0.175040	297.486

time	calc q	calc h
5.00000E-06	14021.4	241.931
1.00000E-05	17511.8	302.237
1.50000E-05	23349.2	403.112
2.00000E-05	24975.1	431.295
2.50000E-05	22770.7	393.289
3.00000E-05	18480.8	319.212
3.50000E-05	19578.2	338.204
4.48500E-03	70709.2	1294.20
4.49000E-03	68437.8	1252.63
4.49500E-03	65230.9	1193.86

avg q	avg h
65614.1	1167.20

```
      program cruncher
*
*   This program reads in a data file of volts and time (the output of a
*   thin film heat flux gauge), along with a measured p5 and ambient (initial
*   wall) temperature.  It then solves for a "measured" T5 by using predicted p5
*   and T5 from SHOCKTUN and measured p5 through an isentropic relation.
*   Using this T5 as stagnation temp. and adiabatic, calorically perfect
*   assumptions, solve for adiabatic wall temp. by using a recovery factor.
*
      real m
      character name*9
      dimension volt(2501), t(2501), temp(2501), vneg(2001), tneg(2001)
      dimension q(2501),h2(2501)
*
      write(*,*) 'enter sqrt(rho*cp*k), temp coefficient (K/Volt)'
      read(*,*) rck,conv
      write(*,*) 'enter file name'
      read(*,*) name
      write(*,*) 'enter ambient temp (F), press. (" Hg) at test time'
      read(*,*) tamb,pamb
      write(*,*) 'enter Volts from subsonic p. gauge, Mach # at h. gauge'
      read(*,*) v5,m
*
      pi=3.1415926535898d0
*   Units conversion
*
      tamb=(tamb+459.67d0)*5.d0/9.d0
      pamb=pamb*3386.38816
*
*   Isentropic solution for p5 and t5 allows calculation of true stagnation
*   conditions using isent. relations on measured subsonic press.
*
      pgau=v5*2.613521724e5+pamb
      p5=pgau*1.0115937
      t5=546.005d0*(p5/7.106733e5)**(.389/1.389)
      tinf=t5/(1.d0+.1945d0*m**2.d0)
      taw=tinf*(1.d0+.1945d0*.892112d0*m**2.d0)
*
*
      write(*,*) 'p5    Temp5    Taw'
      write(*,*) p5,t5,taw
*
      write(2,*) 'time   Volts    Temp'
*
      open(1,file=name,status='old')
*
      open(2,file='crunch.out',status='old')
*
*   Put in here # of points to skip ( up to point where nozzle starts )
*
      do 3 i=1,150
        read(1,*) vneg(i),tneg(i)
3     continue
*
      read(1,*) volt(1),t(1)
      volt1=volt(1)
      volt(1)=0.0d0
      temp(1)=tamb
      write(2,*) t(1),volt(1),temp(1)
*
*   Make the number of iterations here at least enough to cover the action time
*
      do 10 i=2,2500
       read(1,*) volt(i), t(i)
       volt(i)=volt(i)-volt1
       temp(i)=conv*volt(i)+tamb
```

```
          write(2,*) t(i),volt(i),temp(i)
 10       continue
*
*
      write(2,*) name
      write(2,*) 'time        calc q        calc h'
*
*   Make this the same as the 10 do loop
*
       do 20 j=2,2500
*
       term1=0.0d0
*
       term2=0.00d0
       do 30 k=2,j
        sum=(temp(k)-temp(k-1))/(sqrt(t(j)-t(k))+sqrt(t(j)-t(k-1)))
        term2=term2+sum
 30     continue
*
        q(j)=2.d0*rck/sqrt(pi)*(term1+term2)
        h2(j)=q(j)/(taw-temp(j))
        write(2,*) t(j),q(j),h2(j)
 20     continue
*
        qsum=0.d0
        hsum=0.d0
*
*   This loop should iterate the # of points in the action time, but start
*   averaging after about 10 iterations, to get a steady value.
*
        do 40 l=21,2500
         qsum=qsum+q(l)
         hsum=hsum+h2(l)
 40      continue
*
*   Don't forget to divide by the correct # of points!
*
        qave=qsum/2479.d0
        have=hsum/2479.d0
        write(2,*) '   avg q    avg h'
        write(2,*) qave,have
*
        stop
        end
```

INPUT

enter sqrt(rho*cp*k), temp coefficient (K/Volt)

1520, 19.05735

enter file name

blow64

enter ambient temp (F), press. (" Hg) at test time

70, 29.02

enter Volts from subsonic p. gauge, Mach # at h. gauge

1.61, 1.1713

OUTPUT

p5	Temp5	Taw
525068.	501.628	490.228

Time	Volts	Temp
1.00000E-06	0.	294.261
2.00000E-06	3.20001E-04	294.267
3.00000E-06	8.00001E-04	294.276
4.00000E-06	9.60000E-04	294.279
5.00000E-06	1.44000E-03	294.289
6.00000E-06	1.76000E-03	294.295
7.00000E-06	2.24000E-03	294.304
8.00000E-06	2.72000E-03	294.313
9.00000E-06	3.36000E-03	294.325
1.00000E-05	3.68000E-03	294.331
1.10000E-05	4.32000E-03	294.343
2.49600E-03	0.330720	300.564
2.49700E-03	0.330880	300.567
2.49800E-03	0.330720	300.564
2.49900E-03	0.330720	300.564
2.50000E-03	0.330560	300.561

time	calc q	calc h
2.00000E-06	10468.36	53.4206
3.00000E-06	20038.7	102.2632
4.00000E-06	15013.3	76.6183
5.00000E-06	25644.8	130.881
6.00000E-06	25298.3	129.116
7.00000E-06	32359.0	165.161
8.00000E-06	36370.5	185.644
9.00000E-06	44991.3	229.661
1.00000E-05	39821.4	203.277
1.10000E-05	50480.5	257.705
1.20000E-05	55514.0	283.419
1.30000E-05	59824.8	305.446
1.40000E-05	63676.1	325.130
1.50000E-05	72411.9	369.763
1.60000E-05	72706.7	371.292
1.70000E-05	80592.7	411.595
1.80000E-05	85452.3	436.448
1.90000E-05	95090.9	485.722
2.49000E-03	119051.	627.703
2.49100E-03	113468.	598.256
2.49200E-03	116381.	613.615
2.49300E-03	116798.	615.813
2.49400E-03	117001.	616.882
2.49500E-03	117125.	617.535
2.49600E-03	117209.	617.980
2.49700E-03	122504.	645.908
2.49800E-03	114249.	602.372
2.49900E-03	116845.	616.060
2.50000E-03	111880.	589.875

avg q	avg h
202519.	1062.01

```
*************************************************************************
***** Program BLOWDOT calculates the total mass flow through the porous *****
***** material for boundary layer purposes, and the total mass flow     *****
***** up to each heat flux gauge for heat transfer purposes.           *****
*************************************************************************
      PROGRAM BLOWDOT

        IMPLICIT NONE

        REAL*8 rhoinj,Ppl,R,Tpl,uinj,ainj,SA,mdot,mdotinf,B(3),BT
        REAL*8 mdotsum,CF,P,Astar,in2msq,RHOUinf,P0,T0,psi2Pa,Ainf
        REAL*8 M(54),x(54),y(54),GAMMA

        INTEGER*4 i
*
*     Isentrop contains x and y coordinate data and isentropic Mach NO
*     fo the blowing portion of the nozzle.
*
        OPEN(1,file='isentrop.dat',status='old')
*
*     Blowin contains gamma, stagnation pressure based on subsonic pressure
*     transducer data, stagnation temperature based on stagnation pressure,
*     plenum pressure from the plenum transducer, and plenum temp from the
*     plenum thermocouple.
*
        OPEN(2,file='blowin.dat',status='old')
*
*     Blowrat gives the sum of the positive blowing as a percentage of primary
*     flow evaluated at the three heat flux gauge locations.
*
        OPEN(3,file='blowrat.out',status='old')
*
*     Plotmdot gives all incremental blowing and summed blowing up to each
*     iteration step.
*
        OPEN(4,file='plotmdot.out',status='old')

***** Initialization *****
        write(3,*) 'Blowing Ratios at each heat flux gauge and Total Blo
     cwing Ratio'
        write(3,*)
        write(3,*) 'Test Conditions:'
        write(4,*) 'Mass flow data at each interval'
        write(4,*)
        write(4,*) 'Test Conditions:'
        SA=0.0D0
        mdot=0.0D0
        mdotsum=0.0D0
        DO I=1,3
           B(i) = 0.0D0
        ENDDO
        BT=0.0D0

***** Constants *****
        R = 287.0D0                                              !J/(kg-K)!
        in2msq = .00064516D0
        psi2Pa = 6894.7572D0
        Astar = .3679D0*8.0D0*in2msq                                 !m^2!

***** Read in data needed for problem *****
        DO i=1,54
           READ(1,*) x(i),y(i),M(i)
        ENDDO
        READ(2,*) GAMMA,P0,T0,Ppl,Tpl                        !pressure in psi!...
...
        write(3,30) 'Gamma    =',GAMMA
```

```
      write(3,30) 'P0       =',P0
      write(3,30) 'T0       =',T0
      write(3,30) 'Ppl      =',Ppl
      write(3,30) 'Tpl      =',Tpl
      write(4,30) 'Gamma    =',GAMMA
      write(4,30) 'P0       =',P0
      write(4,30) 'T0       =',T0
      write(4,30) 'Ppl      =',Ppl
      write(4,30) 'Tpl      =',Tpl
      P0 = P0*psi2Pa
      Ppl = Ppl*psi2Pa

***** Initial calculations for iteration *****
      write(3,*)
      write(3,*) 'Initial Calculations:'
      write(4,*)
      write(4,*) 'Initial Calculations:'
      mdotinf=DSQRT(GAMMA/(R*T0)*((2.0D0/(GAMMA+1.0D0))**
     c              ((GAMMA+1.0D0)/(GAMMA-1.0D0))))*Astar*P0          !kg/sec!...
...
      write(3,30) 'mdotinf =',mdotinf
      write(4,30) 'mdotinf =',mdotinf
      RHOUinf=mdotinf/Astar                                    !kg/(m^2-sec)!...
...
      write(3,30) 'RHOUinf =',RHOUinf
      write(4,30) 'RHOUinf =',RHOUinf
      rhoinj=Ppl/(R*Tpl)                                           !kg/m^3!...
...
      write(3,30) 'rhoinj  =',rhoinj
      write(4,30) 'rhoinj  =',rhoinj
      write(3,*)
      write(4,*)
      write(4,40)
*
*   Here we find main flow pressure at any point using isentropic relations,
*   but these are corrected for actual losses by a correction factor CF.  CF
*   is based on fitting two curves to the actual pressure transducer data.
*   Static pressure was generally higher than isentropic predictions,
*   indicating some friction losses.
*
      DO i=2,53
         IF (M(i) .lt. 1.6919D0) THEN
             CF=0.0155*M(i)**3.0D0 + 0.9722D0
         ENDIF
         IF (M(i) .ge. 1.6919D0) THEN
             CF=0.0132*M(i)**6.0D0 - 0.0356*M(i)**4.0D0 + 1.0302
         ENDIF
         P=P0/((1.0D0+(GAMMA-1.0D0)/2.0D0*M(i)**2.0D0)**(GAMMA/
     c          (GAMMA-1.0D0)))*CF                                  !Pa!...
...
         uinj=(ABS(Ppl-P)/1.41402e5)**(1.0D0/.9585d0)
         IF ((Ppl - P) .lt. 0.0D0) THEN
             uinj = uinj*(-1.0D0)
         ENDIF
         ainj=DSQRT((((x(i+1)+x(i))/2-(x(i)+x(i-1))/2)**2.0D0)+
     c           (((y(i+1)+y(i))/2-(y(i)+y(i-1))/2)**2.0D0))*3.0D0*
     c           in2msq                                             !m^2!...
...
         mdot=rhoinj*uinj*ainj                                   !kg/sec!...
...
         Ainf=Astar*y(i)/.3679d0
         IF (i .eq. 11) THEN
             B(1) = ((mdotsum + .2853D0*mdot)/(SA + .2853D0*ainj))/
     c                (mdotinf/Ainf)
             write(*,*) 'Writimg Blowing Ratio 1 to file'
             WRITE(3,20) 'B(1) =',B(1)
```

```
            ENDIF
            IF (i .eq. 23) THEN
                B(2) = ((mdotsum + .7828D0*mdot)/(SA + .7828D0*ainj))/
     c                    (mdotinf/Ainf)
                write(*,*) 'Writing Blowing Ratio 2 to file'
                WRITE(3,20) 'B(2) =',B(2)
            ENDIF
            IF (i .eq. 47) THEN
                B(3) = ((mdotsum + .1201D0*mdot)/(SA + .1201D0*ainj))/
     c                    (mdotinf/Ainf)
                write(*,*) 'Writing Blowing Ratio 3 to file'
                WRITE(3,20) 'B(3) =',B(3)
            ENDIF
            SA=ainj+SA                                                    !m^2!…
     …
            mdotsum=mdot+mdotsum                                        !kg/sec!…
     …
            IF (mdotsum .le. 0.0D0) THEN
                mdotsum = 0.0D0
            ENDIF
            write(4,10) (i-1),x(i),CF,(P/psi2Pa),mdot,mdotsum
          ENDDO
          BT = (mdotsum/SA)/RHOUinf
          WRITE(3,20) 'BT =',BT
        STOP
 10       format(I2,3X,F6.4,3X,F6.4,3X,F5.2,3X,F10.8,3X,F10.8)
 20       format(A7,F6.4)
 30       format(A9,F8.4)
 40       format(8X,'x',7X,'CF',7X,'P',9X,'mdot',7X,'mdotsum')
        END
```

Mass flow data at each interval

Test Conditions:
Gamma = 1.3900
P0 = 74.8007
T0 =499.1000
Ppl = 55.0690
Tpl =287.4500

Initial Calculations:
mdotinf = 1.7673
RHOUinf =930.7518
rhoinj = 4.6024

	x	CF	P	mdot	mdotsum
1	6.0410	0.9744	60.65	-.00023263	0.00000000
2	6.1330	0.9754	57.58	-.00009758	0.00000000
3	6.2240	0.9770	53.86	0.00004429	0.00004429
4	6.3160	0.9794	49.47	0.00021550	0.00025979
5	6.4080	0.9828	44.50	0.00041251	0.00067229
6	6.5000	0.9877	39.15	0.00078966	0.00146195
7	6.6390	0.9937	34.31	0.00072203	0.00218398
8	6.6600	0.9945	33.72	0.00019536	0.00237934
9	6.6810	0.9955	33.09	0.00020143	0.00258078
10	6.7020	0.9963	32.52	0.00020692	0.00278770
11	6.7230	0.9973	31.92	0.00021778	0.00300548
12	6.7450	0.9982	31.37	0.00022326	0.00322874
13	6.7660	0.9992	30.79	0.00022377	0.00345251
14	6.7870	1.0003	30.22	0.00022937	0.00368187
15	6.8080	1.0014	29.64	0.00024072	0.00392259
16	6.8300	1.0025	29.06	0.00024645	0.00416904
17	6.8510	1.0036	28.52	0.00024608	0.00441512
18	6.8720	1.0047	27.97	0.00025167	0.00466679
19	6.8930	1.0060	27.40	0.00026340	0.00493019
20	6.9150	1.0072	26.86	0.00189599	0.00682618
21	7.1960	1.0226	21.49	0.00255170	0.00937787
22	7.2550	1.0256	20.67	0.00089267	0.01027054
23	7.3120	1.0285	19.94	0.00089676	0.01116730
24	7.3690	1.0313	19.26	0.00090651	0.01207381
25	7.4250	1.0340	18.66	0.00090624	0.01298005
26	7.4800	1.0367	18.08	0.00092136	0.01390141
27	7.5360	1.0394	17.55	0.00069925	0.01460066
28	7.5630	1.0407	17.30	0.00046657	0.01506723
29	7.5910	1.0420	17.05	0.00047823	0.01554546
30	7.6190	1.0433	16.81	0.00048145	0.01602691
31	7.6470	1.0446	16.58	0.00047584	0.01650274
32	7.6740	1.0459	16.35	0.00047884	0.01698159
33	7.7020	1.0472	16.13	0.00049047	0.01747206
34	7.7300	1.0521	15.97	0.00049252	0.01796458
35	7.7580	1.0562	15.80	0.00050351	0.01846809
36	7.7870	1.0607	15.63	0.00050574	0.01897382
37	7.8150	1.0651	15.48	0.00049889	0.01947271
38	7.8430	1.0698	15.33	0.00050990	0.01998261
39	7.8720	1.0748	15.18	0.00052087	0.02050348
40	7.9010	1.0798	15.04	0.00052281	0.02102629
41	7.9300	1.0850	14.90	0.00052469	0.02155099
42	7.9590	1.0905	14.77	0.00049925	0.02205024
43	7.9850	1.0953	14.65	0.00520600	0.02725624
44	8.5320	1.2009	13.16	0.00566894	0.03292518
45	8.5860	1.2106	13.08	0.00100959	0.03393477
46	8.6390	1.2202	13.00	0.00100190	0.03493667
47	8.6920	1.2296	12.94	0.00100328	0.03593995
48	8.7450	1.2384	12.87	0.00100453	0.03694448
49	8.7980	1.2471	12.82	0.00099638	0.03794086
50	8.8500	1.2559	12.76	0.00098807	0.03892893
51	8.9020	1.2641	12.71	0.00099847	0.03992740

Blowing Ratios at each heat flux gauge and Total Blowing Ratio

Test Conditions:
Gamma = 1.3900
P0 = 74.8007
T0 =499.1000
Ppl = 55.0690
Tpl =287.4500

Initial Calculations:
mdotinf = 1.7673
RHOUinf =930.7518
rhoinj = 4.6024

B(1) =0.0021
B(2) =0.0051
B(3) =0.0113
BT =0.0075

Bibliography

Azavedo, David. "Measured Thrust Losses Associated with Secondary Air Injection Through Nozzle Walls," Journal of Propulsion and Power, 9: 43-50 (January/February 1993).

Bartz, D.R. "An Approximate Solution of Compressible Turbulent Boundary-Layer Development and Convective Heat Transfer in Convergent-Divergent Nozzles," ASME Journal of Engineering for Power,77: 1235-1245 (November 1955).

-----. "A Simple Equation for Rapid Estimation of Rocket Nozzle Convective Heat Transfer Coefficients," Journal of Jet Propulsion, 27: 49-51 (January 1957).

-----. "Survey of Relationships Between Theory and Experiment for Convective Heat Transfer in Rocket Combustion Gasses," Advances in Rocket Propulsion, edited by S.S. Penner. Manchester England: AGARD Technivision Services, 1968.

Beitel, G.R. Boiling Heat Transfer Processes and Their Application in the Cooling of High Heat Flux Devices. Technical Report Arnold Engineering Development Center (AFMC) Arnold AFB TN, 1993.

Bonafede, 1st Lt Joseph Anthony. A Numerical Investigation of Thin Film Heat Transfer Gauges. MS Thesis AFIT/GA/AA/88M-1. School of Engineering, Air Force Institute of Technology (AU), Wright Patterson AFB OH, March 1988.

Bowersox, Dr. Rodney. Blcorr. Version 1.0, Fortran Computer Software. Air Force Institute of Technology (AU), Wright Patterson AFB OH, 1991.

-----. Nozz. Version 1.0, Fortran Computer Software. Air Force Institute of Technology (AU), Wright Patterson AFB OH, 1991.

-----. Shocktun. Version 1.0, Fortran Computer Software. Air Force Institute of Technology (AU), Wright Patterson AFB OH, 1991.

Cook, W.J. and E.J. Felderman. "Reduction of Data from Thin-Film Heat-Transfer Gages: A Concise Numerical Technique," AIAA Journal, 4: 561-562 (March 1966).

Eads, Capt Thomas. Shock Tube Study of the Effects of Large Density Differences and Blowing Ratio on Heat Transfer to a Film-Cooled Flat Plate. MS Thesis, AFIT/GAE/ENY/92D-25. School of Engineering, Air Force Institute of Technology (AU), Wright Patterson AFB OH, December 1992.

Endevco Corporation. "Endevco Model 8530A Piezoresistive Absolute Pressure Transducers," San Juan Capistrano CA. Personal Correspondence. March 1994.

Forth, C.J.P. and T.V. Jones. "Scaling Parameters in Film Cooling," Proceedings of the Eighth International Heat Transfer Conference. 1271-1276. San Fransisco: Hemisphere Publishing Corporation, 1986.

Giedt, W.H. "Investigation of Variation of Point Unit Heat Transfer Coefficient Around a Cylinder Normal to an Air Stream," ASME Transactions, 71: 375-381 (September 1949).

Glass, I.I. Shock Tubes, Part I: Theory and Performance of Simple Shock Tubes. UTIA Review No. 12. Toronto: University of Toronto Institute of Aerophysics, 1958.

Goldstein, R.J. and others. "Film Cooling with Injection through Holes: Adiabatic Wall Temperature Downstream of a Circular Hole," ASME Journal of Engineering for Power, 90: 384-395, 1968.

Hill, Philip G. and Carl R. Peterson. Mechanics and Thermodynamics of Propulsion (Second Edition). New York: Addison-Wesley Publishing Company, 1992.

Kays, William M. and Michael E. Crawford. Convective Heat and Mass Transfer (Second Edition). New York: McGraw-Hill Book Company, Inc., 1980.

Keener, 2nd Lt David N. Investigation of Boundary Layer and Performance Effects of Transpiration Cooling Through a Porous Plate in a Rocket Nozzle. MS Thesis, AFIT/GA/ENY/94D-3. School of Engineering, Air Force Institute of Technology (AU), Wright Patterson AFB OH, December 1994.

May, Lee R. and Wendel M. Burkhardt. "Transpiration Cooled Throat for Hydrocarbon Rocket Engines," Journal of Spacecraft Propulsion and Power: 1-53, December 1991.

Medtherm Corporation. "Report of Calibration for Platinum Thin Film Gages," Part Number PTF-100-20404. Huntsville AL. Personal Correspondence. February 1994.

Mott Metallurgical Corporation. Technical Handbook for Precision Porous Metal Products. Product Catalog No. 1000A. Farmington CT, 1986.

Ozisik, M. Necati. Heat Transfer: A Basic Approach. New York: McGraw-Hill Book Company, Inc., 1985.

Pederson, D.R. and others. "Film Cooling With Large Density Differences Between the Mainstream and the Secondary Fluid Measured by the Heat-Mass Transfer Analogy," ASME Journal of Heat Transfer, 99: 620-627 (November 1977).

Poll, D.I.A. "The Solution of Boundary Problems by the use of Integral Equations: Basic Equations and the Development of the Pressure Gradient Closure Relations," Journal of Fluid Mechanics and Heat Transfer: 31-62, 1991.

Rivir, R.B. and others. "Visualization of Film Cooling Flows Using Laser Sheet Light," Paper No. AIAA-87-1914. New York: American Institute of Aeronautics and Astronautics, 1987.

Seginer, A. and others. "Calibration of Thin Film Resistance Thermometers for Heat Flux Measurements in the Shock Tube," Israel Journal of Technology, 3: 25-30 (December 1964).

Schultz, D.L. and Jones, T.V. Heat Transfer Measurements in Short Duration Hypersonic Facilities. AGARDograph AG-165, February 1973.

Shapiro, Ascher H. The Dynamics and Thermodynamics of Compressible Fluid Flow. In Two Volumes. New York: John Wiley & Sons, 1953.

Sutton, George P. Rocket Propulsion Elements (Fourth Edition). New York: Wiley-Interscience, 1976.

Valencia, Marco R. Experimental Investigation of the Effects of Blowing Ratio Parameter on Heat Transfer to a Film-Cooled Flat Plate. MS Thesis AFIT/GAE/ENY/93J-01. School of Engineering, Air Force Institute of Technology (AU), Wright Patterson AFB OH, January 1993.

White, Frank M. Heat Transfer. Reading MA: Addison-Wesley Publishing Company, 1984.

-----. Viscous Fluid Flow (Second Edition). New York: McGraw-Hill Inc., 1991.

Wittig, S. and V. Scherer. "Heat Transfer Measurements Downstream of a Two Dimensional Jet Entering a Crossflow," ASME Journal of Turbomachinery, 109: 572-578 (October 1987).

Zuppan, Maj Lawrence L. An Investigation of the Variation of Throat Height on the Performance of Convergent-Divergent Nozzles in a Shock Tube. MS Thesis AFIT/GAE/ENY/64D. School of Engineering, Air Force Institute of Technology (AU), Wright Patterson AFB OH, December 1964.

REPORT DOCUMENTATION PAGE

Form Approved
OMB No. 0704-0188

1. AGENCY USE ONLY (Leave blank)	2. REPORT DATE	3. REPORT TYPE AND DATES COVERED
	28 November 1994	Final

4. TITLE AND SUBTITLE

Effects of Blowing Ratio on Heat Transfer to the Throat Region of a Porous-Walled Nozzle

5. FUNDING NUMBERS

6. AUTHOR(S)

Joseph L. Lenertz

7. PERFORMING ORGANIZATION NAME(S) AND ADDRESS(ES)

AFIT/ENY
Wright Patterson AFB OH 45431

8. PERFORMING ORGANIZATION REPORT NUMBER

AFIT/GA/ENY/94D-7

9. SPONSORING/MONITORING AGENCY NAME(S) AND ADDRESS(ES)

Mr. Terence Galati OLAC PL/RKCA, 4 Draco Dr.
Phillips Laboratory, Edwards AFB CA 93524-7190

10. SPONSORING/MONITORING AGENCY REPORT NUMBER

11. SUPPLEMENTARY NOTES

12a. DISTRIBUTION/AVAILABILITY STATEMENT

Approved for public release; distribution unlimited

12b. DISTRIBUTION CODE

13. ABSTRACT *(Maximum 200 words)*

This experiment analyzed the effects of blowing ratio on heat transfer to the throat region of a porous-walled nozzle, using the AFIT low speed shock tube. Heat flux data were taken from both sides of a two-dimensional Mach 2.0 (Re/m=5.2x10e7) nozzle using thin film resistance thermometers. One side was transpiration-cooled by secondary air injection through a sintered wall, while the other side served as a control. Control results were validated using empirical relations, and cooled side results showed up to a 14% reduction in heat transfer coefficient at blowing ratios of only 0.51%. The linear nature of cooling effectiveness at these low blowing ratios allowed a modification of nozzle heat transfer equations to include a blowing ratio parameter. Disturbance of primary flow was also minimized, causing no measurable reduction of nozzle performance.

14. SUBJECT TERMS	15. NUMBER OF PAGES
Heat Flux Gauge Calibration, Shock Tube, Heat Transfer, Transpiration Cooling, Blowing Ratio	107
	16. PRICE CODE

17. SECURITY CLASSIFICATION OF REPORT	18. SECURITY CLASSIFICATION OF THIS PAGE	19. SECURITY CLASSIFICATION OF ABSTRACT	20. LIMITATION OF ABSTRACT
Unclassified	Unclassified	Unclassified	UL